

CONS/9427-1
NASA CR-135368

HYDRODYNAMIC AIR LUBRICATED COMPLIANT SURFACE BEARING FOR AN AUTOMOTIVE GAS TURBINE ENGINE I - JOURNAL BEARING PERFORMANCE

D. Ruscitto, J. Mc Cormick, and S. Gray
Mechanical Technology Incorporated
Latham, New York 12110

April 1978

Prepared for the
NATIONAL AERONAUTICS AND SPACE ADMINISTRATION
Lewis Research Center
Cleveland, Ohio 44135

Contract NAS 3-19427

As a part of the
U.S. DEPARTMENT OF ENERGY
Division of Transportation Energy Conservation



(NASA-CR-135368-1) HYDRODYNAMIC AIR LUBRICATED COMPLIANT SURFACE BEARING FOR AN AUTOMOTIVE GAS TURBINE ENGINE I - JOURNAL BEARING PERFORMANCE Final Report (Mechanical Technology, Inc.) 146 p. 1978

1. Report No. NASA CR-135368		2. Government Accession No.		3. Recipient's Catalog No.	
4. Title and Subtitle HYDRODYNAMIC AIR LUBRICATED COMPLIANT SURFACE BEARING FOR AN AUTOMOTIVE GAS TURBINE ENGINE I - JOURNAL BEARING PERFORMANCE				5. Report Date April 1978	
				6. Performing Organization Code	
7. Author(s) D. Ruscitto, J. McCormick, and S. Gray				8. Performing Organization Report No.	
9. Performing Organization Name and Address: Mechanical Technology Incorporated 968 Albany-Shaker Rd. Latham, New York 12110				10. Work Unit No.	
				11. Contract or Grant No. NAS3-19427	
12. Sponsoring Agency Name and Address: Department of Energy Division of Transportation Energy Conservation Washington, D. C. 20545				13. Type of Report and Period Covered Contractor Report	
				14. Sponsoring Agency Code Report No. CONS/9427-1	
15. Supplementary Notes Final report. Prepared under Interagency Agreement EC-77-A-31-1040. Project Manager, William J. Anderson, Fluid System Components Division, NASA Lewis Research Center, Cleveland, Ohio 44135.					
16. Abstract A 38.1 mm diameter Hydresil™ Compliant Foil Bearing was designed and tested at room temperature and 315° C. Test speeds of 60 000 rpm and loads of 1.75×10^5 N/m ² were obtained. A unique adaptation of capacitance proximity probes mounted in the rotating journal was utilized to directly measure the bearing film thickness. Test bearings with an L/D = 1 and L/D = 1/2 were used and the experimental data have been compared with predicted minimum film thickness values for an L/D = ∞ bearing and the results presented as a series of curves. Experimental data were obtained at 315° C which showed relatively low cooling air flow requirements to remove self-generated heat. The detrimental influence of porous journal surface coatings on bearing load performance was demonstrated.					
17. Key Words (Suggested by Author(s)) Gas bearings Foil bearings Compliant bearings Journal bearings			18. Distribution Statement Unclassified - unlimited STAR Category 37 DOE Category UC-96		
19. Security Classif. (of this report) Unclassified		20. Security Classif. (of this page) Unclassified		21. No. of Pages 148	22. Price A07

TABLE OF CONTENTS

	<u>Page</u>
I. INTRODUCTION	1
BACKGROUND AND APPLICATION	1
PROGRAM OBJECTIVES	2
II. EXISTING STATE OF COMPLIANT BEARING ANALYSIS	4
ONE-DIMENSIONAL HYDRESIL JOURNAL BEARING ANALYSIS	4
III. TEST BEARINGS	9
SENSOR SYSTEM REFERENCE AIR BEARING	9
COMPLIANT SURFACE TEST BEARING	10
IV. TEST FACILITY AND INSTRUMENTATION	20
TEST RIG DESCRIPTION	20
Drive Spindle Assembly	20
Test Journals	24
Test Bearings	24
QUALITY ASSURANCE	26
MEASUREMENTS AND INSTRUMENTATION	26
Rotor Speed	26
Shaft and Test Bearing Motion	27
Test Bearing Load	27
Test Temperatures	27
Test Bearing Cooling Air	28
Bearing Frictional Power Loss	28
Data Acquisition Equipment Calibration	28
V. FILM MEASUREMENT TECHNIQUE	30
INTRODUCTION	30
SELECTION OF ROTATING CAPACITANCE SYSTEM	30
CALIBRATION OF SENSORS	33
FILM MEASUREMENT DATA ACQUISITION	36
VI. TEST PROGRAM	39
FILM THICKNESS TESTS	39
FILM PRESSURE TESTS	40
HIGH TEMPERATURE TESTS	41
VII. TEST RESULTS AND DISCUSSION	42
FILM THICKNESS MEASUREMENT TESTING	42
BASELINE RIGID SURFACE PLAIN SLEEVE BEARING TEST RESULTS	42
COMPLIANT SURFACE JOURNAL BEARING TESTS	45
Test Results of Compliant Bearing Tests	52
Discussion of Compliant Bearing Test Results	64
Changes in film profile due to design parameters	64
Changes in film thickness due to test parameters	73
Bearing attitude angle	78
Influence of bearing accuracy on performance	83
Foil excitation by cooling air	85

	<u>Page</u>
HIGH TEMPERATURE TESTS	87
RESULTS FOR ELEVATED TEMPERATURE TESTING	87
DISCUSSION OF ELEVATED TEMPERATURE TEST RESULTS	93
Effects of Bearing Journal Surface Porosity on Bearing Load Performance	93
Bearing Coolant Air Requirements	98
Method of supplying cooling air	98
Maintaining bearing temperature constant with ambient temperature	101
Comparison of Cooling Flows with Typical Gas Turbine Engine Flows	102
Effects of High Temperature on Load Performance	102
BEARING LIFT OFF SPEED	103
BEARING FRICTIONAL POWER LOSS	106
VIII. ANALYSIS OF FILM THICKNESS TEST DATA	107
IX. CONCLUSIONS AND RECOMMENDATIONS	120
SPECIFIC CONCLUSIONS	120
Journal Bearing Load Capacity Performance	120
Influence of L/D Ratio on Minimum Film Thickness	121
Influence of Bearing Fabrication Accuracy on Load Performance	121
Bearing Journal Surface Porosity	121
Bearing Cooling Air Requirements	121
Effects of Thermal Distortion on Bearing Performance	122
RECOMMENDATIONS	122
Continued Technology Advancement	122
Additional Journal Bearing Tests	122
Thrust Bearing Tests	123
REFERENCES	124
APPENDIX A. FABRICATION OF THE FILM THICKNESS SENSOR	125
APPENDIX B. FABRICATION OF BRUSH AND SLIP RING ASSEMBLY	133

LIST OF FIGURES

Number		Page
II-1	Schematic of Hydresil Journal Bearing	5
II-2	Computer Predicted Test Journal Bearing Performance Curves (One Dimensional Analysis)	7
II-3	Sample Input and Output for Journal Bearing Computer Program (HYDRE)	8
III-1	Hydresil Test Journal Bearing	11
III-2	Mechanical Design of Test Journal Bearing	12
III-3	Compliant Bearing Design Details	13
III-4	Precision Die for Forming Bump Foil	15
III-5	Schematic of Apparatus Used to Determine Bearing Clearance	17
III-6	Example of Load vs Deflection Plot for Determining Bearing Clearance	18
IV-1	Journal Bearing Test Rig (layout)	21
IV-2	Journal Bearing Test Rig (photo)	22
IV-3	Journal Bearing Test Facility with Instrumentation Rack	23
IV-4	Test Shaft with Support Ball Bearings, Drive Turbine and Test Bearing	25
V-1	Film Measurement Probes (photo)	31
V-2	Rotating Sensors and Slip Ring Assembly	32
V-3	Calibration Curve for Film Thickness Sensors	35
V-4	Schematic of Set Up for Obtaining Zero Correction Voltage for Compliant Surface Bearing	37
VII-1	Analytical and Experimental Minimum Film Thickness Values, Rigid Surface Plain Sleeve Bearing	43
VII-2	Typical Oscilloscope Trace of Film Thickness Profile, Rigid Surface Plain Sleeve	44
VII-3	Oscilloscope Traces Showing Effect of Speed on Film Thickness Profile, Rigid Surface Plain Sleeve Bearing	46
VII-4	Expanded Plot of Film Thickness Profile, Rigid Surface Plain Sleeve Bearing	47
VII-5	Polar Plot of Film Thickness Profile, Rigid Surface Plain Sleeve Bearing	48
VII-6	Schematic of Instrumentation Used in Film Thickness Data Acquisition	49

LIST OF FIGURES

Number		Page
VII-7	Typical Oscilloscope Trace of Film Thickness Profile, Compliant Surface Bearing	51
VII-8	L/D=1, C=0.057 mm: Experimental Minimum Film Thickness Values, Compliant Surface Bearing	60
VII-9	L/D=1, C=0.0318 mm: Experimental Minimum Film Thickness Values, Compliant Surface Bearing	61
VII-10	L/D=1/2, C=0.057 mm: Experimental Minimum Film Thickness Values, Compliant Surface Bearing	62
VII-11	L/D=1/2, C=0.0318 mm: Experimental Minimum Film Thickness Values, Compliant Surface Bearings	63
VII-12	Oscilloscope Traces Showing Effect of Bearing Clearance on Film Thickness, Compliant Surface Bearing	65
VII-13	Oscilloscope Traces Showing Effect of Bearing L/D Ratio on Film Thickness, Compliant Surface Bearing	67
VII-14	Film Thickness Profile at Various Axial Positions, Compliant Surface Bearing	68
VII-15	Oscilloscope Traces Showing Effect of Load on Smooth Foil Deflection	69
VII-16	Oscilloscope Traces Showing Effect of Axial Position on Smooth Foil Deflection	70
VII-17	Hydresil Bearing with Inverted Bump Foil	72
VII-18	Oscilloscope Traces Showing Effect of Bearing Load on Film Thickness, L/D=1 Compliant Surface Bearing . .	74
VII-19	Oscilloscope Traces Showing Effect of Bearing Load on Film Thickness, L/D=1/2 Compliant Surface Bearing . . .	75
VII-20	Expanded Plot of Film Thickness Profile, Compliant Surface Bearing	76
VII-21	Polar Plot of Film Thickness Profile, Compliant Surface Bearing	77
VII-22	Oscilloscope Traces Showing Effect of Speed on Film Thickness, L/D=1 Compliant Surface Bearing	79
VII-23	Polar Plot Showing Effect of Speed on Internal Size of Compliant Surface Bearing	80
VII-24	Oscilloscope Film Thickness Trace Showing Method Used to Obtain Attitude Angle, Compliant Surface Bearing . .	81
VII-25	Oscilloscope Film Thickness Trace of 3 Compliant Surface Bearings Having Fabrication Defects..	84
VII-26	Oscilloscope Trace Showing Excitation of Smooth Foil by Cooling Air Supply	86
VII-27	Experimental Data for Bearing Cooling Air Requirements for Compliant Surface Bearing at 315°C	91

LIST OF FIGURES

Number		Page
VII-28	Typical Trace of Test Bearing Temperature.	92
VII-29	Typical Trace of Test Bearing Temperature.	94
VII-30	Taly Surf Traces of Bearing Journal Surfaces	96
VII-31	Schematic Showing Method of Supplying Cooling Air to Test Bearing	99
VII-32	Schematic Showing Alternate Method of Supplying Cooling Air to Bearing	100
VII-33	Typical Trace for Obtaining Lift Off Speed, Compliant Surface Bearing.	104
VIII-1	C=0.057 mm; 30,000 rpm: Dimensionless Minimum Film Thickness Values for 3 L/D Ratios Compliant Surface Bearing (CSB).	110
VIII-2	C=0.057 mm; 45,000 rpm: Dimensionless Minimum Film Thickness Values for 3 L/D Ratios Compliant Surface Bearing.	111
VIII-3	C=0.057 mm; 60,000 rpm: Dimensionless Minimum Film Thickness Values for 3 L/D Ratios Compliant Surface Bearing.	112
VIII-4	C=0.0318 mm; 30,000 rpm: Dimensionless Minimum Film Thickness Values for 3 L/D Ratios Compliant Surface Bearing.	113
VIII-5	C=0.0318 mm; 45,000 rpm: Dimensionless Minimum Film Thickness Values for 3 L/D Ratios Compliant Surface Bearing.	114
VIII-6	C=0.0318 mm; 55,000 rpm: Dimensionless Minimum Film Thickness Values for 3 L/D Ratios Compliant Surface Bearing.	115
VIII-7	C=0.0213 mm; 10,000 rpm: Dimensionless Minimum Film Thickness Values for 3 L/D Ratios Rigid Surface Plan Sleeve Bearing	117
VIII-8	Expanded Plot of Predicted and Experimental Film Thickness Profile.	118
A-1	Detail Cross Section of Film Thickness Probe	126
A-2	Detail Cross Section of Film Thickness Sensor System Installed in Test Shaft.	127
A-3	Rotating Film Measurement Sensors and Test Shaft	129
A-4	Film Measurement Sensors	130
A-5	Detail Cross Section of Slip Ring.	132
B-1	Brush Housing and Brushes.	135
B-2	Brush Housing Installed on Test Rig.	136

LIST OF TABLES

<u>Number</u>		<u>Page</u>
VII-1	Compliant Bearing Data from Test #101.	53
VII-2	Compliant Bearing Data from Test #102.	54
VII-3	Compliant Bearing Data from Test #103.	55
VII-4	Compliant Bearing Data from Test #106.	56
VII-5	Compliant Bearing Data from Test #107.	57
VII-6	Compliant Bearing Data from Test #108.	58
VII-7	Compliant Bearing Data from Test #112.	59
VII-8	Tabulated Data for Bearing Attitude Angle.	82
VII-9	Compliant Bearing Data from Test #219.	88
VII-10	Compliant Bearing Data from Test #220.	89
VII-11	Compliant Bearing Data from Test #220.	90
VII-12	Compliant Bearing Data from Test #221.	95
VII-13	Tabulated Data from Lift Off Speed Test.	105

SUMMARY

A 38.1 mm (1.5 inch) diameter Hydresil™ Compliant Surface Air Lubricated Journal Bearing was designed and tested to obtain bearing performance characteristics at both room temperature and 315°C (600°F). Testing was performed at various speeds up to 60,000 rpm with varying loads. A maximum steady state bearing load of $1.75 \times 10^5 \text{ N/m}^2$ (25.4 psi) at 315°C (600°F) was obtained during the test program.

The program objectives centered around two phases of testing. The first test phase was conducted at room temperature for the purpose of obtaining direct film characteristics. To achieve this objective, a unique method of instrumentation was designed, fabricated and tested by Mechanical Technology Incorporated to measure directly the minimum film thickness value and film thickness profile in the compliant surface bearing. The measurement system utilized specially fabricated capacitance proximity probes mounted in the rotating journal surface. The electrical signal was obtained from the rotating shaft using an adaptation of a conventional brush and slip ring assembly. Testing was conducted on test bearings with an $L/D = 1$ and $L/D = 1/2$ at two bearing clearances each, at a variety of speeds and loads. The experimental data has been compared with predicted minimum film thickness values for an $L/D = \infty$ bearing obtained using an existing computer program which is based on a one-dimensional analysis. Minimum film thickness values as a function of load are presented in dimensionless form as a series of curves which allow approximate finite bearing factors to be obtained.

The rotating sensors provided an opportunity to examine the film characteristics of the compliant surface bearing. In addition to providing minimum film thickness values and profiles, many other insights into bearing operation were gained such as the influence of bearing fabrication accuracy and the influence of smooth foil deflection between the bumps.

I. INTRODUCTION

This report describes Part I of a technology program performed for the NASA Lewis Research Center for the development of hydrodynamic air lubricated compliant journal bearings for an automotive gas turbine engine. Part I of the program focused on advancing compliant surface journal bearing technology by providing design information through an experimental and analytical effort. Part II of the program, which is currently in progress, will investigate and test materials and coatings for compliant surface bearings and journals suitable for operation in a 537° - 648°C (1000° - 1200°F) environment.

The rotating film measurement system was designed by Leo Hoogenboom of the Measurement Science Section of MTI. Fabrication of the components for the measurement sensors and their installation into the test shafts were performed by Robert Moss of MTI. William Miller of MTI's Fluid Film Tribology Section assisted in the analytical correlation of the film thickness test data.

BACKGROUND AND APPLICATION

The U.S. Energy Research and Development Agency is currently funding the development of an automotive gas turbine engine that will meet proposed Federal emission standards and demonstrate improved fuel economy over a comparable internal combustion engine. To enable future automotive gas turbine engines to achieve the performance requirements, the engine must be compact, operate at high rotational speeds, utilize high turbine gas temperatures, and be cost competitive. The high turbine gas temperatures will impose temperature requirements on turbine end support bearings that will eliminate the practical use of oil lubricated support bearing systems in these areas. The hydrodynamic air lubricated compliant journal bearing is a likely candidate to fill this requirement. Potentially, the compliant air lubricated bearing offers the following advantages:

- Higher cycle operating temperatures.
- Elimination of oil requirements and limitations.

- Greater accommodation of thermal distortions, assembly variations, and dynamic shaft motion because of bearing compliance.
- Reduced frictional power loss.
- Reduced rotor noise.
- Lower bearing costs.

Under a separate contract (ERDA/Chrysler 68-01-0459-7.5) MTI has designed, fabricated, and tested a HydresilTM air lubricated compliant journal bearing for the A-926 Upgraded Chrysler/ERDA Automotive Gas Turbine Engine. The bearing is being used at the drive turbine end of the gas generator and is subjected to a temperature range of -34°C (-30°F) to +275°C (525°F).

The program reported here was performed to advance the technology of compliant surface air lubricated bearings and to assist in the design and application of bearing systems for the automotive gas turbine engine.

PROGRAM OBJECTIVES

The basic objective of this program was to conduct a fundamental study of air lubricated compliant journal bearings in a combined precise test rig measurement and analytical effort. Specific program objectives included:

- Modification of an existing MTI owned test facility to program requirements.
- Design and fabrication of a Hydresil compliant surface journal bearing.
- Design and fabrication of a rotating capacitance sensor system for obtaining direct film measurements.
- Testing of the journal bearing over a range of speeds up to 60,000 rpm and loads up to $2.1 \times 10^6 \text{ N/m}^2$ (30 psi) as measured on the bearing projected area for the purpose of obtaining bearing performance characteristics to include: bearing film characteristics, bearing cooling air requirements, and bearing power loss.
- Analysis of experimental test data and correlation with existing infinite width bearing theory.

A significant portion of the program included the design, fabrication, installation, and testing of the sensor system used to obtain the direct film measurements. It is believed that this work represents the first time that direct film measurements of a compliant surface bearing have been obtained at speeds typical of turbomachinery that would utilize the compliant surface bearing.

The test program was designed to obtain experimental data that could be used to correct an existing infinite length bearing theory for side leakage effects and to construct design charts to assist in the design of rotor bearing systems that would utilize the compliant surface bearing.

Testing was conducted at 315°C (600°F) bearing temperature to determine bearing cooling air flow requirements and to investigate the influence of thermal distortions on bearing performance. The film thickness data was obtained at room temperature conditions.

II. EXISTING STATE OF COMPLIANT BEARING ANALYSIS

The Hydresil test bearings used in this program were designed utilizing existing MIT computer programs. A detailed description of the analysis together with the Journal Bearing Computer Program HYDRE is given in Reference [2]. The program is written for use on the GE Mark II Time Sharing System.

The following discussion describes the assumptions and highlights of the one dimensional analysis and includes the design curves generated for the test bearing and an example of the computer input and output.

ONE-DIMENSIONAL HYDRESIL JOURNAL BEARING ANALYSIS

A schematic showing the geometry and the coordinate system used in the analysis is given in Figure II-1. A load, W , is applied to the test bearing causing it to displace a distance, e . The shaft is rotating at speed, ω , and has a radius, R . The bearing casing is rigid and contains an elastic bump foil covered by a smooth top foil.

Under zero load, the clearance between the shaft and a seated foil would be, C . The minimum film thickness for a rigid bearing under load would thus be $C-e$. This is not the case for a Hydresil bearing because the foils are free to deflect and the film thickness can be substantially larger than $C-e$ and in fact e can, for sufficiently compliant bearings, be considerably greater than C .

The two modes of deflections of the foils which have been considered in the analysis are shown schematically in the bottom portion of Figure II-1. First, the bump foils are free to deform under load and the deflection of these foils will have a dominant role in the bearing stiffness. Second, the upper foils can dip down under pressure between the bumps causing grooving to occur which could have an effect on the film thickness.

A narrow groove theory is used in computing the effects of grooving on film thickness coupled with the elastic bending theory which dictates the extent to which grooving will occur under the hydrodynamic pressure.

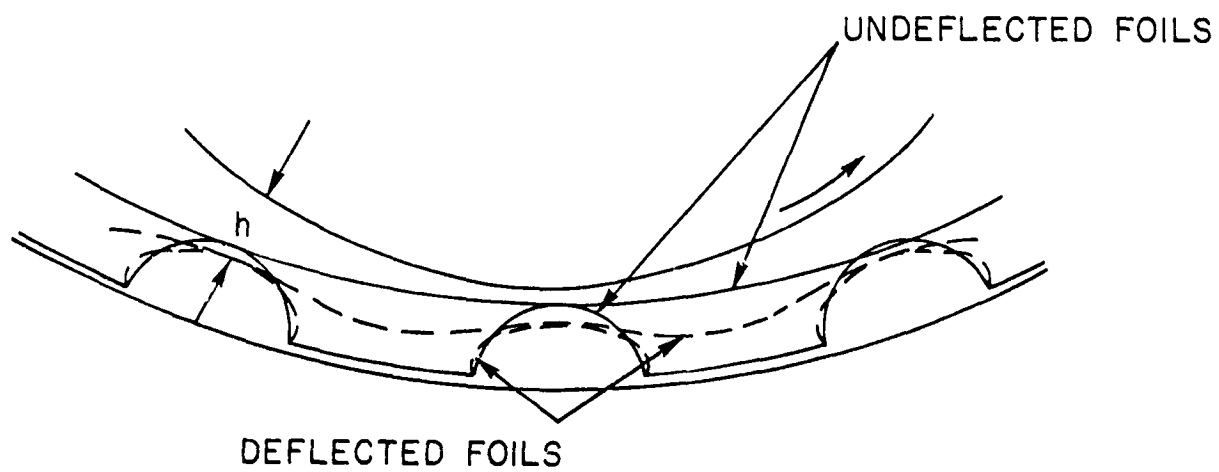
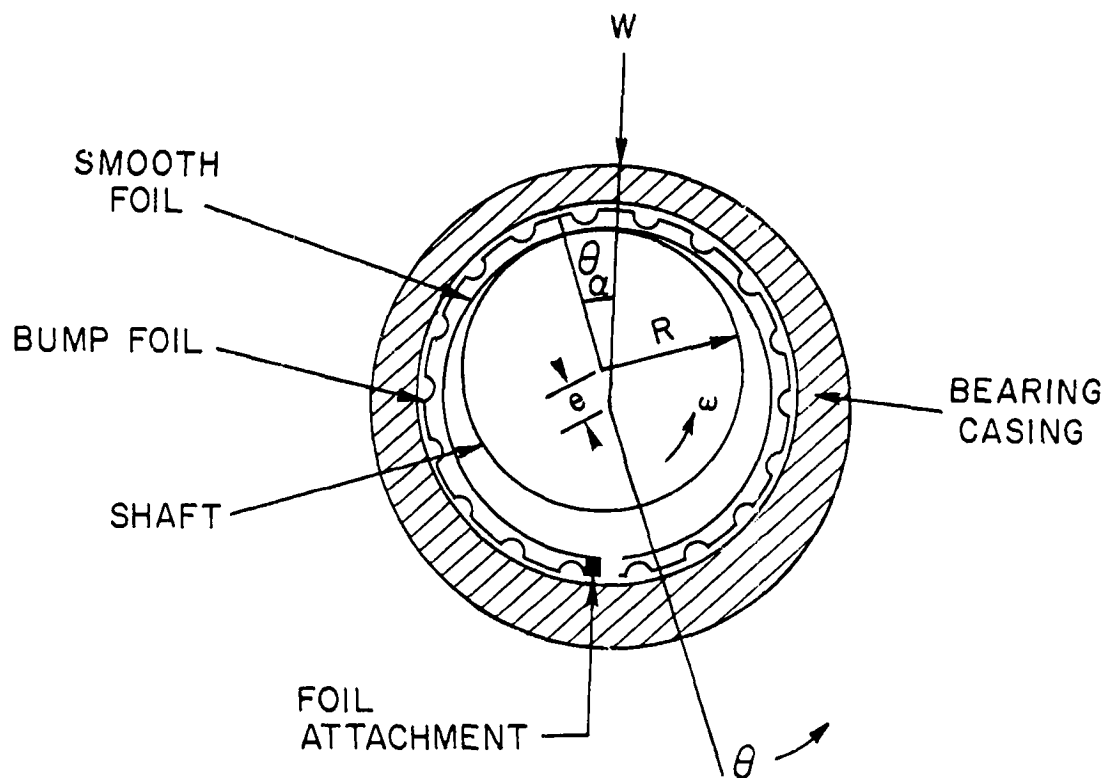


Fig. 11-1 Schematic of Hydrofoil Journal Bearing

Analyses have been performed to predict the deflection of circular arc bumps under load applied at their center. These analyses include the effects of the height, length, and thickness of the bumps and the effects of friction between the bump foil and the housing. The bump deflection analysis is then coupled with the top foil analysis which is further coupled with the global hydrodynamic analysis to result in the full analysis for a one-dimensional journal bearing.

All analyses thus far have been performed for a single 360° pad rather than an assembly of pads.

Figure II-2 shows as a function of bearing load, the shaft deflection, minimum film thickness, and frictional power loss predicted for the Hydresil test bearing at 60,000 rpm. The shaft motion shown in the figure represents the relative radial displacement e between the rotating shaft and the rigid bearing casing. Figure II-3 is a sample of the input and output dimensional parameters required by the Hydresil computer program.

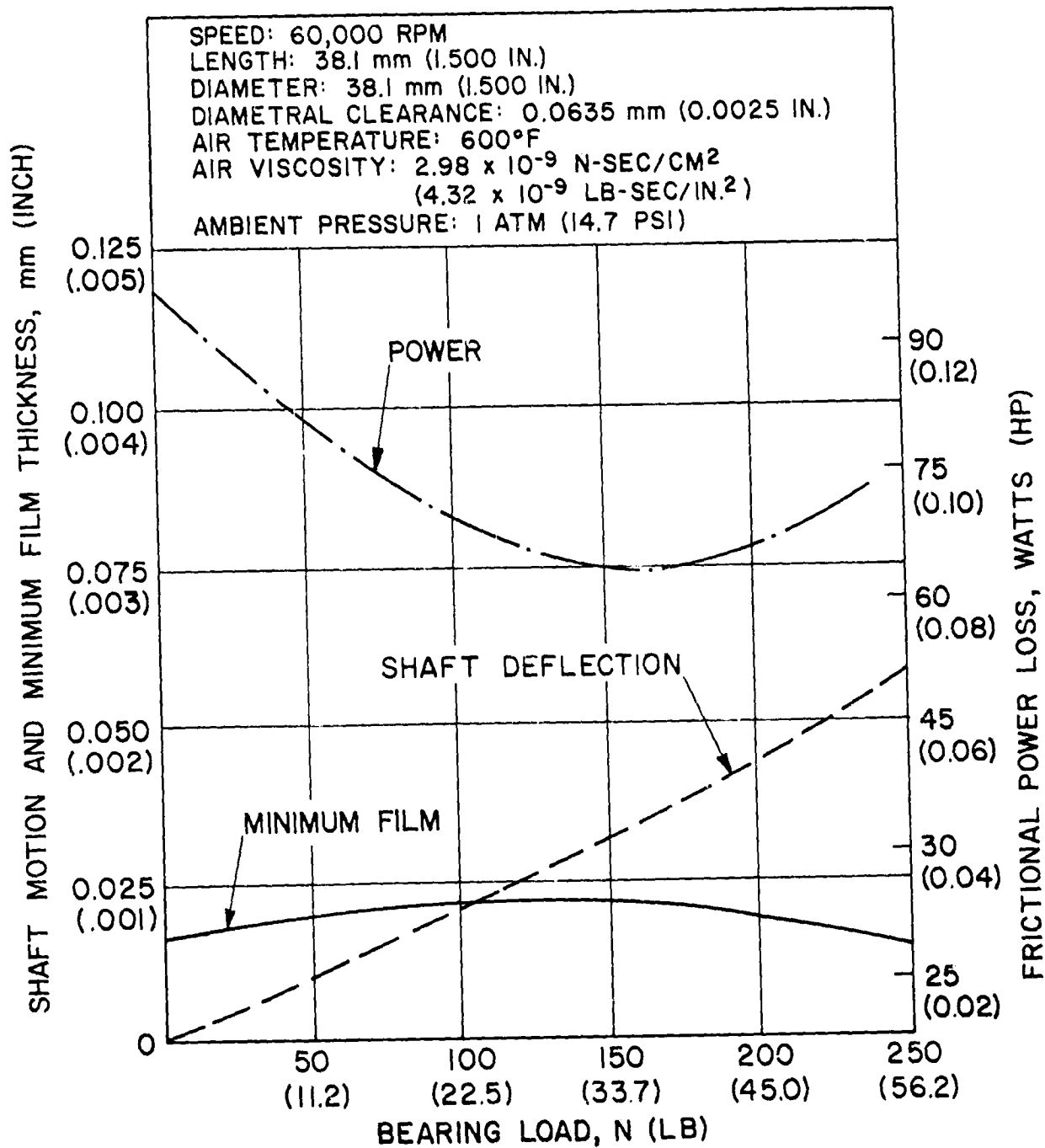


Fig. 11-2 Computer Predicted Test Journal Bearing Performance Curves (One Dimensional Analysis)

INPUT

1. LENGTH (IN), 2. DIAM. (IN), 3. BUMP HEIGHT (IN) =?1.5,1.5,2.E-2
4. BUMP LENGTH (IN), 5. BUMP PITCH (IN), 6. BUMP THICK. (IN) =?1.4E-1,1.8E-1,4.E-3
7. TAPE THICK. (IN), 8. CLEARANCE (IN), 9. TEMP. (F) =?4.E-3,1.25E-3,1.E2
10. AMB. PRES. (PSI), 11. SPEED (RPM), 12. E/C =?1.47E1,4.5E4,5.E-1

∞

OUTPUT

LENGTH (IN) = 1.500000E+00 DIAM. (IN) = 1.500000E+00 BUMP HEIGHT (IN) = 2.000000E-02
BUMP LENGTH (IN) = 1.400000E-01 BUMP PITCH (IN) = 1.900000E-01 BUMP THICK. (IN) = 4.000000E-03
TAPE THICK. (IN) = 4.000000E-03 CLEARANCE (IN) = 1.250000E-03 TEMP. (F) = 1.000000E+02
AMB. PRES. (PSI) = 1.470000E+01 SPEED (RPM) = 4.500000E+04 E/C = 5.000000E-01
LOAD (LB) = 1.308849E+01 MIN. FILM THICK. (IN) = 1.028773E-03 ATT. ANG. (DEG) = 2.409605E+01
POWER (HP) = 2.624948E-02

Fig. II-3 Sample Input and Output for Journal Bearing
Computer Program (HYDRE)

III. TEST BEARINGS

SENSOR SYSTEM REFERENCE AIR BEARING

Three self-acting rigid surface bearing designs were considered for the initial checkout bearing of the rotating sensor system. For each of the three bearing designs considered, sufficient analytical and experimental data existed for use in comparing the program test data. The three bearing designs considered and their limitations were:

- Rigid Surface Plain Sleeve Bearing - This type bearing while simple to fabricate tends to operate in an unstable regime at high rotational speeds.
- Tilting Pad Bearing - Space available for the floating sleeve housing was limited, and a difficult mechanical design would be required to incorporate a tilting pad bearing. The high fabrication cost was another significant factor.
- Spiral Groove - The best high speed performance of this type bearing is achieved with the grooving on the shaft. If a spiral groove bearing was to be used, the grooving would have to be placed on the bearing. The high cost involved with grooving the bearing was a significant factor.

The rigid surface, plain sleeve bearing was selected as the initial sensor system check-out bearing. This selection was based on the following:

- The bearing could be conveniently adapted to fit in the same floating housing as the compliant test bearing.
- Reliable analytical work was available.
- Initial fabrication cost was low.

The analytical work of A.A. Raimondi [3] was selected for comparison with the experimental data. Raimondi's analysis was chosen since his numerical technique is believed to be the most accurate available for solving Reynold's Equation for a finite 360° gas journal bearing. In addition, his analysis has been shown to have good agreement with experimental data in the range of compressibility numbers anticipated in the testing. The bearing was designed to operate in a stable regime at speeds up to 15,000 rpm.

The bearing was fabricated of SAE 660 Bronze and installed in the floating sleeve housing with a light press fit prior to final machining of the bore. The bearing bore was lapped to a diameter of 38.1287 mm (1.5013 inches) and had a total out of roundness of 0.0015 mm (0.00006 inch). The radial bearing clearance with the film thickness measurement shaft was 0.0213 mm (0.00084 inch).

COMPLIANT SURFACE TEST BEARING

A single pad 360° arc design MTL Hydresil Journal Bearing, shown in Figure III-1, was selected as the compliant surface test bearing. Figure III-2 shows the basic mechanical design of the bearing. A single pad Hydresil was selected over the multiple pad design for the following reasons:

- Existing infinitely long bearing analysis programs are based on the 360° arc configuration.
- The single pad design has the minimum number of foil interruptions around the circumference resulting in simplified test data.
- Single pad bearings can be manufactured with greater accuracy and consistency.
- The single pad bearing has a greater load capacity for a given operating speed.
- The single pad Hydresil bearing is currently in use in the Chrysler/ERDA Automotive Gas Turbine.

Test bearings with two L/D ratios were designed using existing computer programs for infinite length bearings. The bearing design characteristics shown in Figure III-3 were as follows:

Smooth (top) Foil Thickness:	0.1016 mm (0.004 inch)
Bump Foil Thickness:	0.1016 mm (0.004 inch)
Bump Geometry:	
length	3.556 mm (0.140 inch)
pitch	4.572 mm (0.180 inch)
height	0.508 mm (0.020 inch)
type	partial arc

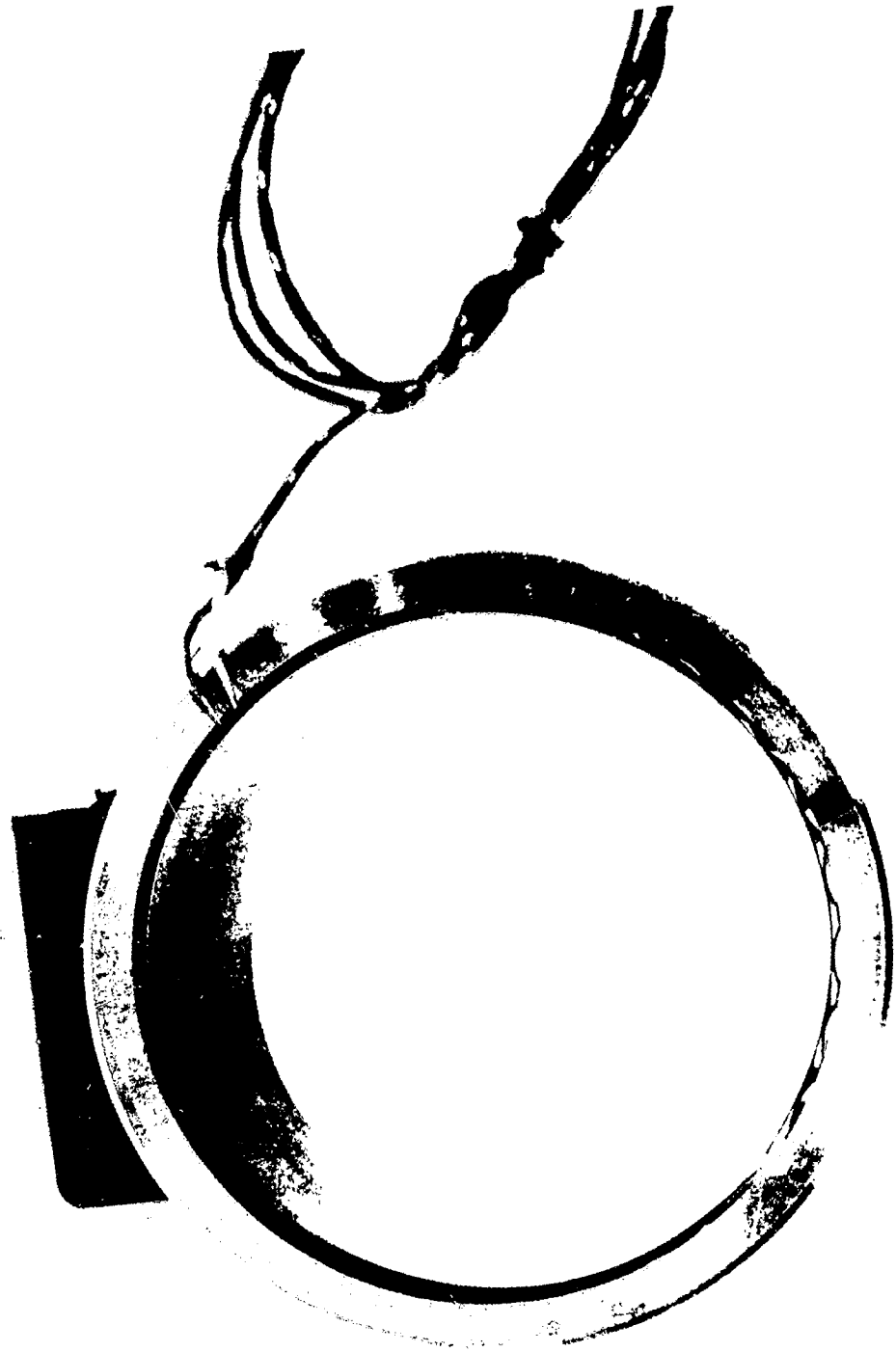


FIG. III-1 Hydresil Test Journal Bearing

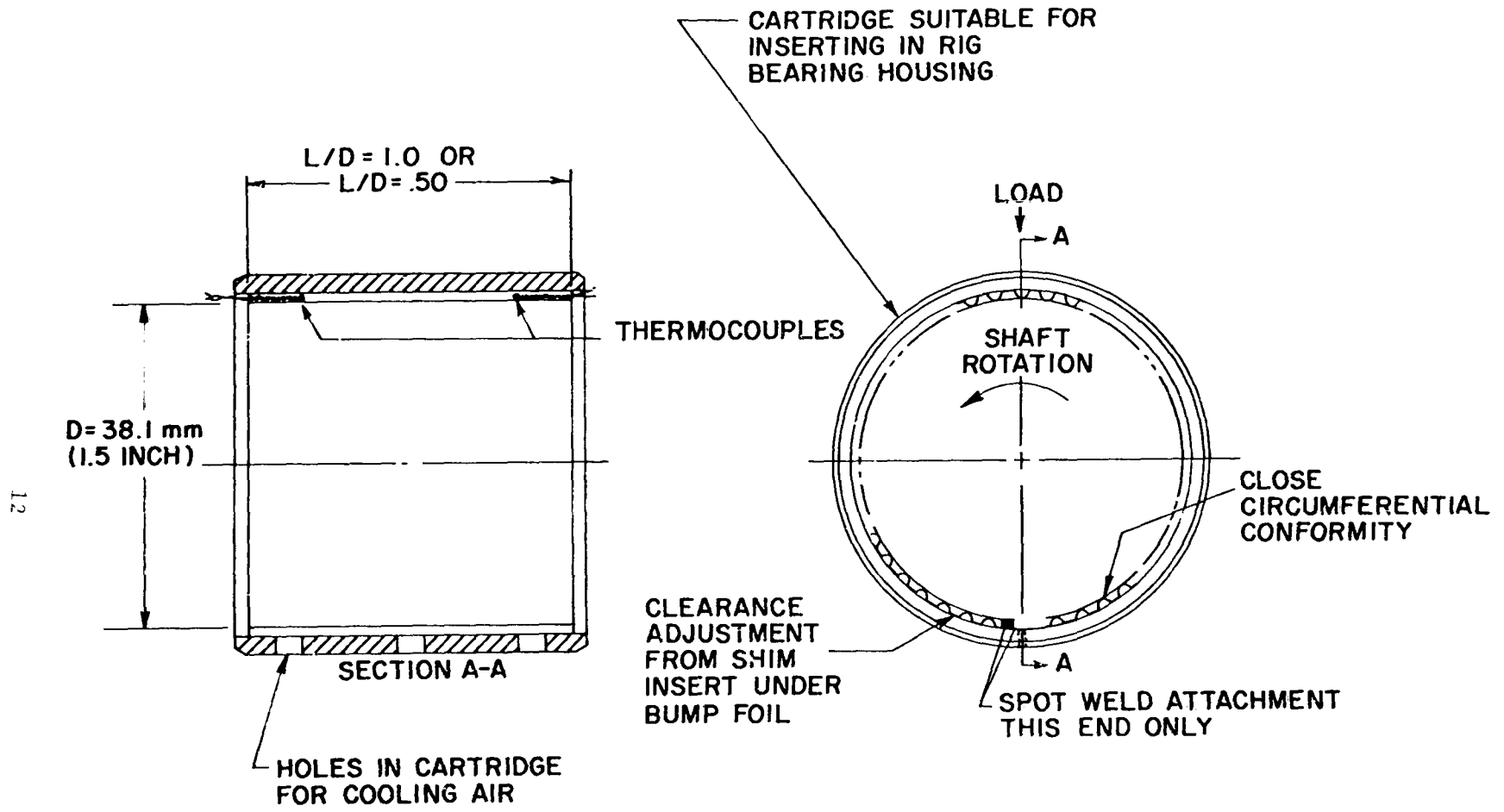
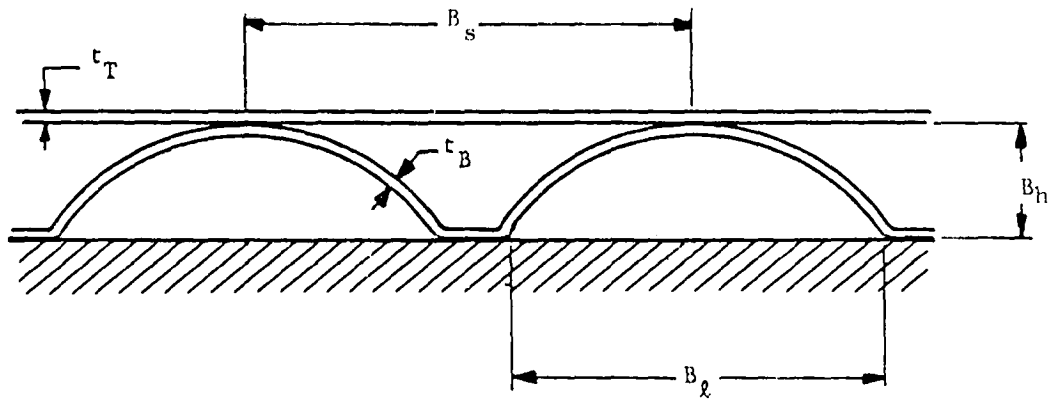


Fig. III-2 Mechanical Design of Test Journal Bearing



- B_h = Bump Height
- B_l = Bump Length
- B_s = Bump Pitch
- t_B = Bump Foil Thickness
- t_T = Top Foil Thickness

Fig. III-3 Compliant Bearing Design Details

Bearing Diameter :	38.1 mm (1.500 inch)
L/D Ratio :	1 and 1/2
Dry Film Lubricant (Hohman M-1284):	0.005-0.007 mm (0.0002 - 0.0003 inch)

The material used for both the smooth foil and bump foil was Inconel X-750. The material, obtained in the annealed condition, is aged before use at 705°C (1300°F) for 20 hours which results in the following mechanical properties at room temperature:

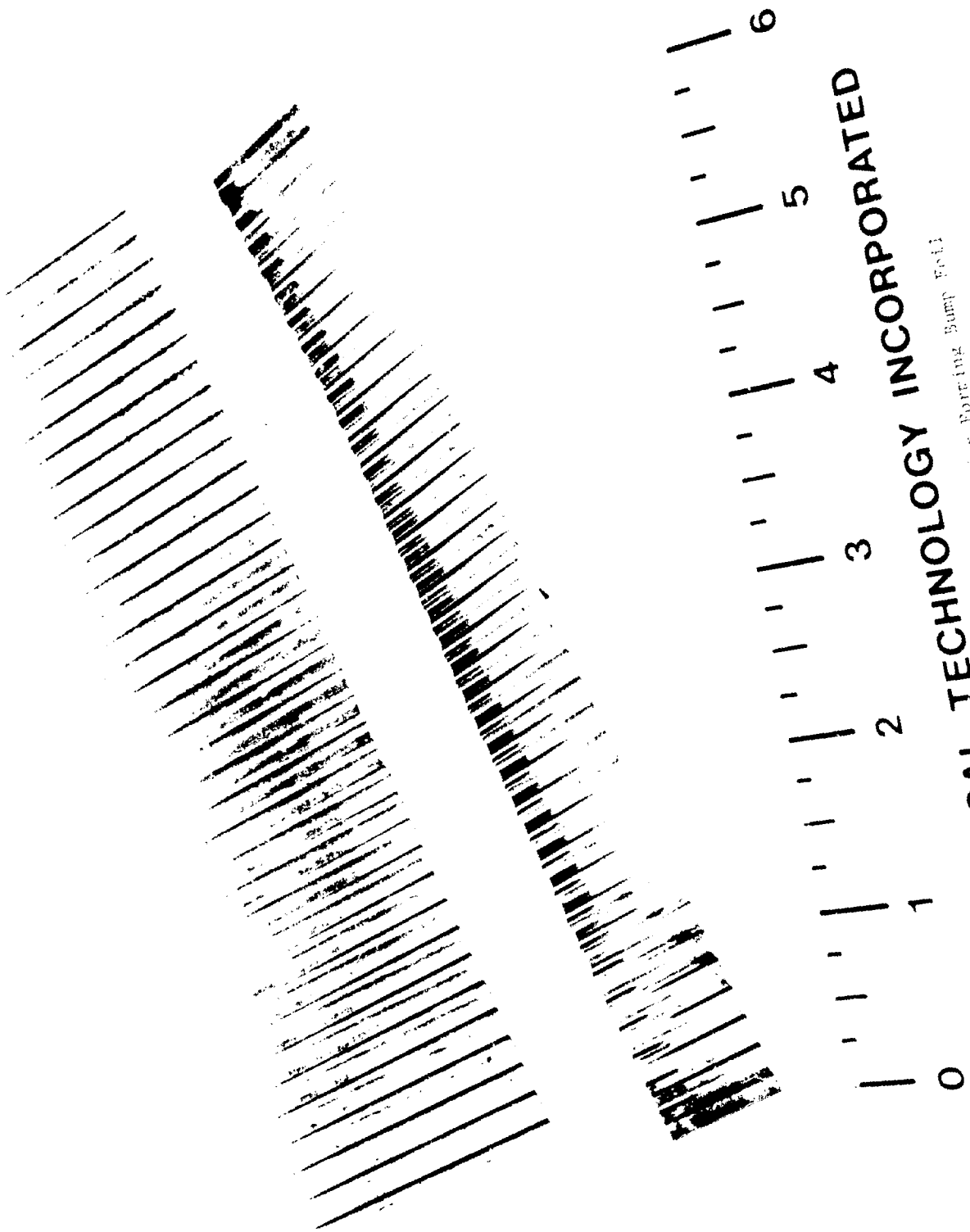
0.2% Yield Strength:	$6.55 \times 10^8 \text{ N/m}^2$ (95,000 psi)
Ultimate Tensile Strength:	$9.65 \times 10^8 \text{ N/m}^2$ (140,000 psi)
Endurance Limit (10^8 cycles).	$1.38 - 2.07 \times 10^8 \text{ N/m}^2$ (20-30,000 psi)

The bearing was mechanically designed to support a $2.07 \times 10^5 \text{ N/m}^2$ (30 psi) load. The maximum bump stress associated with this loading was one of the important factors in the bearing design and was calculated with the use of the computer program BUMSTR. Various factors such as foil thickness and bump geometry could be varied independently in the computer program to obtain a bump foil design in which the maximum bump stress would not exceed the 0.2% yield strength of the Inconel X-750. The maximum bump stress in the test bearing design, calculated at a load of $2.07 \times 10^5 \text{ N/m}^2$ (30 psi), was $6.09 \times 10^8 \text{ N/m}^2$ (88,358 psi).

The bump foils were formed on a precision steel die utilizing rubber pad forming techniques. The precision die and a formed foil are shown in Figure III-4. This method of forming enables an entire bump foil to be formed in one operation and provides the greatest bump uniformity and accuracy. The bump foils were formed with the material in the annealed condition.

Each bump foil used in a bearing was inspected prior to assembly into the test bearings. Two methods were used to inspect the parts. The bump geometry was checked using a comparator with a 10X magnification. This procedure allowed the bump pitch, length, arc radius, and height to be checked. In addition, the height of each bump was checked using the

REPRODUCIBILITY OF THE ORIGINAL PAGE IS POOR



MECHANICAL TECHNOLOGY INCORPORATED
FIG. III-4 Precision Die for Forming Bump Field

following procedure. The bump foil was placed on a surface plate with a parallel bar weighing approximately .9 kg (2 pounds) on top of it. An electronic dial indicator was then used to check the height of each bump. The total variation in bump heights was less than 0.0127 mm (0.0005 inch). Two thermocouples were attached to the bump foil as shown in Figure III-2. The thermocouples were formed by fusing the ends of 0.25 mm (0.010 inch) diameter iron-constantan thermocouple wire together to form the junction. The iron wire of the thermocouple was then spot welded to the bump foil. The leads were carefully brought out of the bearing in a manner to allow complete freedom of dynamic movement of the foil members.

The smooth foil was checked for thickness uniformity after heat treatment. Total variation in thickness was less than 0.0077 mm (0.0003 inch). The dry film lubricant was applied to the smooth foil after the heat treatment process by spraying. The coating was cured and then burnished to obtain the proper thickness.

Each foil was first formed to conform to the journal diameter then individually spot welded into the bearing cartridge. The bump and smooth foils are welded at only one end and are separated by a spacer block.

The internal bearing clearance of a finished bearing is determined by performing a load deflection test on the bearing. A schematic of the test apparatus used to perform this test is shown in Figure III-5. Figure III-6 is a plot of the test data obtained from the load deflection test. The internal clearance of the bearing is defined as the total motion of the bearing when a 0.9 kg (2 pound) load is applied first downward then upward. The bearing clearance is indicated on Figure III-6. The 0.9 kg (2 pound) load value used roughly corresponds to the static load on the bearing due to the weight of the bearing housing and load support mechanism. This value is also sufficient to seat the foils against each other and the bearing housing.

The internal clearance can be varied in a finished bearing assembly by inserting an adjustment shim between the bump foil and bearing cartridge bore as shown in Figure III-2.

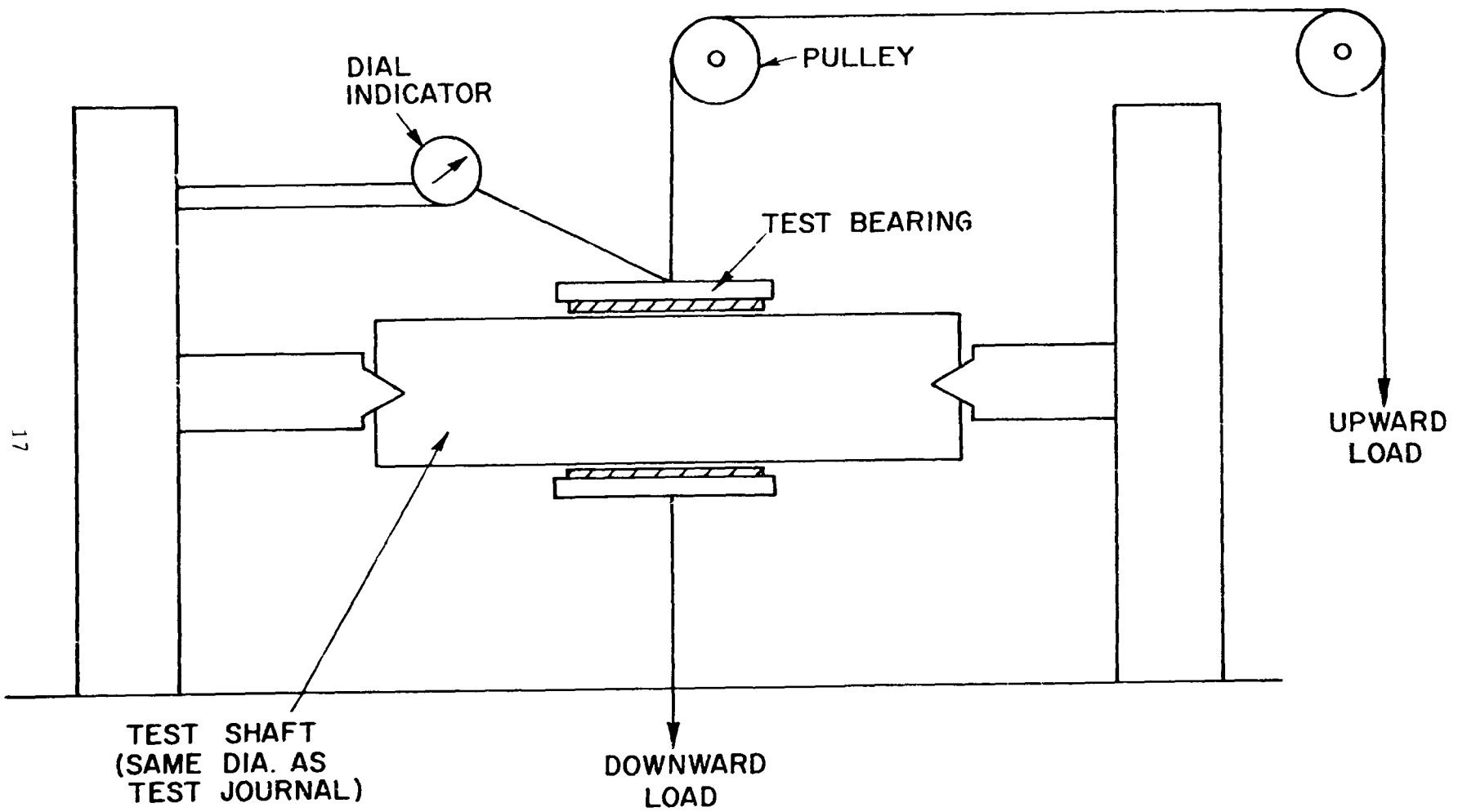


Fig. III-5 Schematic of Apparatus Used to Determine Bearing Clearance

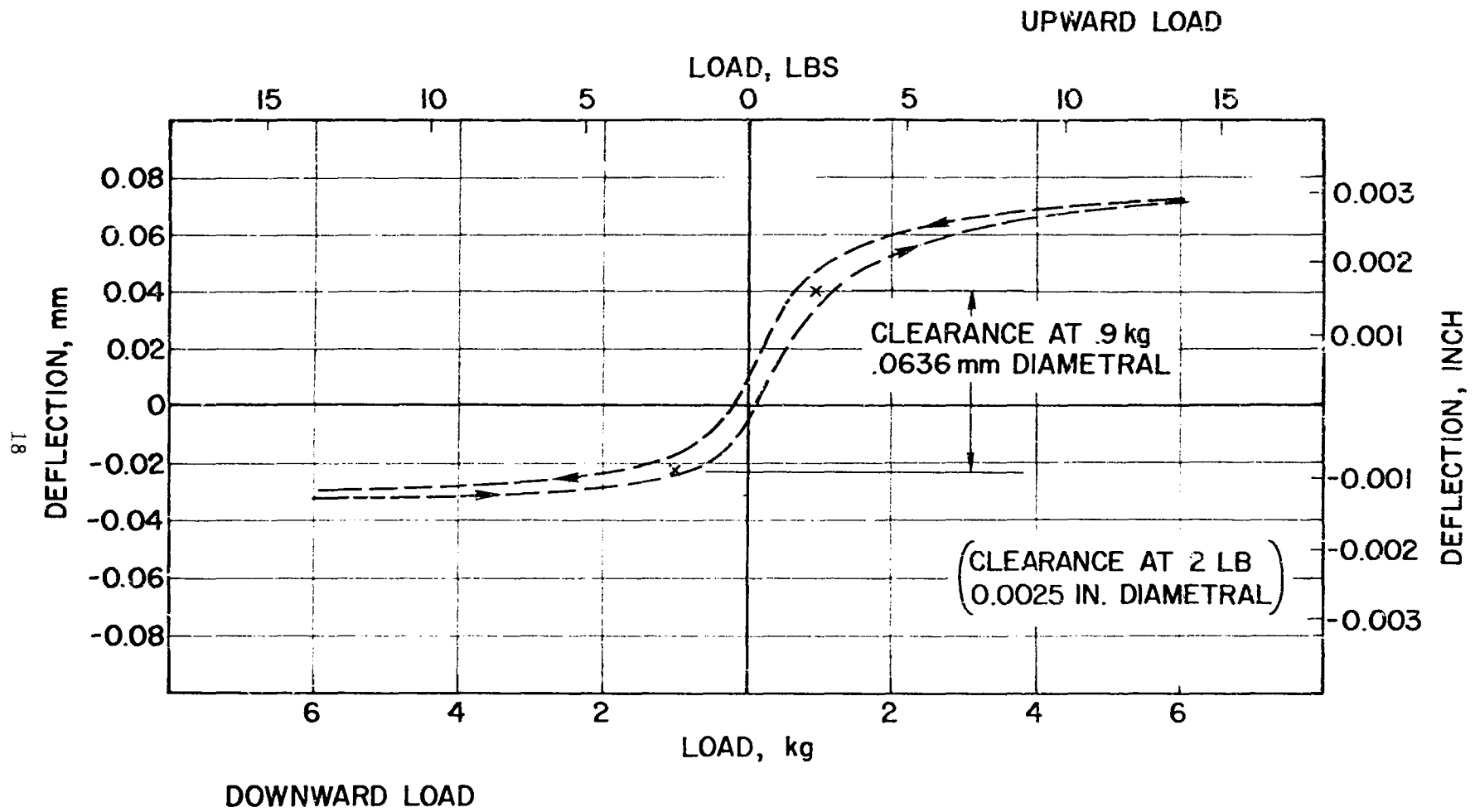


Fig. III-6 Example of Load Versus Deflection Plot for Determining Bearing Clearance

The bearing stiffness is determined from the slope of the curve of shaft motion versus bearing load which is generated from data obtained from the computer program output. Figure II-2 shows the plot for the program test bearing which had a stiffness of approximately $1.38 \times 10^8 \text{ N/m}^2$ (20,000 lb/inch). Bearing stiffness can be varied by changes to the bump foil design characteristics such as foil thickness and/or bump pitch. Since the majority of the bearing compliance in this design is due to a soft bump foil rather than the air film, the bearing stiffness will be quite sensitive to the mechanical characteristics of the bump foil and relatively insensitive to the air film characteristics.

IV. TEST FACILITY AND INSTRUMENTATION

TEST RIG DESCRIPTION

Drive Spindle Assembly

An existing MTL owned test rig was upgraded and modified to meet the specific requirements of this program. The test rig is shown in Figures IV-1 and IV-2. Figure IV-3 shows the test facility.

The air turbine driven high speed spindle was supported on two preloaded angular contact ball bearings. Both support bearings were standard class 7 bearings supplied by the Barden Company. The bearing at the test end was a 107H (35 mm bore), and at the drive turbine end a 105H (25 mm bore). Both bearings contained bronze retainers.

Oil for lubricating and cooling the support ball bearings was supplied through two oil jets 180° apart at each bearing. The jets were sized to produce a jet velocity of approximately 20 m/sec (65 ft/sec) at $4.4 \times 10^5 \text{ N/m}^2$ (64 psig) supply pressure with 2.27 kg/min (5 lb/min) total oil flow. A water cooled heat exchanger in the oil supply loop removed heat from the oil.

A double labyrinth seal with pressurized air supplied between the seals prevented the oil from traveling down the test shaft into the test bearing area.

During the high temperature tests, eight 500 watt quartz heaters were used to heat the test bearing. A 10 mm (.250 inch) thick Mycalex 500 disk acted as an insulator between the quartz heater box and support housing. A water jacket in the support housing assisted in removing heat from the support ball bearings.

The drive air supply was provided by a three stage centrifugal air compressor having the following maximum output characteristics:

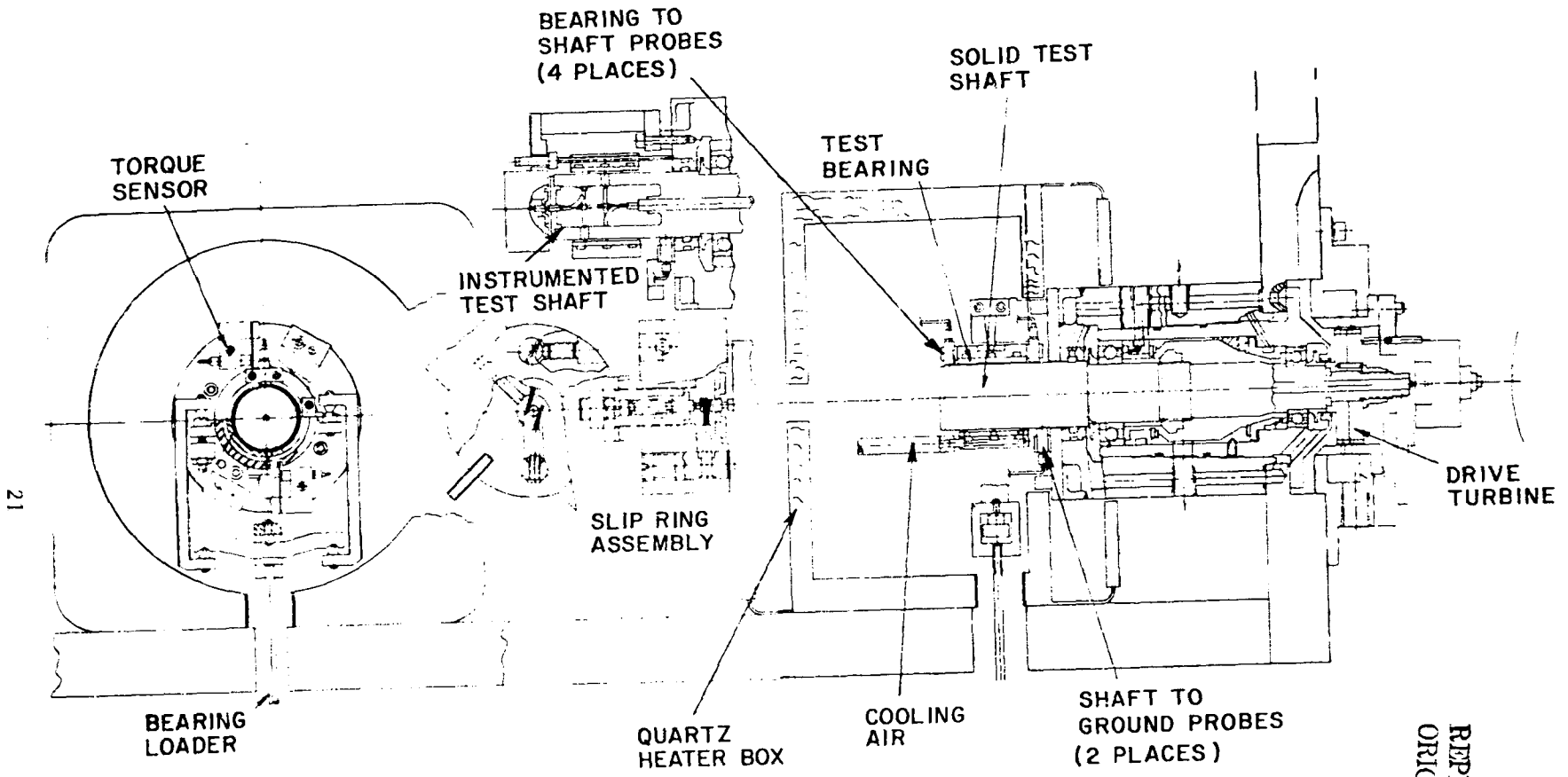
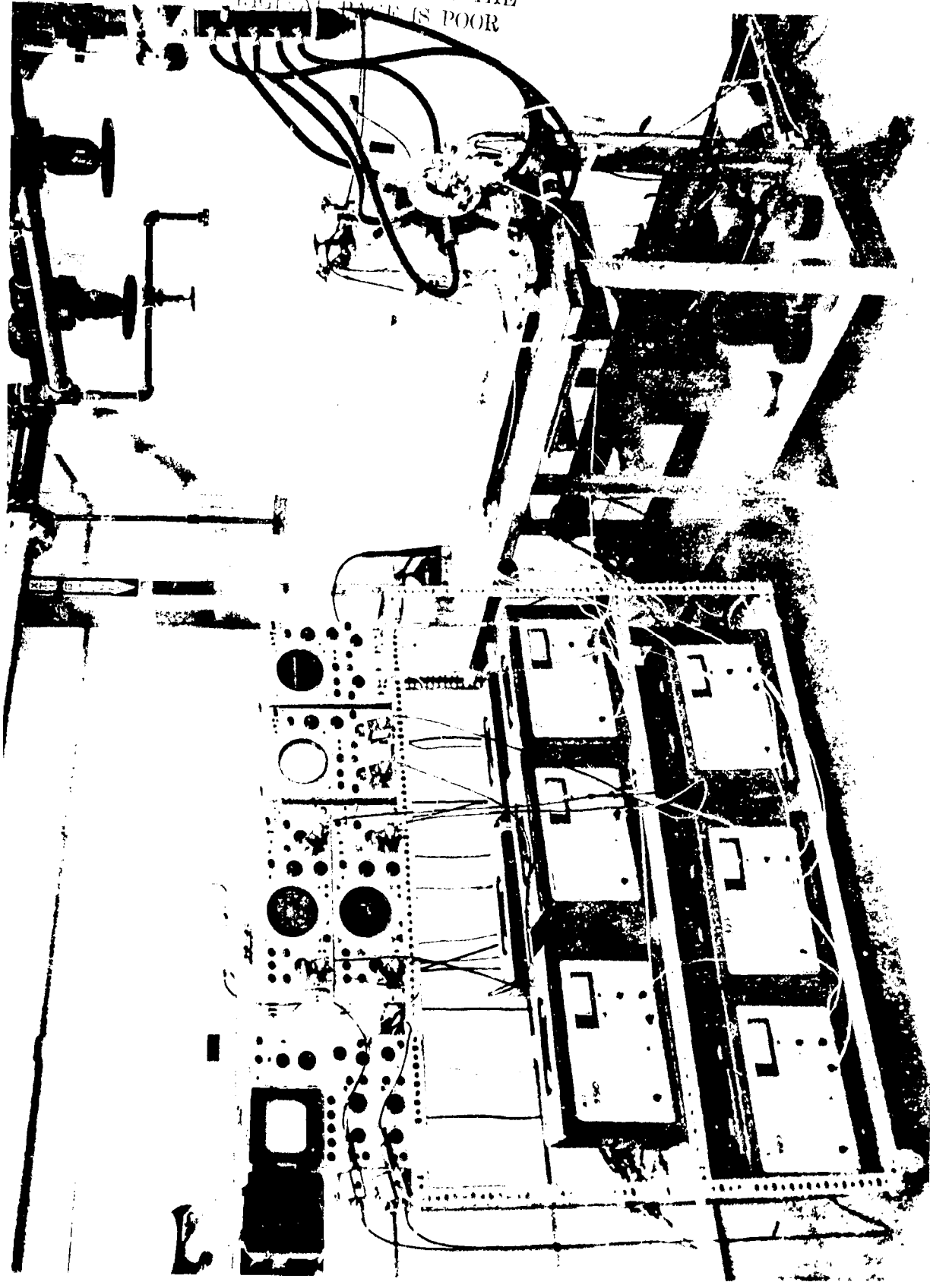


Fig. IV-1 Journal Bearing Test Rig

REPRODUCIBILITY OF THE ORIGINAL PAGE IS POOR



REPRODUCIBILITY OF THE
ORIGINAL PAGE IS POOR



Pressure:	$6.89 \times 10^5 \text{ N/m}^2$ (100 psig)
Flow:	22.66 m ³ /min (800 scfm)
Temperature:	93.3°C (200°F)

A fixed test speed could be accurately maintained utilizing this compressor because of its constant pressure output characteristics.

Rotor balancing was performed on a conventional low speed two plane "Dynamic Balancer", Model MU-6, manufactured by Micro-Balancing, Inc. Each test shaft was first balanced as a detail while supported on teflon vee-blocks. The rotor was then completely assembled, installed in the ball bearing cartridge, and balanced on its own support bearings at 1750 rpm. Residual unbalance levels were 0.018 gm.cm (0.000250 oz.in.) in each of two planes. The test rig design allowed for the rotor assembly to be installed into the support housing without disrupting the assembly after balancing.

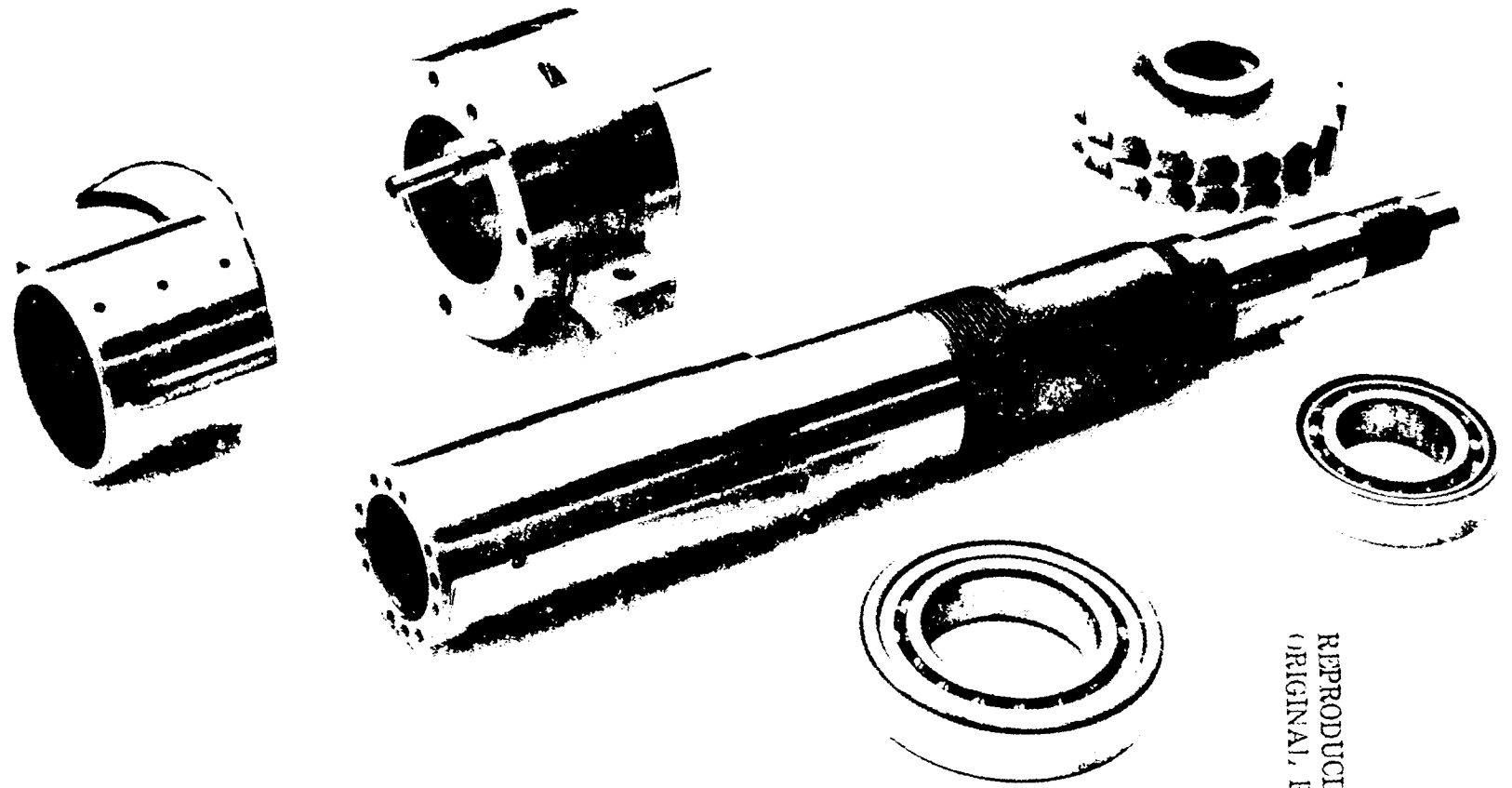
In addition, the test rig contained provisions to allow MTI CommandTM multiplane multispeed balancing to be performed if required.

Test Journals

The foil test journal was an integral part of the test shaft and was overhung to facilitate access to the test bearing and rotating sensors. Three test shafts were fabricated for the program: two to be instrumented with the rotating sensor system (the rotating sensor system is discussed in Section V) and one for high temperature testing. The test journal surfaces on the two shafts that were to be instrumented were initially left uncoated and relatively soft to enable modifications to be made if required during installation of the rotating sensor system. The journal surface on the shaft used for pressure measurements was later coated with a thin hard chromium alloy by the Electroplating Company. The test journal surface on the third shaft, which was to be used for the high temperature testing, was coated with a plasma sprayed chrome carbide coating. A test shaft with support bearings and drive turbine is shown in Figure IV-4.

Test Bearings

The test bearings, which have been previously discussed in Section III, were mounted with a light press fit in a floating bearing housing.



REPRODUCIBILITY OF THE
ORIGINAL, PAGE IS POOR

Fig. IV-- Test Shaft with Support Ball Bearings, Drive Turbine and Test Bearing

Loading of the test bearing was accomplished by applying dead weight through a knife edge loading parallelogram mounted on the floating bearing housing. A lead screw, which was threaded into the floating housing, allowed the axial position of the test bearing to be varied relative to the rotating sensors installed in the shaft, for obtaining an axial film thickness profile.

Dry filtered cooling air was supplied to the test bearing through three (3) 2.29 mm (.09 inch) diameter holes located at the gap in the smooth foil. The bearing cooling air line was connected to the floating housing through a flexible connection to avoid introducing a moment load to the bearing. During the high temperature tests, two (2) PureFlow air heaters were used to heat the test bearing cooling air.

QUALITY ASSURANCE

All components used in this test program underwent a quality assurance check to insure conformity with the applicable drawings. Specific items checked and recorded include: the physical and chemical characteristics of raw material; heat treatment procedures; and dimensions, tolerances, and finishes. During assembly of the spindle, particular care was taken to insure that the static runout of the test journal was at the lowest level possible. Runout checks and residual unbalance level of each assembly were recorded.

MEASUREMENTS AND INSTRUMENTATION

The success of this program was dependent upon obtaining high quality test data utilizing both routine and sophisticated measurement methods. The film measurement systems are discussed in detail in Section V of this report.

Rotor Speed

Rotational speed was measured by an MTI Fotonic SensorTM fibre optic probe which responds to the once per revolution passing of a dark band painted on the face of the drive turbine. A Monsanto digital frequency counter Model #103A measured the output of the Fotonic Sensor speed pickup and provided a continuous digital display of rotor speed.

Shaft and Test Bearing Motion

Radial motions were measured using capacitance type displacement probes. Two sets of X-Y probes were mounted on the floating bearing housing to measure test bearing to shaft motion and one set was mounted on the support housing to monitor shaft to ground motion. Wayne-Kerr DM100 Distant Meters were used as signal conditioners for the capacitance probes. The output of each horizontal-vertical pair of probes was displayed on a cathode-ray oscilloscope. Tektronix Model 503 Oscilloscopes were used and provided a continuous orbital motion display at each of the three probe locations.

Special high temperature capacitance probes rated to 537°C (1000°F) were used during the high temperature testing. The sensitivity of both the standard and high temperature probes were 100 millivolts/.0254 mm (100 millivolts/.001 inch).

Test Bearing Load

Test bearing loading was accomplished by applying calibrated commercial dead weights to the test bearing floating housing. A knife edge parallelogram mechanism was used to minimize introducing a moment into the bearing.

Test Temperatures

Temperatures were measured by using thermocouples mounted at the following locations.

- Two on Test Bearing Bump Foil (see Figure III-2)
- *Ambient Chamber
- *Floating Housing
- Cooling Air at Bearing Inlet
- Cooling Air at Flow Meter
- Support Bearing Oil Inlet and Outlet

The two thermocouples located on the test bearing were Type J, Iron-Constantan. One of these thermocouples was displayed on an X-Y plotter, Houston Omni-plotter Model 2000, against a time base, and the second used a Technique Associates Model 93 Potentiometer as the readout device. The remaining

* During testing at 315°C (600°F) only.

thermocouples were Type K, Chromel-Alumel, and were recorded on a Honeywell multipoint chart recorder.

Test Bearing Cooling Air

A standard Fisher-Porter flowmeter was used to measure the total cooling air flow entering the test bearing. The flowmeter is calibrated by the manufacturer at 1 atmosphere (14.7 psia) and 20°C (68°F). A correction factor is applied to the reading based on the actual air pressure and temperature at the flowmeter.

Bearing Frictional Power Loss

The mechanical arrangement selected for the frictional torque measurement and dead weight loading of the bearing is shown in Figure IV-1. The floating housing is restrained from rotation by two flexures in the vertical plane through the bearing centerline. Bearing friction torque which causes deflection of the flexures is measured with two capacitance probes and read with a digital voltmeter. Two flexures at positions 180° apart were used to reduce the effect of lateral (horizontal) motion of the floating bearing housing on the torque measurement. The range of the displacement probes used in the torque sensing system was 0.254 mm (0.010 inch).

Data Acquisition Equipment Calibration

All equipment used for the acquisition of test data was calibrated at the start of the test program. The equipment ~~is periodically checked~~ to insure its accuracy, stability, and repeatability at intervals recommended by the equipment's manufacturer. The following is a discussion of the calibration procedures used:

- Film Thickness and Pressure Sensors - The calibration procedures used for these special sensors is discussed in Section V.
- Capacitance Displacement Probes - All standard and high temperature capacitance probes were calibrated in a standard micrometer test stand. Total accuracy of the probe and capacitance meter system is rated at 0.00254 mm (0.0001 inch).
- Bearing Torque - The capacitance probes used in the torque measuring system were first calibrated using the method just described then

installed in the test rig. Each flexure was calibrated individually by attaching a light steel wire to the flexure in the loading area. The wire was then guided horizontally to and over a pulley on ball bearings to where the wire could be dropped vertically. Weights were then hung from the wire and the probe output recorded. A calibration curve for each flexure was generated. This calibration was valid only for the room temperature tests.

- Cooling Air Flow - The calibration supplied by the manufacturer of the flow meter was used. The correction curves used for correcting air flow based on actual air temperature and pressure at the flow meter were also supplied by the manufacturer.
- Capacitance Meters - The Wayne-Kerr capacitance meters are checked at 6 month intervals with a standard capacitor, referenced to the National Bureau of Standards, for linearity and sensitivity.
- Oscilloscopes - Oscilloscopes are checked at 6 month intervals for voltage and time base accuracy. Accuracy of voltage was $\pm 2\%$ of range and time base $\pm 3\%$ of range.
- Voltage Calibration - A voltmeter referenced to the National Bureau of Standards is maintained for the purpose of calibration of meters and oscilloscopes. Accuracy of voltmeters used in the test program was $\pm 0.05\%$ of range ± 1 digit.
- Thermocouple Readout - Potentiometers are calibrated using a referenced millivolt meter and are then used to calibrate the multi-point chart recorders. Accuracy of the potentiometers used was $\pm 0.2\%$ of range and the chart recorder was $\pm 2.2^{\circ}\text{C}$ (4°F).

V. FILM MEASUREMENT TECHNIQUE

INTRODUCTION

A number of sensor measurement systems* were considered for use in obtaining direct film measurements in the compliant surface bearing and are discussed later in this section. The capacitance system which was selected utilized a unique adaptation of the standard proximity probe modified to be conveniently mounted in a rotating journal and a brush and slip ring assembly for obtaining the electrical signal from the rotating shaft. The film thickness sensor consisted of a 3.25 mm (0.128 inch) diameter probe that continuously measured the distance between the probe tip and the smooth foil of the test bearing.

The pressure sensor consisted of a diaphragm supported by a flanged tube which covered a 2.083 mm (0.082 inch) diameter probe. This sensor continuously measured the distance between the probe tip and the diaphragm, sensing diaphragm deflections caused by pressure variations in the film. The probes are shown in Figure V-1.

Two shafts were instrumented each containing two similar type probes. The sensors were designed to be mechanically stable at 60,000 RPM at which point the center electrode was subjected to approximately 60,000 "g's", and to operate in a temperature range of 24°C - 55°C (75°F to 130°F). Figure V-2 shows the rotating sensor system and slip ring assembly.

SELECTION OF ROTATING CAPACITANCE SYSTEM

Two locations for the placement of the sensors were considered; a rotating sensor in the journal or an embedded stationary sensor in the foil bearing assembly. The rotating sensor arrangement was selected for the following reasons:

- Obtains a complete film trace around the bearing.
- Does not affect the local stiffness, damping, or mass characteristics of the foil.
- One sensor can scan several axial positions by moving the bearing axially along the journal.

* In this report, "sensor" refers to the entire rotating system and "probe" refers to the actual capacitance proximity probe which is only a part of the rotating system.



FILM THICKNESS
PROBE

PRESSURE PROBE



ASSEMBLY



PROBE



PRESSURE DIAPHRAGM

REPRODUCIBILITY OF THE
ORIGINAL PAGE IS POOR.

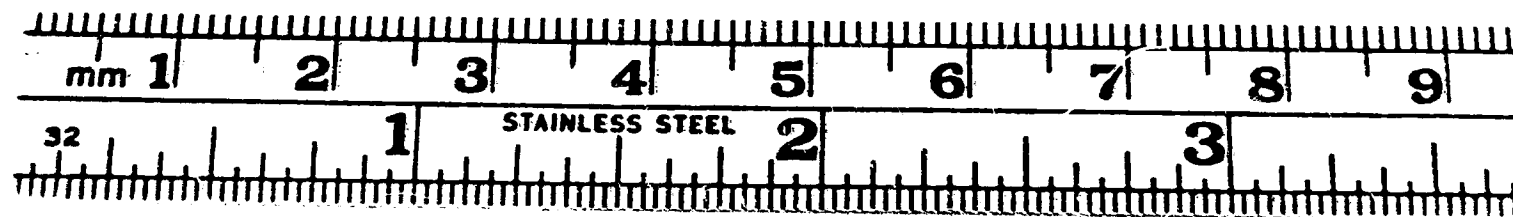


Fig. V-1 Film Measurement Probes

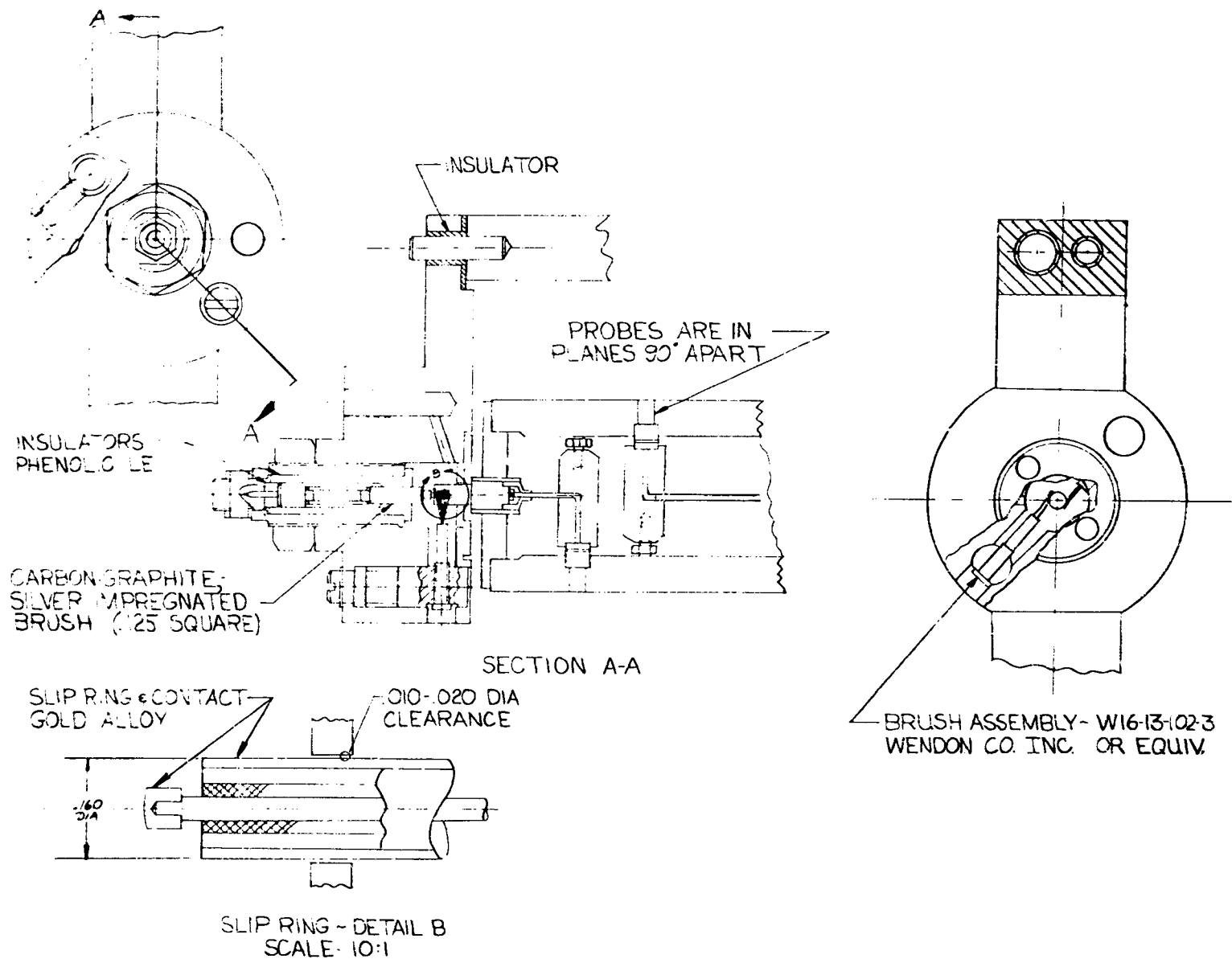


Fig. V-2 Rotating Sensors and Slip Ring Assembly

Three types of sensor systems were examined for use in this application.

- Wayne-Kerr capacitance proximity system.
- Fotonic sensor fiber optic proximity system
- Inductive sensor with ferrite core

A comparative study of the characteristics of each type of system and consideration of methods for obtaining the signal from the rotating shaft led to the selection of a capacitance proximity system with a metal-fiber brush slip ring. Reasons for this selection included:

- Capacitance systems meet the accuracy requirements with the lowest overall noise to signal ratio.
- Capacitance systems have the best resolution.
- The foil surface condition will have the minimum influence on the accuracy of the clearance measurements.
- The capacitance system assembly can be designed to prevent mechanical shifting of the probe in the high "g" operating environment.
- A capacitance system is the least difficult to calibrate from a linearity stand point.
- The same type of probe can be used for both film thickness and pressure measurements.
- The fundamental slip ring design and manufacturing problems have been solved in similar commercial applications.

The selection of the capacitance sensor and the metal-fiber brush slip ring proved to be an excellent choice since the film thickness measurement system was proven during the testing phase of this program to be accurate, reliable, and extremely durable.

Appendices A and B contain a detailed discussion of the procedures used to fabricate the rotating sensor system and the brush and slip ring assembly.

CALIBRATION OF SENSORS

Final calibration of the sensors was performed after installation into the test shaft. The calibration was repeated while the test shaft was installed

In the test rig and after the test shaft had been rotated to full speed. During the final calibration, the electrical signal from the sensors was obtained through the brush and slip ring assembly. The Wayne-Kerr, electrical leads, oscilloscope, and digital voltmeter used for the final calibration were the same components used during data acquisition. Sufficient calibration trials were performed on each sensor to assure repeatability. In addition, periodically throughout the test program calibration checks were performed on the sensors.

A target, machined to conform to the test shaft radius, was mounted to a micrometer head, which had been installed in a modified vee-block. The micrometer used was graduated in 0.00254 mm (0.0001 inch) increments. The test shaft was then clamped in the vee-block with the target over a probe. The micrometer was moved in increments of 0.0127 mm (0.0005 inch) and the output voltage from the sensor recorded. Figure V-3 shows the calibration curve for the film thickness sensors used. Both sensors were highly linear over the intended range and showed no change throughout the test program.

The overall error in the system is estimated to be at a maximum $\begin{matrix} +10 \\ -5 \end{matrix}$ millivolts. With the 0.0127 mm (0.005 inch) range probe used this error equates to $\begin{matrix} +1.27 \\ -0.635 \end{matrix} \mu\cdot m$ ($\begin{matrix} +50 \\ -25 \end{matrix} \mu\cdot in.$) and consists of the following:

- Noise level of Wayne-Kerr DM-100;
 ± 1 mv or $\pm 0.127 \mu\cdot m$ ($\pm 5 \mu\cdot in.$).
- Error in dc voltage peak detector;
 $\begin{matrix} +5 \\ -0 \end{matrix}$ mv or $\begin{matrix} +0.635 \\ -0 \end{matrix} \mu\cdot m$ ($\begin{matrix} +25 \\ -0 \end{matrix} \mu\cdot in.$).
- Error in voltmeter; ± 2 mv or $\pm 0.253 \mu\cdot m$ ($\pm 10 \mu\cdot in.$).
- Error in basic gap calibration: ± 2 mv or $\pm 0.254 \mu\cdot m$ ($\pm 10 \mu\cdot in.$).

Since each probe was recessed approximately 0.038 mm (0.0015 inch) below the journal surface, a zero correction voltage had to be obtained to compensate for the recess. The correction voltage was obtained by two similar

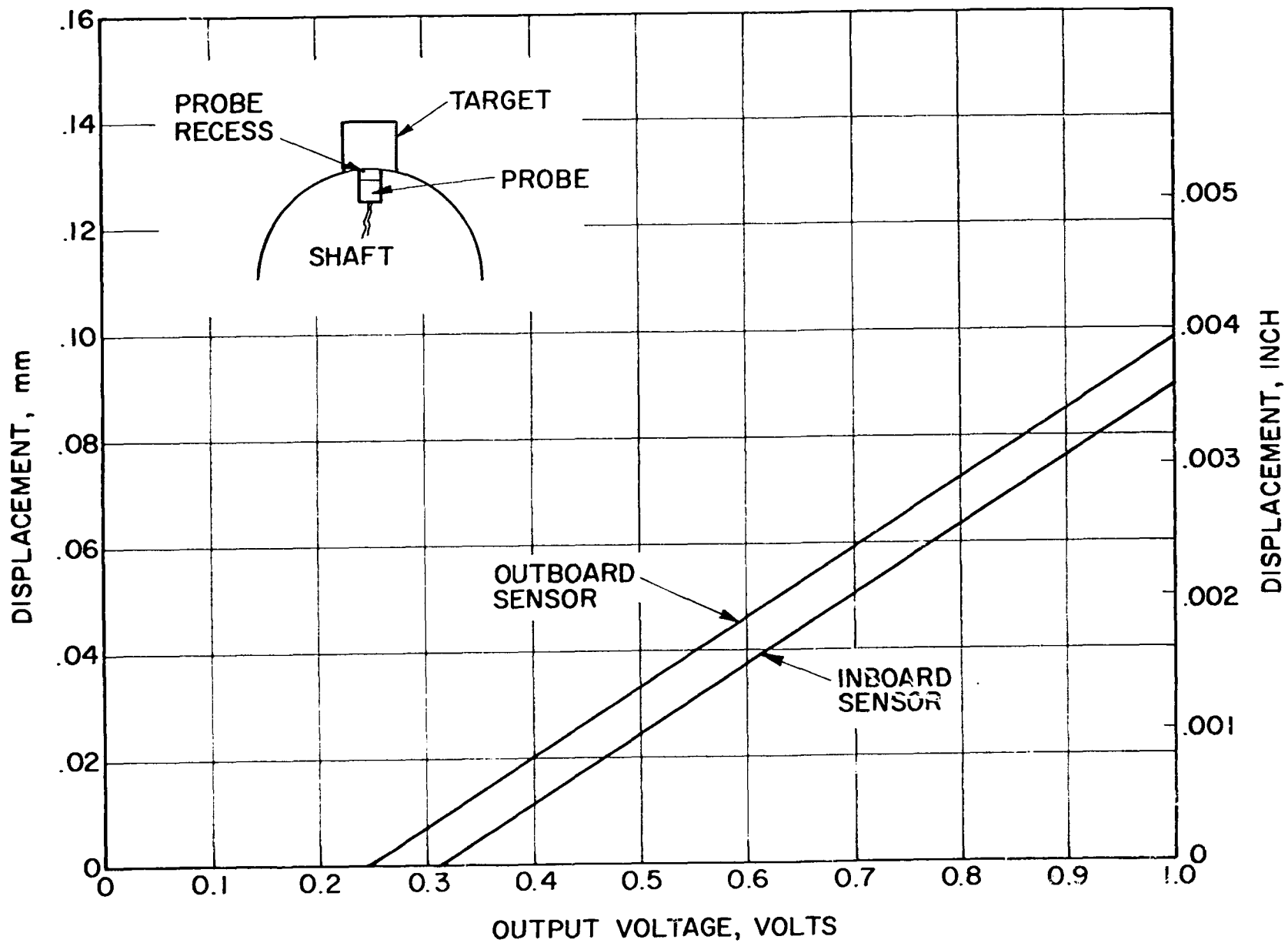


Fig. V-3 Calibration Curve for Film Thickness Sensors

methods. The shaft was locked from rotation in the test rig with one probe located at top dead center. The rigid surface journal bearing, which was 0.0426 mm (0.00168 in.) larger in diameter than the test journal, was installed on the test journal. A downward load was applied to the rigid surface bearing through the parallelogram loading mechanism and the output voltage from the sensor recorded. A point was reached after a relatively light load had been applied to the bearing after which an increasing load would not change the output voltage from the sensor. The procedure was repeated for the second sensor. The minimum output voltage recorded for each sensor represented the recess of the probe and was used as the zero correction voltage for film thickness tests conducted with the rigid surface journal bearing.

The second method used was for obtaining the zero correction voltage for testing with the compliant surface journal bearing. The shaft was again locked from rotation in the test rig with one probe at top dead center. An inconel smooth foil and bump foil identical to the ones used in the compliant journal bearing were placed on the test journal over the probe. A rubber pad and another smooth foil from which a hanger was attached was then placed over the journal to give the arrangement shown in Figure V-4. Weight was added to the hanger and the output voltage from the sensor recorded. Again a point was reached after which an increasing load would not change the output voltage. The procedure was repeated for the second sensor. The minimum output voltage recorded for each sensor was used as the zero correction voltage for testing with the compliant surface bearing.

The difference in the zero correction voltage obtained by the two methods was approximately 3.5% of full scale (F.S. = .127mm).

FILM MEASUREMENT DATA ACQUISITION

The electrical signals from the rotating sensors were conditioned by Wayne-Kerr DM-100 displacement meters which have a frequency response of 10 Kc/s. Each meter was connected to two readout devices: a dual beam Tektronics Oscilloscope and a digital dc voltmeter. The signal to the dc meter was first conditioned by a dc voltage peak detector.

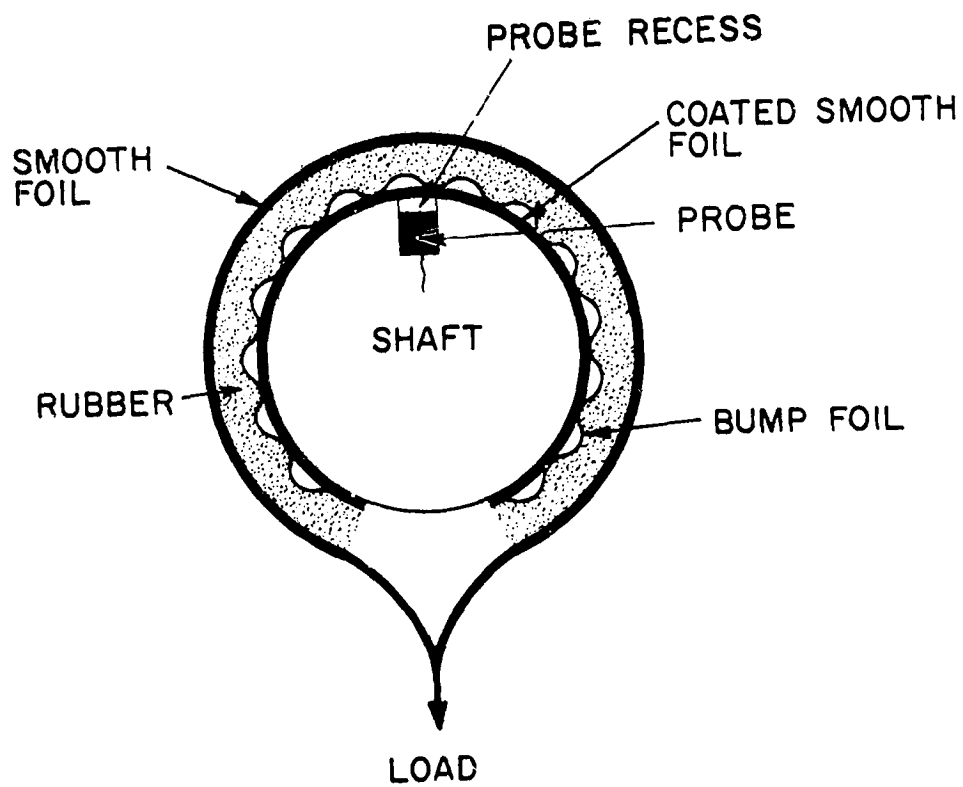


Fig. V-4 Schematic of Set Up for Obtaining Zero Correction Voltage for Compliant Surface Bearing

The oscilloscope was used to obtain the complete film profile around the test bearing. Prior to the start of each test, the dc trace from each sensor was positioned on the oscilloscope to correspond with the bottom horizontal grid line. Sufficient load was applied to the test bearing while the trace was being positioned to ensure contact between the bearing and the shaft over the probe. The bottom grid line then represented zero film and displacement of the dc level above the bottom grid represented the film thickness in the bearing. A detailed explanation of a typical film thickness trace is contained in Section VII.

In addition to the minimum film thickness being obtained from the oscilloscope trace, it was also obtained utilizing a dc voltage peak detector and digital voltmeter. The same signal that went to the oscilloscope was also fed to the peak detector. This peak detector, which was fabricated for the program, detected the minimum dc voltage level in the signal and displayed the dc level on a digital voltmeter. This dc voltage level represented the minimum distance from the probe tip to the bearing surface. The zero correction voltage, obtained during the sensor calibration described previously, was then subtracted from the meter reading and the resulting dc voltage level represented the minimum film thickness.

This method provided a quick and extremely accurate method of obtaining the minimum film thickness, and complemented the oscilloscope trace which provided the actual film profile around the complete foil bearing.

VI. TEST PROGRAM

The test program was designed to obtain precise experimental data of the hydrodynamic film characteristics of a compliant surface journal bearing and to evaluate bearing performance at high bearing temperatures. Specific test objectives included:

- Film thickness measurements
- Pressure profile measurements
- Bearing cooling air requirements at 315°C (600°F)
- Effects of 315°C (600°F) ambient and bearing temperatures on bearing performance.

Two bearing L/D ratios were tested to allow comparative data to be obtained for use in determining effects of L/D ratio on bearing performance (end leakage effects). Since the existing analyses are based on infinite length theory, it would have been desirable to test a bearing with an L/D of 2 or 3 which would closely approximate infinite length behavior and then use the data to directly validate the theory and correct it if necessary. However, a bearing of this configuration would be speed and load limited with the overhung journal arrangement. A compromise was accepted at the start of the program in favor of a high speed high load test rig using test bearings with L/D ratios of 1 and 1/2.

FILM THICKNESS TESTS

During the first series of tests, the rotor assembly was built utilizing the test shaft containing the film thickness sensors. Direct film thickness measurement tests were first conducted with a plain sleeve rigid surface air bearing. Use of the rigid surface bearing allowed a direct comparison between experimental data and existing analytical work. Since the analysis for a simple rigid surface gas bearing under the conditions of interest can be considered very reliable, close agreement between theory and test data at this point provided a check-out of the overall film thickness measuring apparatus. Testing with the rigid surface bearing was performed at three (3) speeds and varying loads. Only one bearing clearance was tested.

The 38.1 mm (1.5 inch) diameter Hydresil compliant surface bearing described in Section III was then installed in the test rig and operated at the test conditions listed below:

Test Bearing Configuration	Test Speed RPM	Test Load N
L/D = 1	30,000	8N to maximum load
C = 0.057 mm	45,000	↓
(C = 0.00225 in)	60,000	
L/D = 1	30,000	8N to maximum load
C = 0.0318 mm	45,000	↓
(C = 0.00125 in)	55,000	
L/D = 1/2	30,000	8N to maximum load
C = 0.057 mm	45,000	↓
(C = 0.00225 in)	55,000	
L/D = 1/2	30,000	8N to maximum load
C = 0.0318 mm	45,000	↓
(C = 0.00125 in)	55,000	

Initially, a bearing with an L/D = 1 was tested. The bearing clearance was held constant while the rotational speed and load were independently varied. Film thickness test data as a function of load was obtained at primarily three (3) speeds: 30,000 RPM; 45,000 RPM; and 60,000 RPM. The clearance in the bearing was changed by the insertion of a shim into the test bearing and the testing repeated. The test bearing was then replaced with another 38.1 mm (1.5 inch) diameter Hydresil bearing with an L/D = 1/2. The entire test sequence was repeated.

FILM PRESSURE TESTS

Following completion of the film thickness measurement tests, the rotor was disassembled and rebuilt utilizing the test shaft containing the film pressure sensors. It was anticipated that the same sequence of tests conducted for the film thickness measurements would be repeated for the film pressure measurements. However, during initial testing with the rigid surface bearing there were significant differences between the predicted analytical

pressures and the pressures being obtained using the rotating pressure sensors. The maximum test pressure from the pressure sensors was below the unit loading of the bearing. A static pressure probe, 0.33 mm (0.013 inch) in diameter, was installed in the rigid bearing under the load to obtain pressure data at one location for comparison with the data being obtained from the rotating sensors. Pressure data obtained from the static probe confirmed that the rotating sensors were not functioning properly and were providing pressure data below the actual values.

The pressure value discrepancy was determined to be caused by the dead air volume created by the recess of the sensor in the shaft. Although the recess of the sensor is only 0.0381 mm (0.0015 inch) below the shaft surface, it is large compared to the film thickness. The air from the hydrodynamic film over the sensor must expand to fill the recess, resulting in a local low pressure area which the pressure sensor measured.

Several attempts to fill the recess were tried, but no solution was found that would allow meaningful data to be obtained. An alternate sensor system considered was a solid non-deflecting sensor, such as a quartz crystal mounted flush with the journal surface. However, because of program limitations this concept was not tested.

HIGH TEMPERATURE TESTS

The final series of tests were conducted at elevated ambient and bearing temperatures using a solid non-instrumented shaft with a hard chrome carbide journal surface. Testing was conducted on the 38.1 mm (1.5 inch) diameter Hydresil bearing with an L/D = 1 and a bearing clearance of 0.0318 mm (0.00125 inch). During these tests the ambient and bearing temperatures were maintained constant at 315°C (600°F) throughout each test. Cooling air at 205°C (400°F) was supplied to the test bearing. Test speed and load were varied independently and the quantity of cooling air required to maintain the constant 315°C (600°F) bearing temperature was determined. It was also the objective of this series of tests to determine the effect of possible thermal distortions, which may occur at the elevated ambient and bearing temperatures, on bearing load performance.

Results of the test program are given in Section VII.

VII. TEST RESULTS AND DISCUSSION

FILM THICKNESS MEASUREMENT TESTING

BASELINE RIGID SURFACE PLAIN SLEEVE BEARING TEST RESULTS

Film thickness measurement tests were first performed on the rigid surface plain sleeve bearing for two purposes. It first allowed a preliminary check to be performed on the rotating sensors and slip ring assembly at relatively low speeds which was not possible with the compliant surface bearing because of the higher lift-off speed. It also served as a functional check of the instrumentation system using the analytical work of A. A. Raimondi as a baseline for comparison of the test data.

Initially, testing was conducted to establish the stability regime of the rigid test bearing. As anticipated, the bearing was unstable at speeds above 15,000 rpm and at very light loads at 14,000 rpm.

Testing was conducted at three speeds and a comparison between the predicted and test values of the minimum film thickness is presented in Figure VII-1 in non-dimensional form. The largest deviation of the test data from the analytically predicted values was -17 percent which occurs at the lightest load tested. The deviation for the remaining seventeen (17) test points was less than 10 percent of the predicted values, and the average deviation for the eighteen (18) test points was 6.8 percent. The correlation of test and analytical data improved with increasing speed and loads. During testing it became obvious that the load could not be applied exactly through the axial centerline of the bearing. This resulted in slight axial cocking of the bearing with respect to the test shaft causing the minimum film thickness measurements between the two probes to vary.

Figure VII-2 shows the location of the measurement sensors with respect to the test bearing and an explanation of a typical oscilloscope trace. The attitude angle reference mark was generated by using a Fotonic Sensor fibre optic probe to cause the oscilloscope trace to become saturated

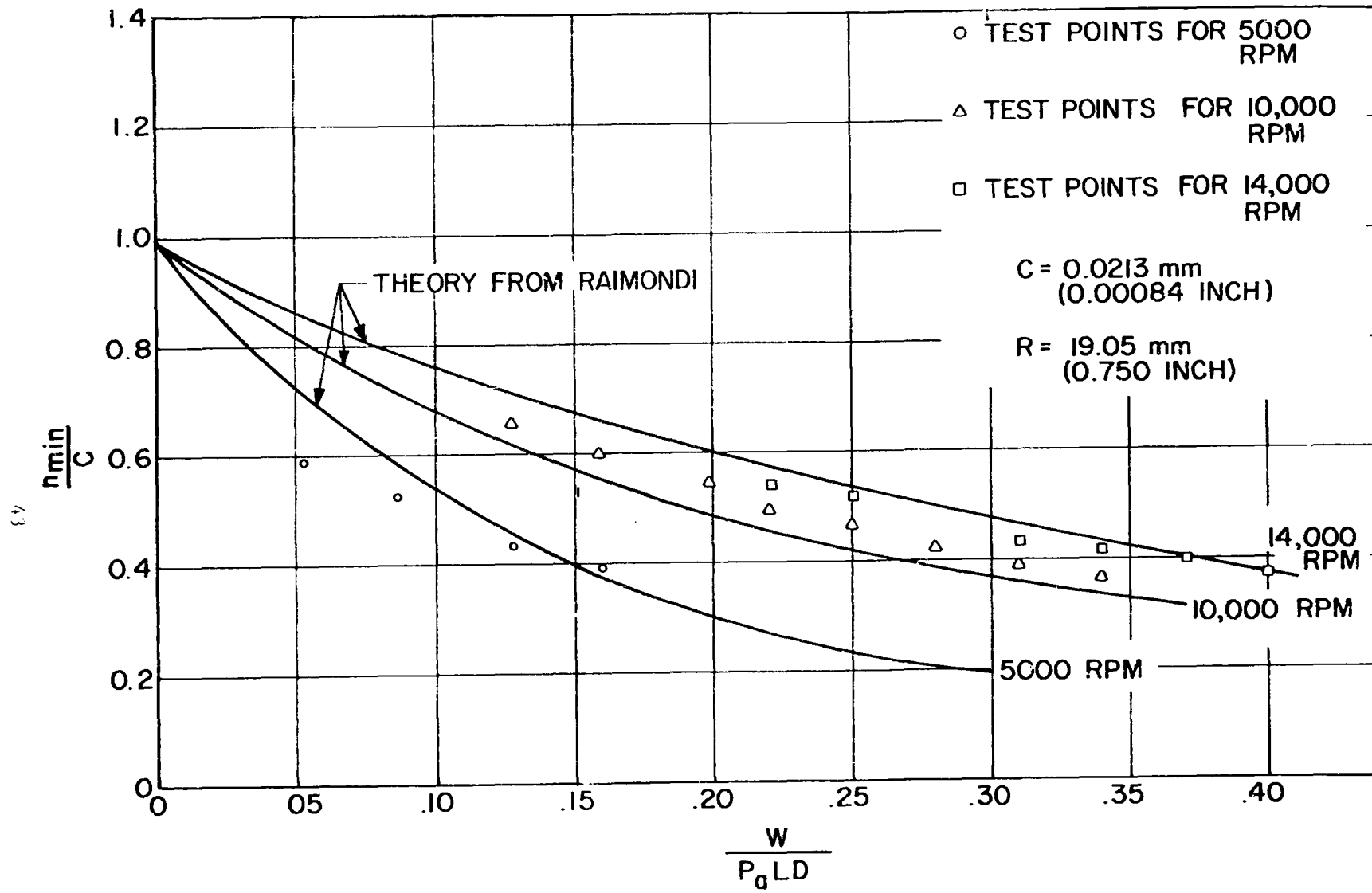


Fig. VII-1 Analytical and Experimental Minimum Film Thickness Values, Rigid Surface Plain Sleeve Bearing

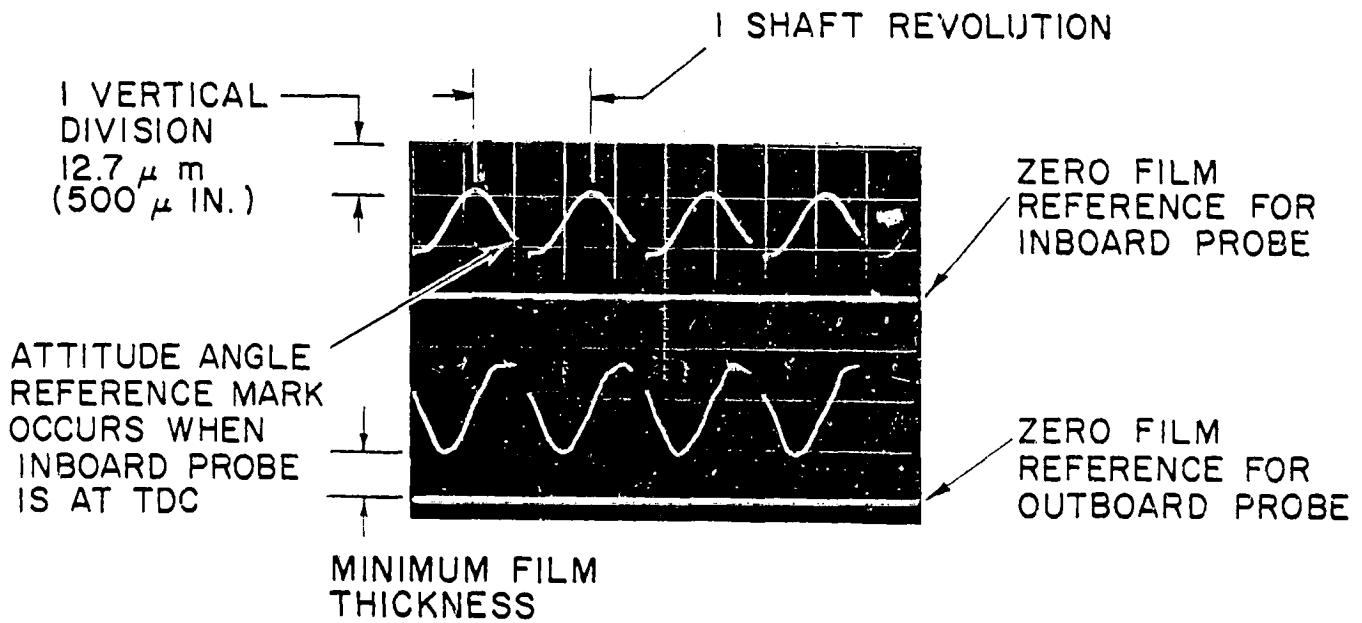
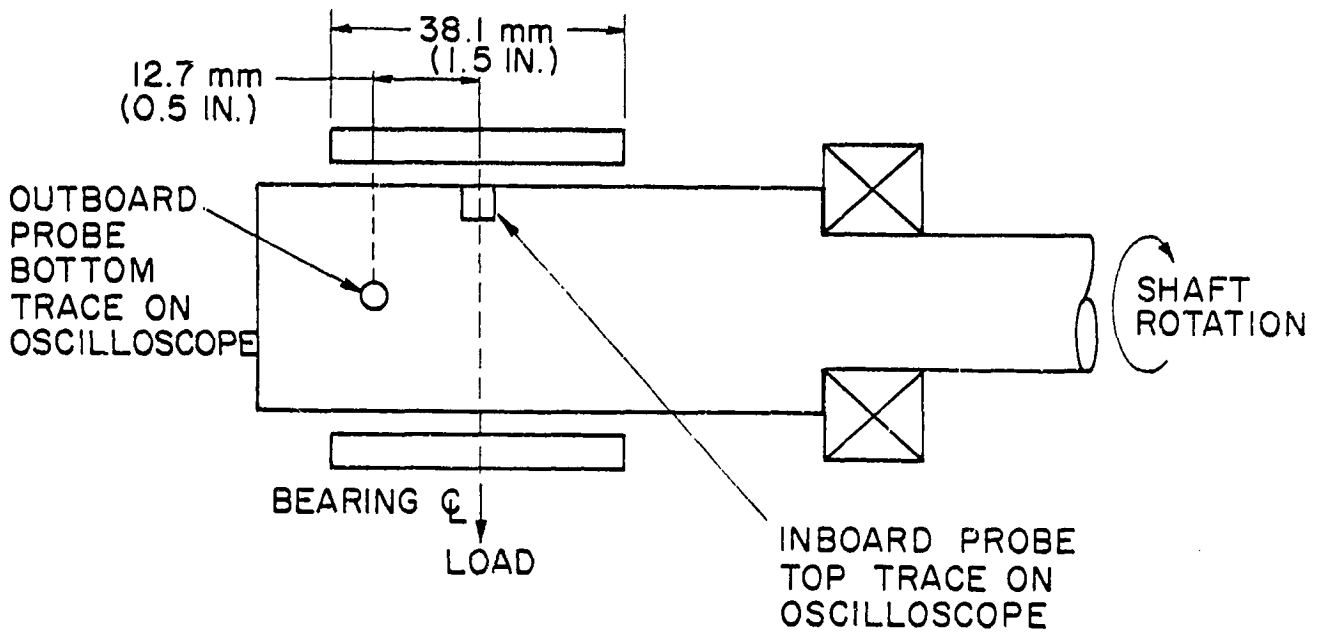


Fig. VII-2 Typical Oscilloscope Trace of Film Thickness Profile,
Rigid Surface Plain Sleeve Bearing

precisely when the inboard probe was directly under the load, in this case, top dead center. By scaling from where the reference mark first starts, to where the minimum film thickness occurs, the attitude angle of the bearing can be determined.

The oscilloscope traces in Figure VII-3 show the effect of speed on minimum film thickness and bearing attitude angle at a constant load. The minimum film thickness value listed with each trace is obtained utilizing the dc voltage peak detector.

The ac amplitude of the film profile traces should ideally be identical for both sensor locations at a given test condition. The film thickness profiles shown in Figure VII-3 exhibit a distinct difference in the ac amplitude at each of the two sensor locations for a given test condition. The difference was determined to be caused by cocking of the bearing, which was previously discussed, and a slight taper in the test journal. The journal was lapped to remove the taper prior to the start of testing with the compliant surface bearing.

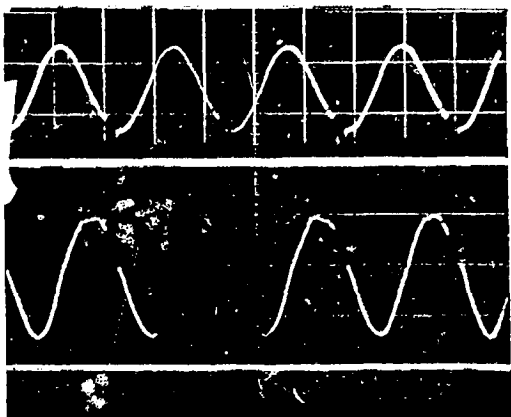
Figure VII-4 shows the film thickness profile obtained from an oscilloscope trace plotted on an expanded scale. Figure VII-5 plots the same data on polar coordinate graph paper and shows the bearing attitude angle and bearing eccentricity.

COMPLIANT SURFACE JOURNAL BEARING TESTS

Testing conducted with the compliant surface journal bearing utilizing the film thickness sensors provided a unique method of examining the effect of various operating conditions and bearing design characteristics on the overall fluid film. By independently varying test speed, bearing load, bearing clearance, and L/D ratio, the effect on the minimum film thickness value and profile was directly observed. Selected test data is presented in this section in tabulated form and as a series of film thickness oscilloscope traces.

To better understand the test data, a detailed description of a typical oscilloscope trace is given. Figure VII-6 shows the location of the film measurement sensors with respect to the test bearing and a schematic of the

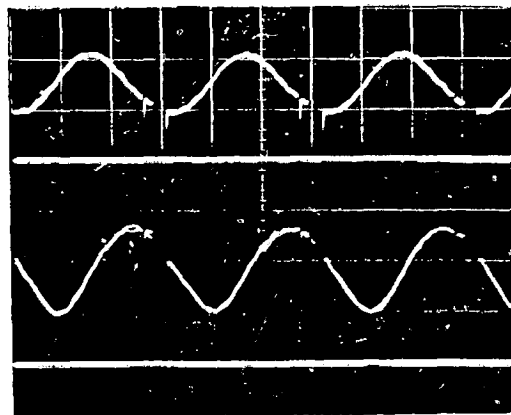
REPRODUCIBILITY OF THE
 PRESENT PAGE IS POOR



TEST SPEED: 5000 RPM
 TEST LOAD: $1.516 \times 10^4 \text{ N/m}^2$
 (2.2 PSI)

	<u>MINIMUM FILM THICKNESS</u>	<u>ATTITUDE ANGLE</u>
INBOARD:	$7.62 \mu\text{m}$ ($300 \mu\text{IN.}$)	60°
OUTBOARD:	$7.62 \mu\text{m}$ ($300 \mu\text{IN.}$)	60°

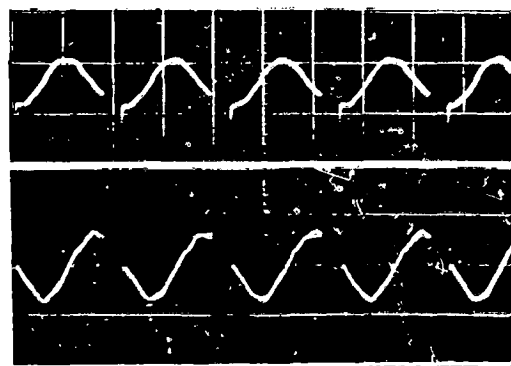
A



TEST SPEED: 10,000 RPM
 TEST LOAD: $1.516 \times 10^4 \text{ N/m}^2$
 (2.2 PSI)

	<u>MINIMUM FILM THICKNESS</u>	<u>ATTITUDE ANGLE</u>
INBOARD:	$12.1 \mu\text{m}$ ($475 \mu\text{IN.}$)	63°
OUTBOARD:	$12.7 \mu\text{m}$ ($500 \mu\text{IN.}$)	66°

B



TEST SPEED: 14,000 RPM
 TEST LOAD: $1.516 \times 10^4 \text{ N/m}^2$
 (2.2 PSI)

	<u>MINIMUM FILM THICKNESS</u>	<u>ATTITUDE ANGLE</u>
INBOARD:	$14.6 \mu\text{m}$ ($575 \mu\text{IN.}$)	67°
OUTBOARD:	$15.7 \mu\text{m}$ ($620 \mu\text{IN.}$)	72°

C

Fig. VII-3 Oscilloscope Traces Showing Effect of Speed on Film Thickness Profile, Rigid Surface Plain Sleeve Bearing

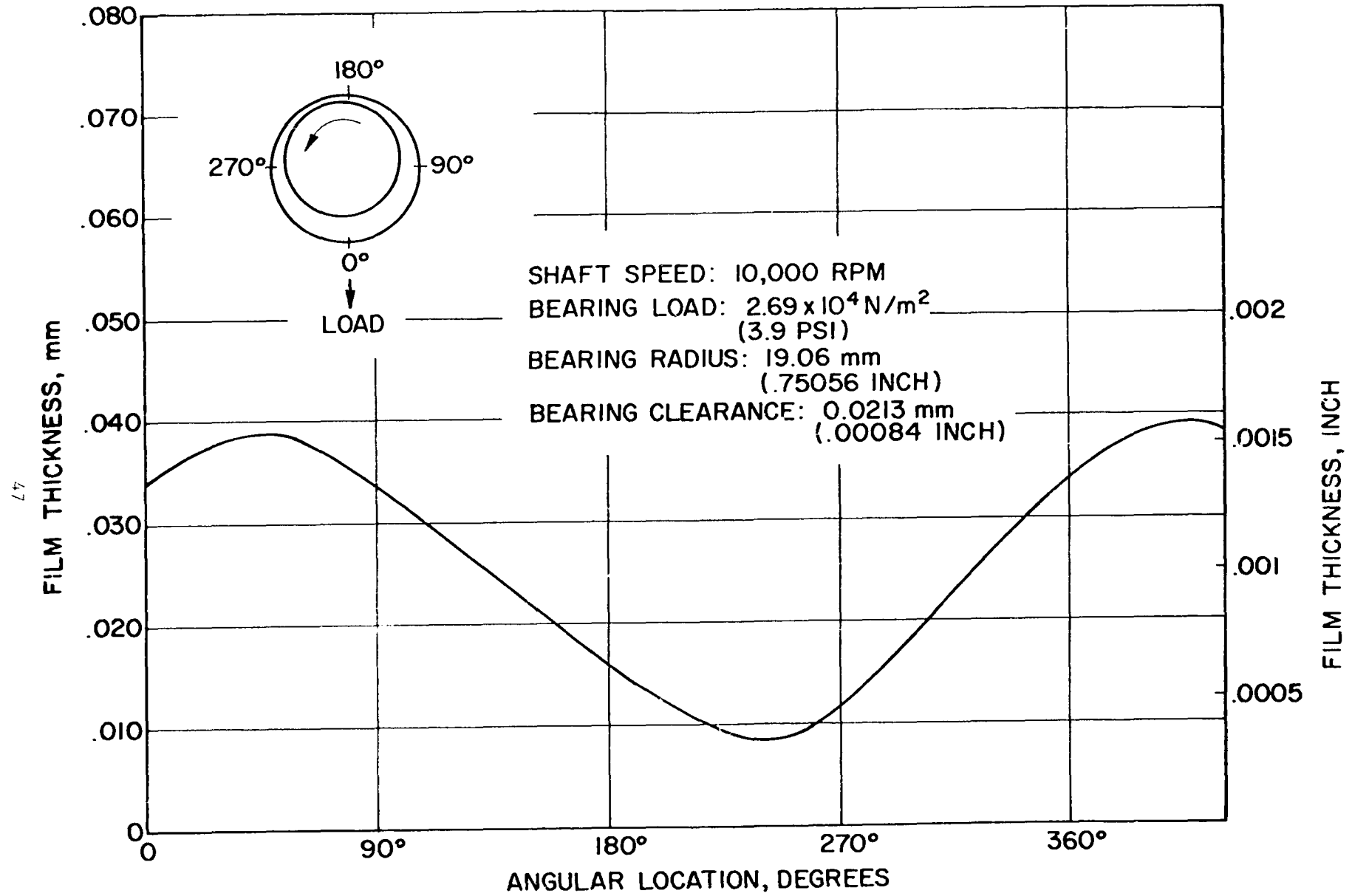


Fig. VII-4 Expanded Plot of Film Thickness Profile, Rigid Surface Plain Sleeve Bearing

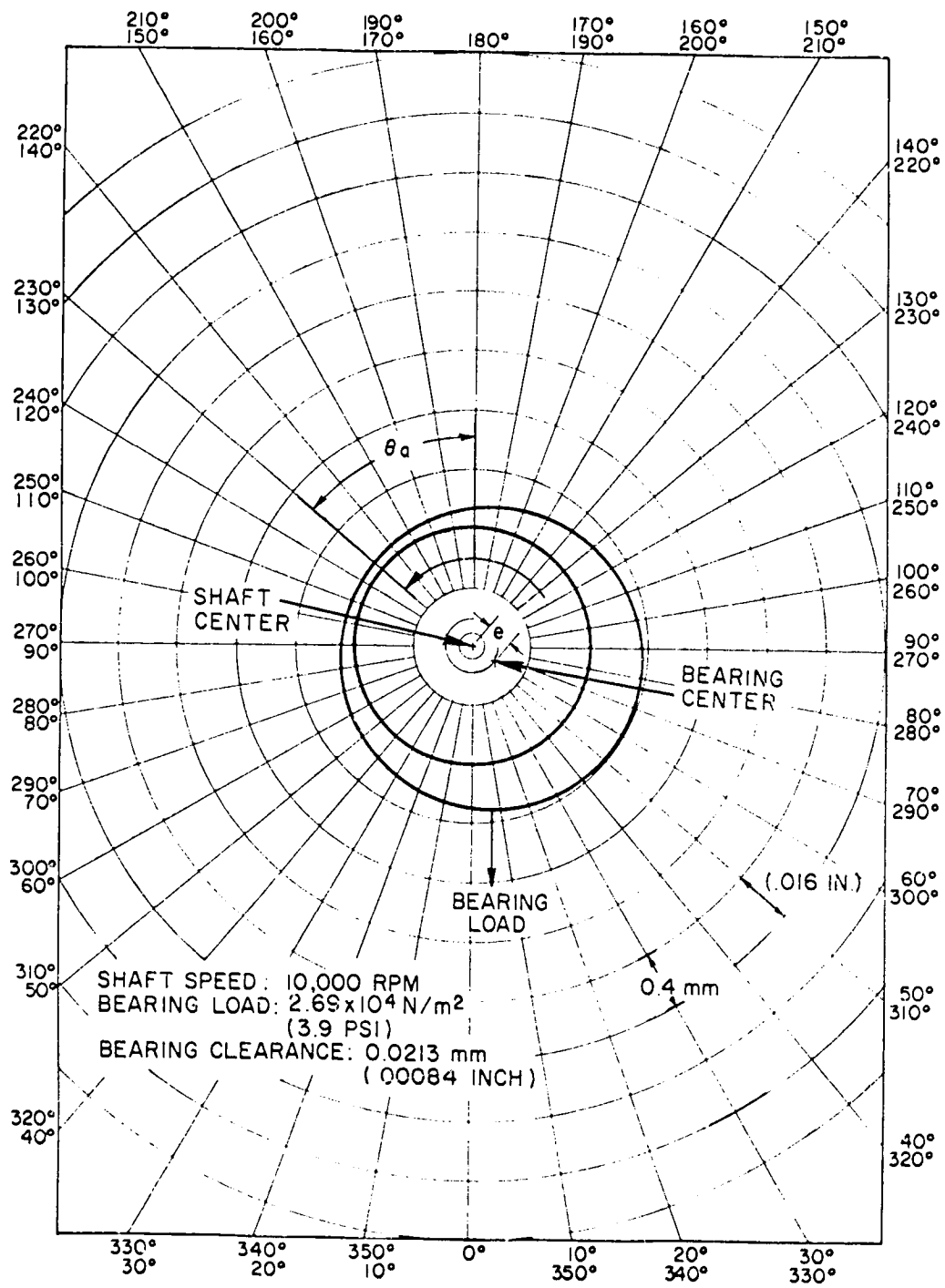


Fig. VII-5 Polar Plot of Film Thickness Profile, Rigid Surface Plain Sleeve Bearing

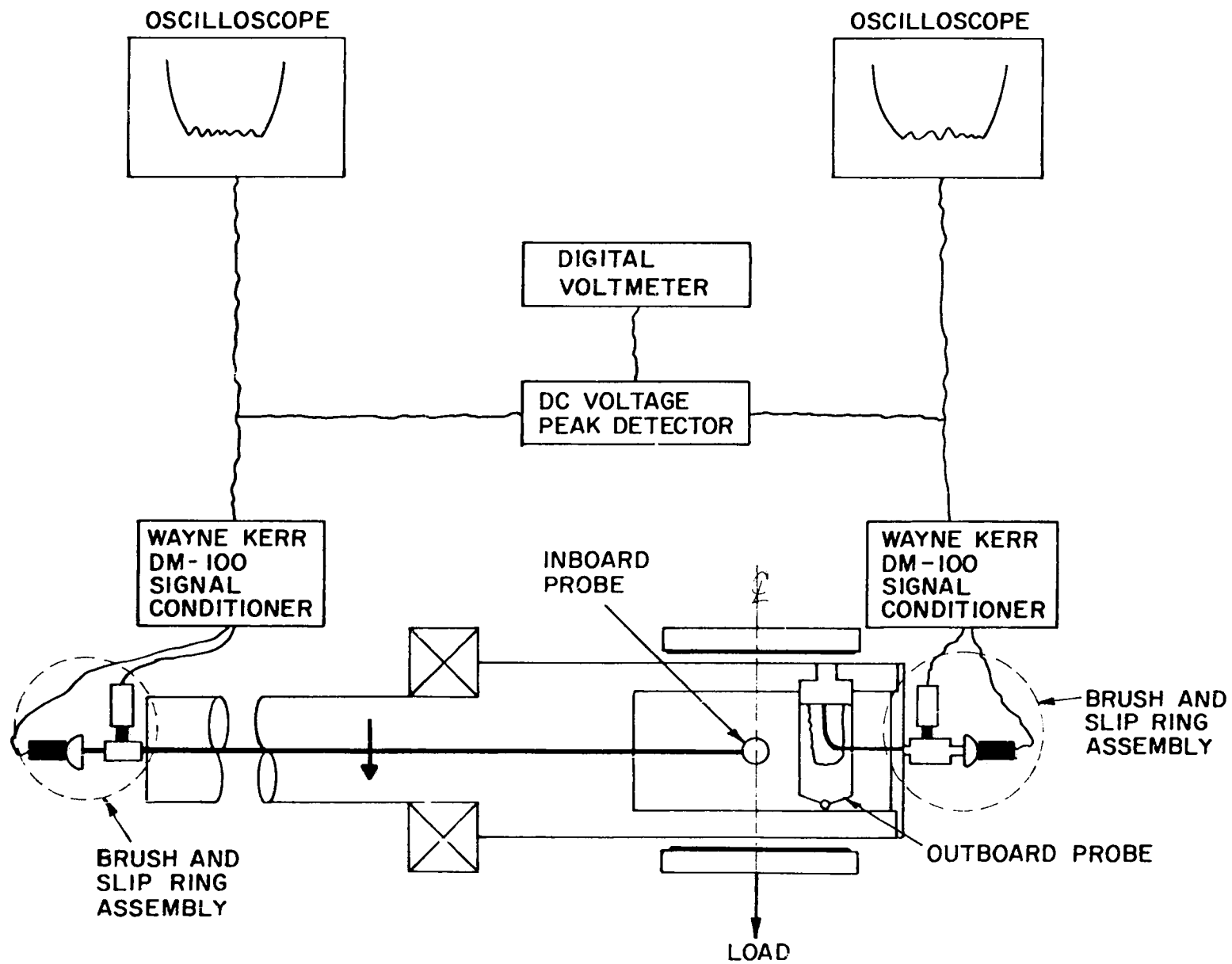


Fig. VII-6 Schematic of Instrumentation Used in EEM Thickness Data Acquisition

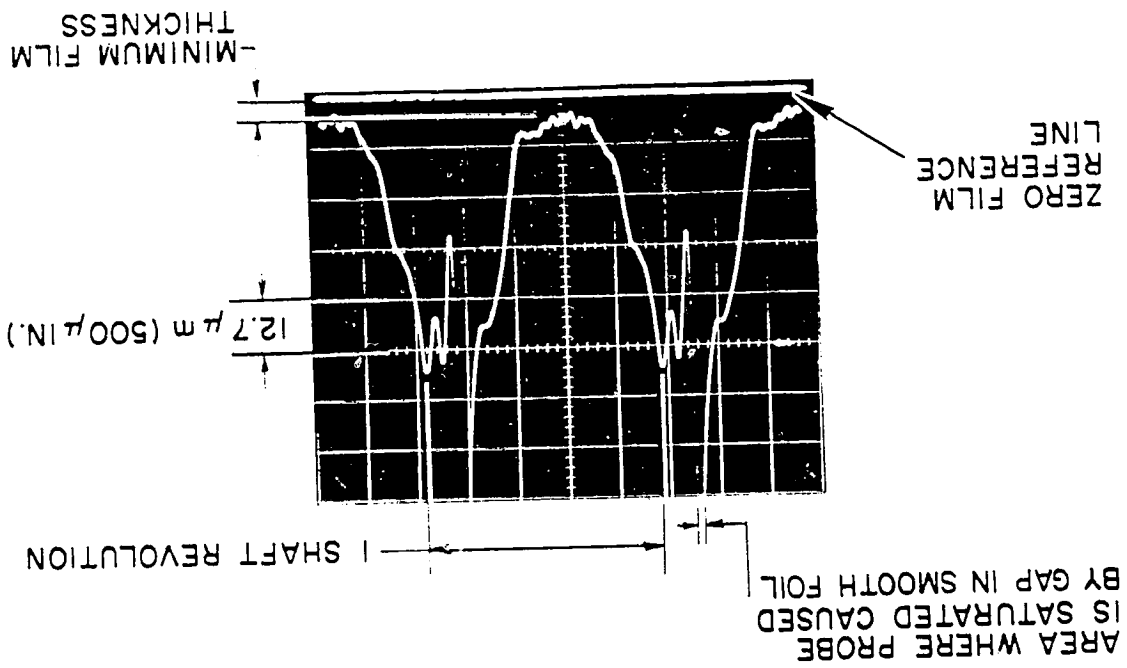
instrumentation used in obtaining the film thickness data. All of the oscilloscope traces shown, unless otherwise stated, represent the film thickness profile at the bearing centerline. The minimum film thickness value listed with each trace is the value obtained using the dc voltage peak detector also at the bearing centerline.

Figure VII-7 is a typical film thickness oscilloscope trace for the compliant surface journal bearing. The bottom horizontal grid line represents zero film thickness. Each vertical division above the bottom grid line equals 12.7 μm (500 $\mu\text{-in.}$) of film thickness. The minimum film thickness for the trace shown is 4.83 $\mu\text{-m}$ (190 $\mu\text{-in.}$). The horizontal scale or time base was varied for each test speed. In the trace shown, one shaft revolution requires 4.6 divisions, so each horizontal division is equal to approximately 80° of shaft rotation.

The gap in the smooth foil of the test bearing was used to reference the trace to the bearing. When the sensor passes over the gap in the smooth foil, the distance from the probe tip to the target is much greater than the probe range causing the probe to become saturated. As a result of this, the trace is driven off the oscilloscope screen. During all testing, the gap was located 180° from the point at which the load was being applied. In the trace shown, the maximum load is distributed over approximately 80° of the bearing.

The internal bearing clearances used in the test program were selected based on test experience obtained during development work on the Gas Generator Simulator for the Chrysler/ERDA Upgraded Gas Turbine Engine. The Hydresil bearings that are currently being tested by Chrysler in the Gas Turbine Engine are being supplied with a radial clearance of 0.031 - 0.038 mm (0.00125 - 0.0015 inch). The two clearances tested in this program are considered to be approximately the tolerance extremes for a 38.1 mm (1.5 inch) diameter Hydresil bearing operating at the temperature and speed requirements of an automotive gas turbine engine.

FIG. 10-1
A. 1000-10000 cps
B. 1000-10000 cps



Test Results of Compliant Bearing Tests

Tabulated test data for selected tests is presented in Tables VII-1 through VII-7. The complete film thickness test results are represented in the plots of Figures VII-8 through VII-11. These graphs show in dimensional form the minimum film thickness at various loads for the different test speeds, L/D ratios, and bearing clearances tested.

Examination of the tabulated data shows significant differences between the minimum film thickness values measured at the bearing centerline by the inboard probe and the value obtained from the outboard probe located 6.35 mm (0.250 inch) from the bearing edge.

The primary factor contributing to the difference in film thickness is the end leakage effect in the bearing causing an axial pressure gradient to occur, with the maximum pressure developed at the bearing midplane. Because the bearing is compliant, the foils deform unevenly with the largest deflection occurring in the area where the greatest pressure is developed, thereby causing an axial variation in film thickness. Axial film profiles are shown later in this section.

A second factor contributing to the variation in film thickness is axial cocking of the bearing sleeve due to the load not being applied exactly through the bearing centerline. This effect, first noticed during testing with the rigid surface bearing, is considered small when compared to the effect of the axial pressure gradient.

The minimum film thickness value obtained at the bearing centerline was used to plot the graphs of Figures VII-8 through VII-11. This value was used as it is located in the region where the maximum pressure is generated and therefore supports most of the bearing load. In addition, any effect due to cocking is not a factor.

The oscilloscope traces obtained as a result of these tests are presented in the discussion portion of this section.

TABLE VII - 1
COMPLIANT BEARING DATA FROM TEST # 101

L/D = 1; L x D = 14.6 cm² (2.25 in²) Test Speed: 30,000 RPM
 Bearing Clearance = 0.057 mm Test Temperature: Room Ambient
 (0.00225 in)

Bearing Load		Bearing Temp.		Dynamic Shaft Orbit		Minimum Film Thickness			
N	Pounds	°C	°F	mm	inch	Inboard		Outboard	
						μ-m	μ-in	μ-m	μ-in
18.9	4.25	32.2	90	<0.005	<0.0002	9.65	380	13.34	525
41.1	9.25	33.3	92	<0.005	<0.0002	7.62	300	10.29	405
63.4	14.25	35.0	95	<0.005	<0.0002	7.11	280	7.49	295
72.3	16.25	36.1	97	<0.005	<0.0002	6.86	270	5.72	225
81.2	18.25	36.7	98	<0.005	<0.0002	6.35	250	5.08	200
90.1	20.25	37.8	100	<0.005	<0.0002	5.08	200	4.83	190
99.0	22.25	38.3	101	<0.005	<0.0002	5.08	200	4.70	185
107.8	24.25	37.8	100	<0.005	<0.0002	4.82	190	4.45	175
72.3	16.25	36.1	97	<0.005	<0.0002	6.60	260	5.72	225
41.1	9.25	35.0	95	<0.005	<0.0002	7.62	300	17.40	460
4.4	1	33.3	92	<0.005	<0.0002	11.68	460	18.54	730

TABLE VII - 2
COMPLIANT BEARING DATA FROM TEST # 102

L/D = 1; L x D = 14.6 cm² (2.25 in²)
Bearing Clearance = 0.057 mm
(0.00225 in)

Test Speed: 45,000 RPM
Test Temperature: Room Ambient

Bearing Load		Bearing Temp.		Dynamic Shaft Orbit		Minimum Film Thickness			
N	Pounds	°C	°F	mm	inch	Inboard		Outboard	
						μ-m	μ-in	μ-m	μ-in
4.4	1	37.8	100	0.005	0.0002	22.10	870	26.42	1040
18.9	4.25	41.7	107	0.005	0.0002	19.56	770	18.92	745
41.1	9.25	43.3	110	0.005	0.0002	16.26	640	13.07	550
54.0	12.13	*	*	0.005	0.0002	15.11	595	11.05	435
76.2	17.13	*	*	0.005	0.0002	13.34	525	8.76	345
98.4	22.13	*	*	0.005	0.0002	12.19	480	7.24	285
111.8	25.13	*	*	0.005	0.0002	11.56	455	6.60	260
125.1	28.13	*	*	0.005	0.0002	11.18	440	6.35	250
142.3	32.0	*	*	0.005	0.0002	10.03	395	5.84	230
155.7	35.0	*	*	0.005	0.0002	9.53	375	5.46	215
169.0	38.0	*	*	0.005	0.0002	8.64	340	5.46	215
182.4	41.0	54.4	130	0.005	0.0002	8.38	330	5.33	210
194.0	43.62	57.8	136	0.005	0.0002	8.00	315	5.33	210
203.8	45.32	58.3	137	0.005	0.0002	6.86	270	4.95	195
142.3	32.0	47.8	118	0.005	0.0002	8.89	350	5.08	200
76.2	17.13	44.4	112	0.005	0.0002	12.19	480	8.64	340
18.9	4.25	40.6	105	0.005	0.0002	18.80	740	19.43	765
4.4	1	40.0	104	0.005	0.0002	21.59	850	22.35	880

*-temperature readout equipment was not functioning properly at these points

TABLE VII - 3
COMPLIANT BEARING DATA FROM TEST # 103

L/D = 1; L x D = 14.6 cm² (2.25 in²)
 Bearing Clearance = 0.057 mm
 (0.00225 in)

Test Speed: 60,000 RPM
 Test Temperature: Room Ambient

Bearing Load N	Pounds	Bearing Temp.		Dynamic Shaft Orbit		Minimum Film Thickness			
		°C	°F	mm	inch	Inboard		Outboard	
						μ-m	μ-in	μ-m	μ-in
18.9	4.25	43.3	110	0.018	0.0007	29.46	1160	21.84	860
41.1	9.25	46.1	115	0.018	0.0007	23.37	920	13.34	525
67.2	15.10	49.4	121	0.018	0.0007	20.19	795	10.92	430
93.2	20.95	53.9	129	0.018	0.0007	13.84	545	7.24	285
123.7	27.8	57.8	136	0.018	0.0007	12.07	475	5.84	230
145.9	32.8	60.0	140	0.018	0.0007	10.80	425	5.33	210
159.2	35.8	61.1	142	0.018	0.0007	9.27	365	5.08	200
174.3	39.2	63.3	146	0.018	0.0007	7.87	310	4.45	175

TABLE VII -4
COMPLIANT BEARING DATA FROM TEST # 106

L/D = 1; L x D = 14.6 cm² (2.25 in²)
Bearing Clearance = 0.0318 mm
(0.00125 in)

Test Speed: 30,000 RPM
Test Temperature: Room Ambient

Bearing Load		Bearing Temp.		Dynamic Shaft Orbit		Minimum Film Thickness			
N	Pounds	°C	°F	mm	inch	Inboard		Outboard	
						μ-m	μ-in	μ-m	μ-in
4.4	1.0	28.9	84	<0.005	<0.0002	13.97	550	18.42	725
18.9	4.25	30.6	87	<0.005	<0.0002	13.21	520	15.88	625
41.4	9.25	31.1	88	<0.005	<0.0002	12.45	490	13.72	540
63.4	14.25	33.3	92	<0.005	<0.0002	9.27	365	7.24	285
76.7	17.25	32.8	91	<0.005	<0.0002	8.26	325	6.10	240
90.1	20.25	33.9	93	<0.005	<0.0002	7.75	305	5.72	225
103.4	23.25	35.0	95	<0.005	<0.0002	6.73	265	5.33	210
116.8	26.25	35.6	96	<0.005	<0.0002	6.35	250	5.46	215
130.1	29.25	35.0	95	<0.005	0.0002	6.10	240	5.21	205
143.5	32.25	36.7	98	<0.005	<0.0002	5.59	220	5.08	200
116.8	26.25	35.6	96	<0.005	<0.0002	6.60	260	5.33	210
76.7	17.25	35.0	95	<0.005	<0.0002	8.38	330	5.21	205
41.1	9.25	34.4	94	<0.005	<0.0002	12.57	495	10.80	425
18.9	4.25	33.3	92	<0.005	<0.0002	12.83	505	15.75	620
4.4	1.0	32.8	91	<0.005	<0.0002	13.84	545	18.92	745

TABLE VII - 5

COMPLIANT BEARING DATA FROM TEST # 107

L/D = 1; L x D = 14.6 cm.² (2.25 in.²)
 Bearing Clearance = 0.0318 mm
 (0.00125 in)

Test Speed: 45,000 RPM
 Test Temperature: Room Ambient

Bearing Load N	Pounds	Bearing Temp.		Dynamic Shaft Orbit		Minimum Film Thickness			
		C	F	mm	inch	Inboard		Outboard	
						μ-m	μ-in	μ-m	μ-in
4.4	1.0	37.8	100	0.005	0.0002	19.56	770	18.54	730
18.9	4.25	40.6	105	0.005	0.0002	15.49	610	16.00	630
41.4	9.25	43.3	110	0.005	0.0002	13.59	535	12.19	480
66.0	14.85	45.0	113	0.005	0.0002	11.56	455	9.02	355
86.5	19.45	47.2	117	0.005	0.0002	10.41	410	7.11	280
108.8	24.45	48.3	119	0.005	0.0002	9.27	365	6.35	250
122.1	27.45	48.9	120	0.005	0.0002	8.64	340	6.10	240
135.4	30.45	50.6	123	0.005	0.0002	8.13	320	5.97	235
148.8	33.45	51.7	125	0.005	0.0002	7.37	290	5.33	210
163.0	36.65	53.3	128	0.005	0.0002	6.22	245	4.06	160
178.2	40.05	53.3	128	0.008	0.0003	5.21	205	4.06	160
191.5	43.05	56.7	134	0.008	0.0003	4.45	175	3.81	150
200.4	45.05	56.7	134	0.008	0.0003	4.32	170	3.81	150
178.2	40.05	54.4	130	0.008	0.0003	5.72	225	3.94	155
148.8	33.45	53.9	129	0.005	0.0002	8.00	315	5.46	215
108.8	24.45	52.2	126	0.005	0.0002	9.65	380	6.35	250
86.5	19.45	50	122	0.005	0.0002	10.54	415	7.11	280
52.7	11.85	50	122	0.005	0.0002	12.07	475	10.41	410
18.9	4.25	47.2	117	0.005	0.0002	15.62	615	15.88	625
4.4	1.0	46.1	115	0.005	0.0002	17.02	670	18.92	745

TABLE VII - 6
COMPLIANT BEARING DATA FROM TEST # 108

L/D = 1; L x D = 14.6 cm² (2.25 in²)
Bearing Clearance = 0.0318
(0.00125 in)

Test Speed: 55,500 RPM
Test Temperature: Room Ambient

Bearing Load N	Pounds	Bearing Temp.		Dynamic Shaft Orbit		Minimum Film Thickness			
		°C	°F	mm	inch	Inboard		Outboard	
						μ-m	μ-in	μ-m	μ-in
18.9	4.25	44.4	112	0.008	0.0003	20.96	825	10.67	425
57.2	12.85	47.8	118	0.010	0.0004	16.38	645	8.13	340
79.4	17.85	50.0	122	0.010	0.0004	14.76	660	7.49	295
106.9	24.05	51.7	125	0.013	0.0005	13.97	550	6.22	245
129.2	29.05	54.4	130	0.013	0.0005	12.83	505	5.46	215
142.5	32.05	55.6	132	0.013	0.0005	10.67	420	4.19	165
155.9	35.05	56.1	133	0.013	0.0005	10.03	395	5.59	220
169.3	38.05	56.7	134	0.013	0.0005	9.78	385	4.95	195
185.2	41.65	62.2	144	0.013	0.0005	8.76	345	4.70	185
198.6	44.65	63.3	146	0.013	0.0005	8.13	320	4.32	170

TABLE VII - 7
COMPLIANT BEARING DATA FROM TEST # 112

L/D = $\frac{1}{2}$; L x D = 7.25 cm² (1.125 in²)
Bearing Clearance = 0.0318 mm
(0.00125 in)

Test Speed: 45,000 RPM
Test Temperature: Room Ambient

N	Bearing Load pounds	Bearing Temp.		Dynamic Shaft Orbit		Minimum Film Thickness					
		°C	°F	mm	inch	Outboard		Center		Inboard	
						μ-m	μ-in	μ-m	μ-in	μ-m	μ-in
4.4	1.0	41.7	107	0.008	0.0003	6.99	275	10.92	430	5.84	230
18.9	4.25	45.6	114	0.008	0.0003	5.97	235	8.26	325	5.08	200
28.7	6.45	46.1	115	0.008	0.0003	5.33	210	6.48	255	4.83	190
37.6	8.45	47.2	117	0.008	0.0003	5.08	200	5.98	235	4.45	175
46.5	10.45	48.9	120	0.008	0.0003	4.32	170	5.21	205	4.06	160
55.4	12.45	50.0	122	0.008	0.0003	3.94	155	5.33	210	3.81	150
64.2	14.45	52.2	126	0.008	0.0003	3.56	140	5.08	200	3.43	135

09

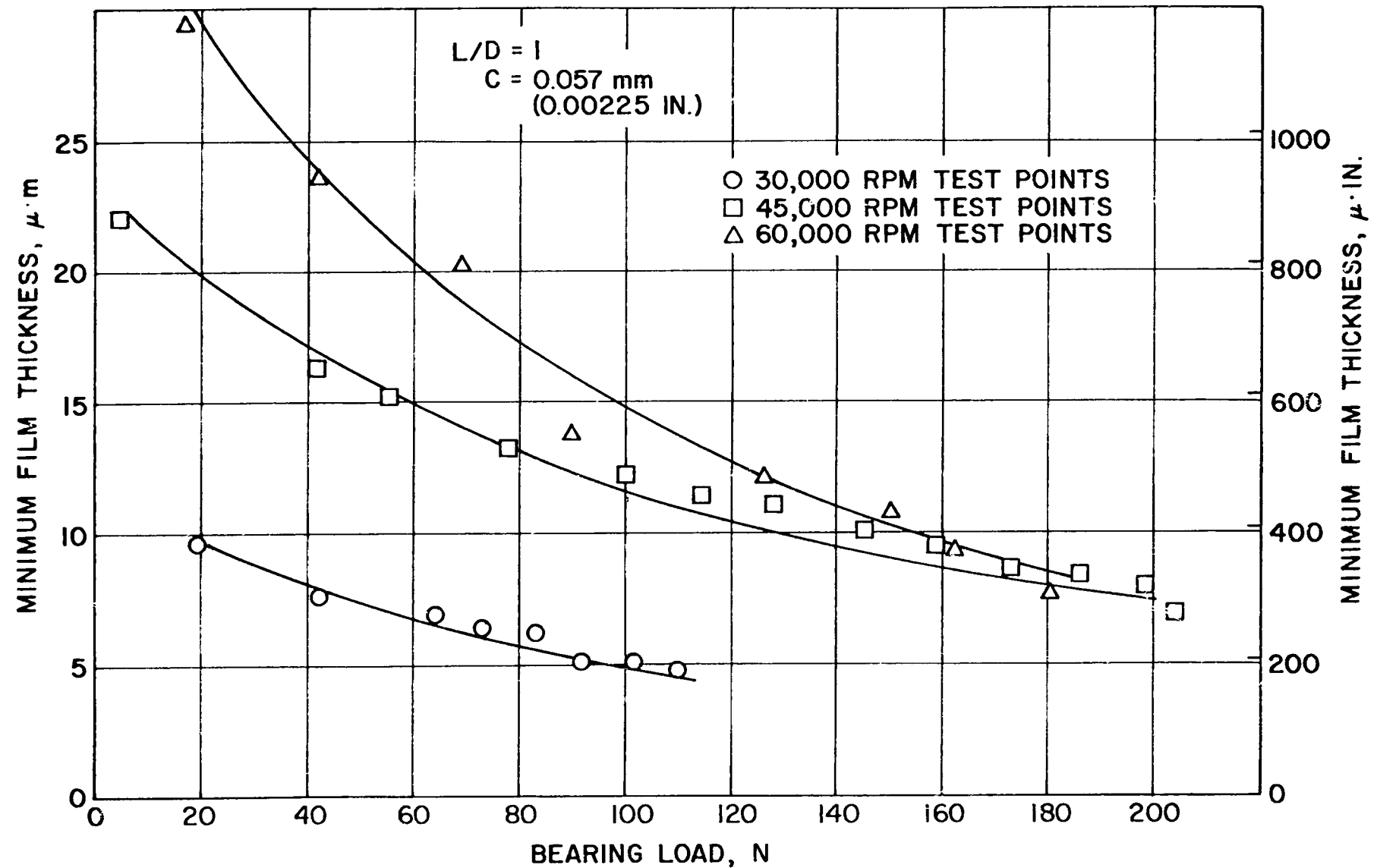


Fig. VII-8 $L/D=1, C=0.057 \text{ mm}$: Experimental Minimum Film Thickness Values, Compliant Surface Bearing

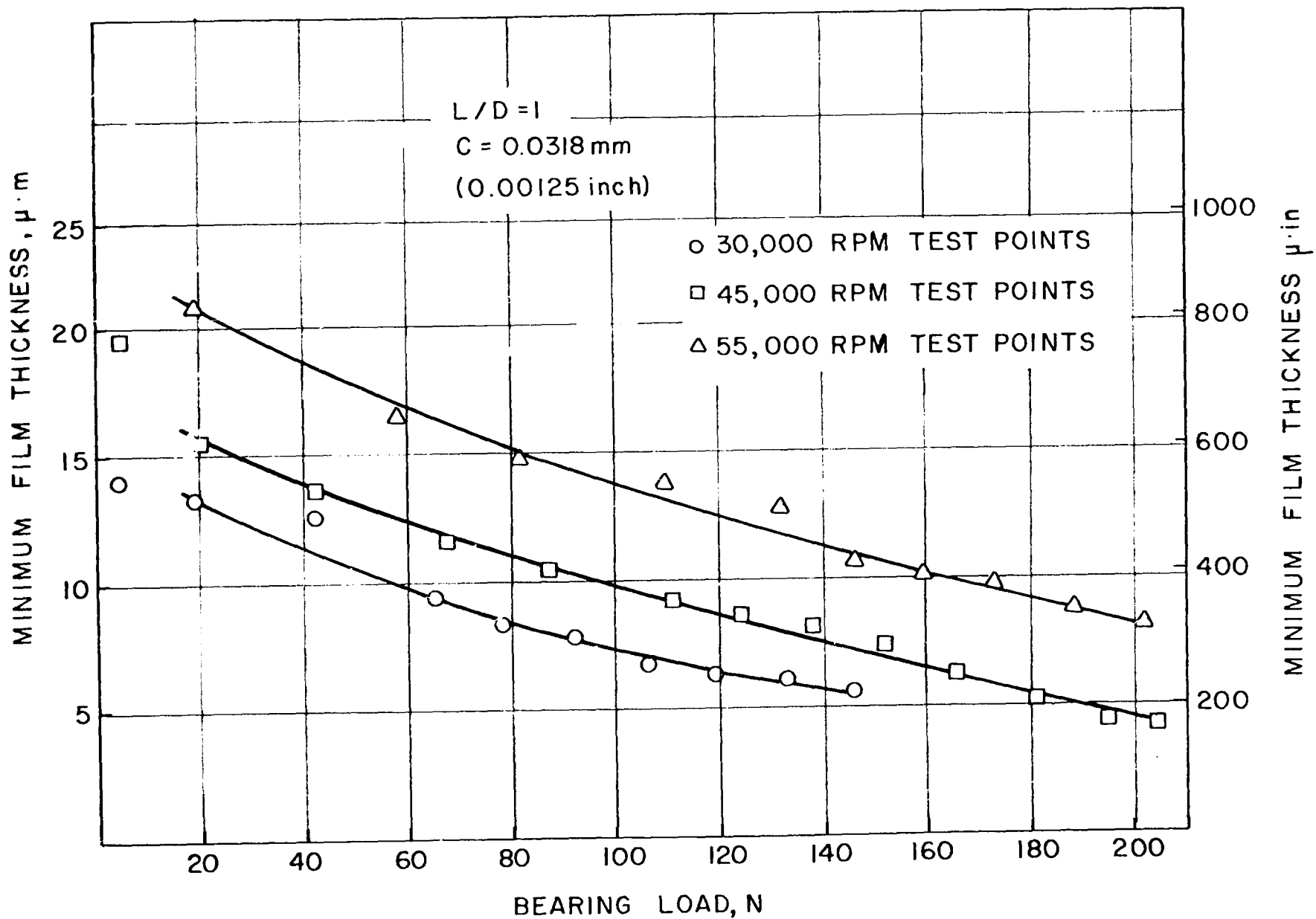


Fig. VII-9 $L/D=1$, $C=0.0318 \text{ mm}$: Experimental Minimum Film Thickness Values, Compliant Surface Bearing

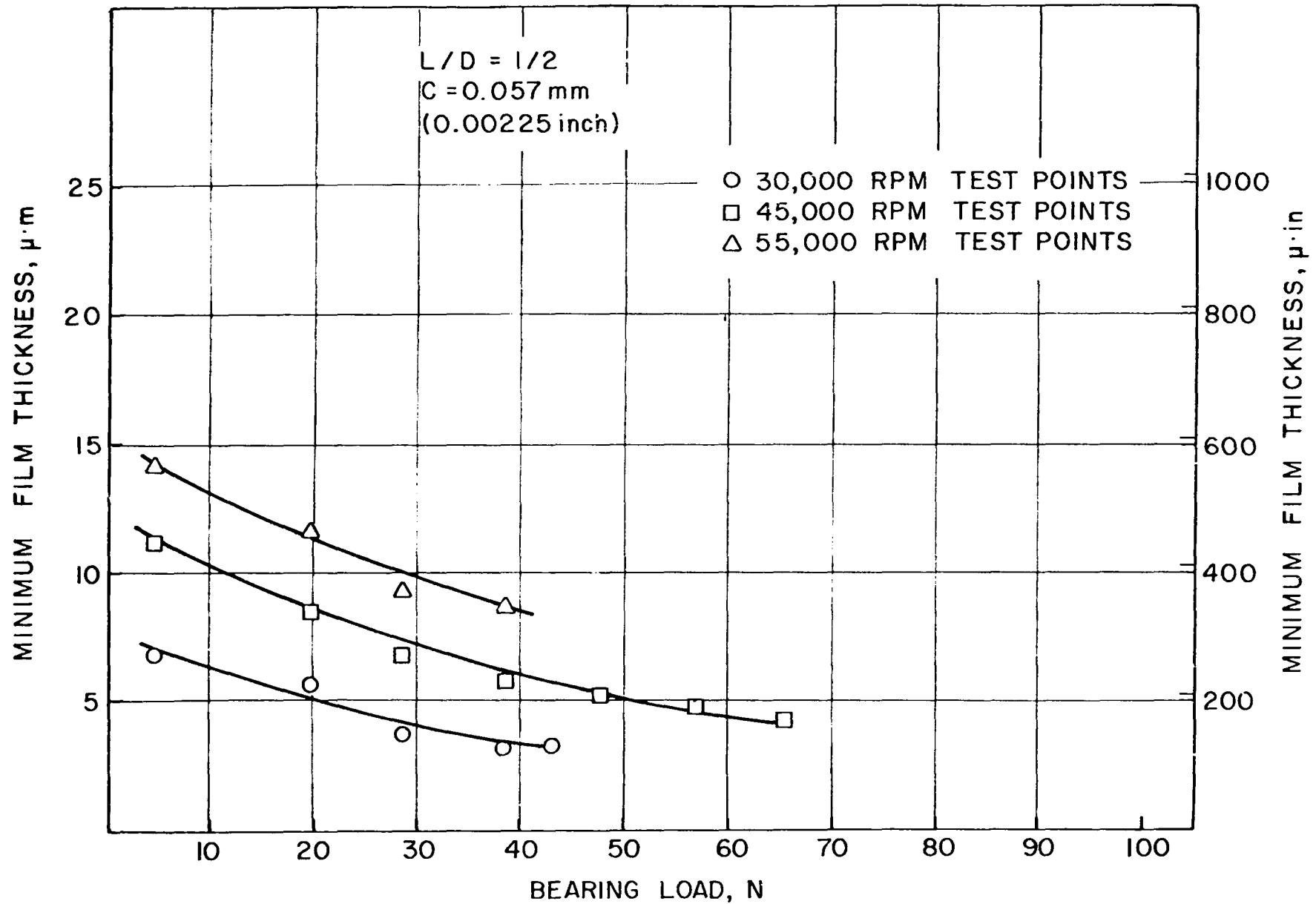


Fig. VII-10 $L/D=1/2$, $C=0.057 \text{ mm}$: Experimental Minimum Film Thickness Values, Compliant Surface Bearing

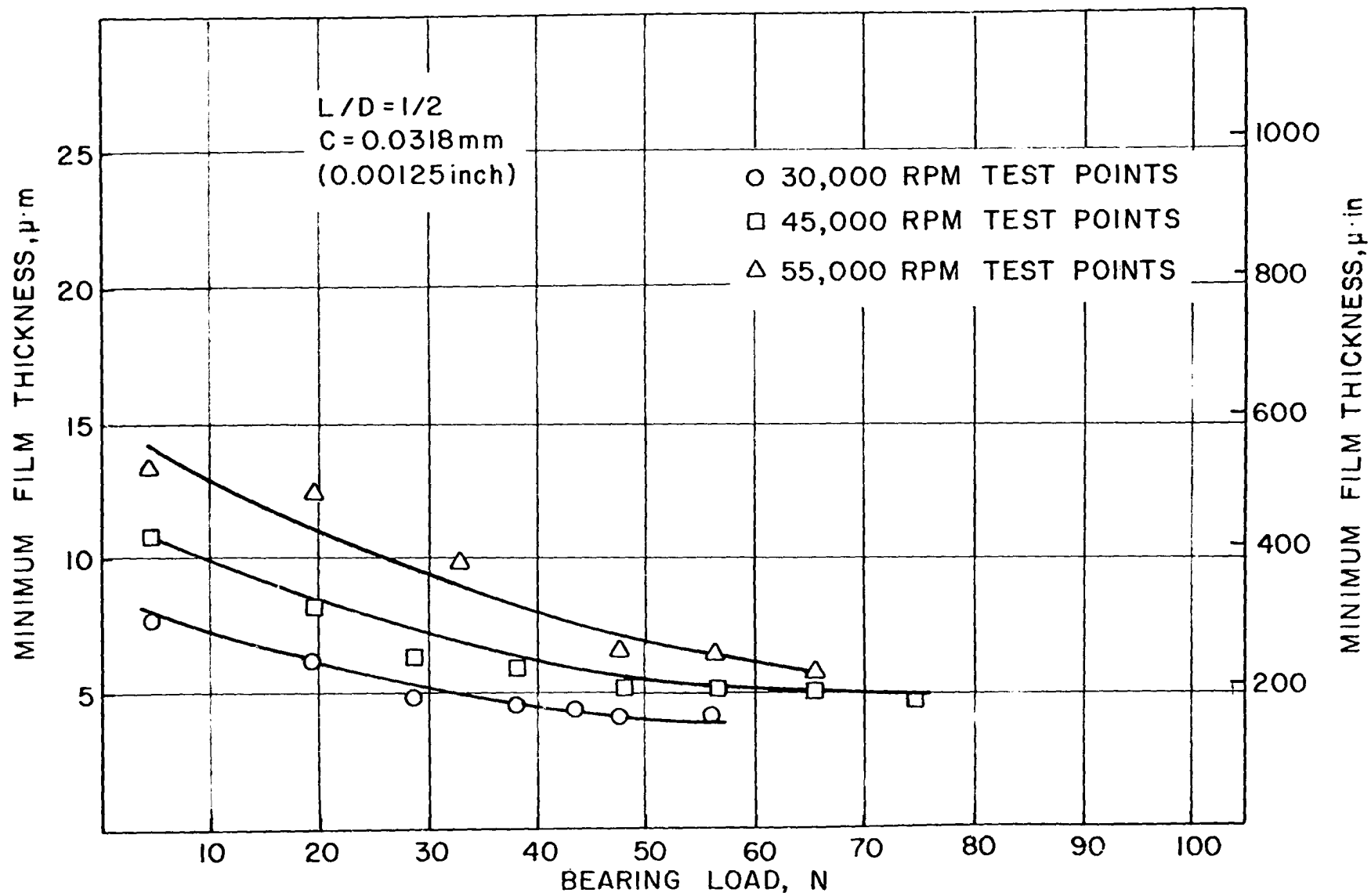


Fig. VII-11 $L/D=1/2, C=0.0318$ ∴ Experimental Minimum Film Thickness Values, Compliant Surface Bearing

Discussion of Compliant Bearing Test Results

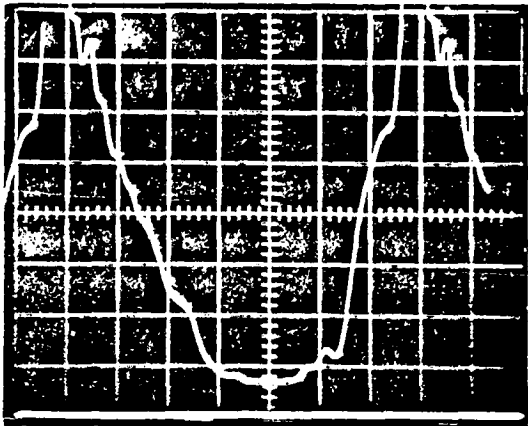
Testing was to be conducted at three speeds: 30,000 rpm; 45,000 rpm; and 60,000 rpm. Although testing was conducted at 60,000 rpm, and data obtained at this speed, the majority of the high speed test data was obtained at 55,000 rpm. The dynamic shaft orbit diameter increased from 0.0076 mm (0.0003 inch) to 0.0178 mm (0.0007 inch) when the shaft speed was increased from 55,000 rpm to 60,000 rpm. This increase in dynamic shaft motion was enough to cause some small motion of the bearing cartridge and housing which resulted in multiple traces of the film thickness profile on the oscilloscope. This motion, although very small, did hinder obtaining clear film profile traces at the 60,000 rpm speed condition.

Utilization of the rotating film thickness sensors provided a unique method of examining the effect of design and operating parameters on the film thickness profile of the Hydresil Compliant Bearing. The film profiles for the compliant bearing, unlike the symmetrical trace of the rigid sleeve bearing, contain many non-uniform characteristics, some of which cannot yet be completely explained. The following sections contain a discussion of various film profile traces that have been selected to show the effect of various design and test parameters.

Changes in film profile due to design parameters

During this test program, two bearing design parameters were varied, bearing clearance and bearing L/D ratio. Figure VII-12 shows the effect of changing bearing clearance while maintaining all other test conditions constant. The basic principle that improved conformity between bearing and journal increases load performance applies to the compliant bearing. The smaller clearance increases bearing conformity, therefore, load capacity or film thickness at a given set of test conditions generally increases with decreasing clearance. Detailed examination of all film thickness test data shows that larger minimum film thickness values were obtained with the smaller bearing clearance for all test conditions except one. Minimum film thickness test data for the L/D = 1 bearing at 45,000 rpm was slightly larger for the test bearing with the larger bearing clearance. No explanation for this can be given at this time.

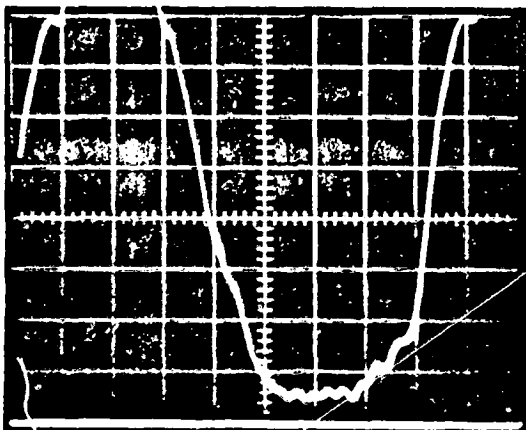
REPRODUCIBILITY OF THE
ORIGINAL PAGE IS POOR



A

L/D = 1
TEST SPEED: 30,000 RPM
TEST LOAD: 6.2×10^4 N/m²
(9 PSI)

MINIMUM FILM
THICKNESS: $7.75 \mu\text{m}$
($305 \mu\text{IN.}$)
C: 0.0318 mm
(0.00125 IN.)



B

L/D = 1
TEST SPEED: 30,000 RPM
TEST LOAD: 6.2×10^4 N/m²
(9 PSI)

MINIMUM FILM
THICKNESS: $5.08 \mu\text{m}$
($200 \mu\text{IN.}$)
C: 0.0572 mm
(0.00225 IN.)

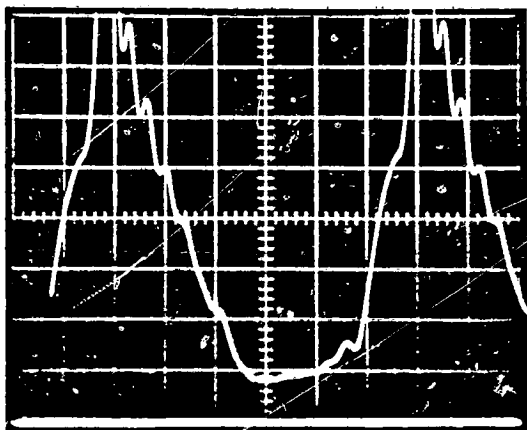
Fig. 11-11. Comparison of film thickness profiles showing effect of surface finish on film thickness, constant surface finish.

Figure VII-13 shows the effect of two L/D ratios. At the same test conditions, the minimum film thickness value for the L/D = 1 bearing is approximately twice the value for the L/D = 1/2. All the data shows a substantial reduction in bearing load capacity for the L/D = 1/2 bearing compared to the L/D = 1 bearing. This can be attributed to the L/D = 1/2 bearing being "all edge" and end leakage becoming more significant in its effect on bearing performance.

An axial profile of the minimum film thickness value was obtained for the L/D = 1 test bearing. The film thickness profile and minimum value was obtained at 3/175 mm (0.125 in) increments between the bearing centerline and 1.65 mm (0.065 inch) from the bearing edge. An accurate trace could not be obtained at the bearing edge as the guard electrode and center electrode of the capacitance probe sensor must both be inside the edge of the smooth foil. The profile and value obtained from the sensor are at the centerline of the sensor. Figure VII-14 shows the film thickness profile at four (4) axial positions and the axial profile of the minimum film thickness.

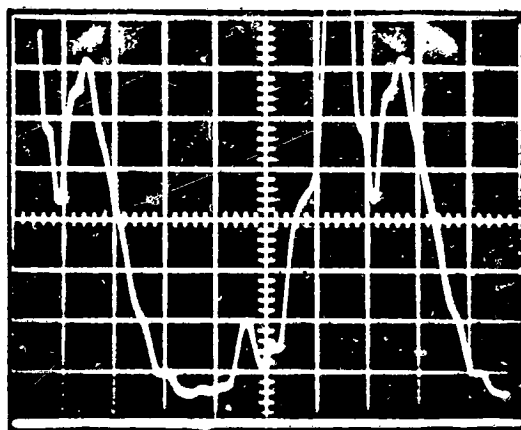
An objective of the film thickness measurement testing was to obtain data that would assist in improving the load performance capability of the compliant surface journal bearing. Examination of the film thickness traces show that in the loaded region of the trace, a low amplitude sine wave pattern appears. As the load is increased, the amplitude of the pattern increases. The cause of this pattern is attributed to the smooth foil "dipping" between the convolutions in the bump foil. Figure VII-15 shows a schematic of the smooth foil "dipping between the bumps and the period of the sine wave trace corresponding to the pitch of the bumps. Also included are two oscilloscope traces which show the "dipping" and the variation in the amount due to bearing loading. Shown in Figure VII-16 are two oscilloscope traces obtained at the same test conditions; Trace A is at the bearing centerline and Trace B is obtained 6.35 mm (0.25 inch) from the bearing edge. The "dipping" is very prominent in Trace A, but cannot be distinguished in Trace B. This comparison shows that pressure generated by the bearing is substantially different at the two points, and the bearing load is being predominately carried by a narrow

REPRODUCIBILITY OF THE
ORIGINAL PAGE IS POOR



L/D = 1
TEST SPEED: 45,000 RPM
TEST LOAD: 6.78×10^4 N/m²
(9.83 PSI)

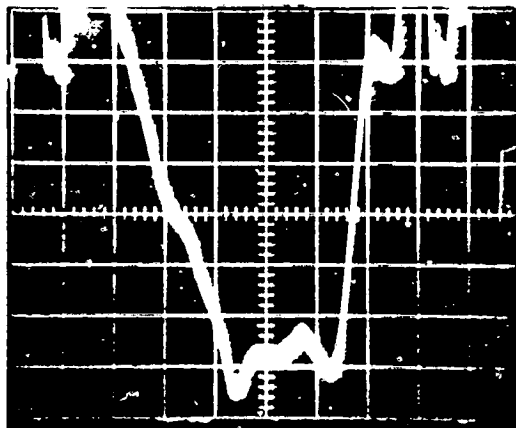
MINIMUM FILM
THICKNESS: $10.16 \mu\text{m}$
($400 \mu\text{IN.}$)
C: 0.0318 mm
(0.00125 IN.)



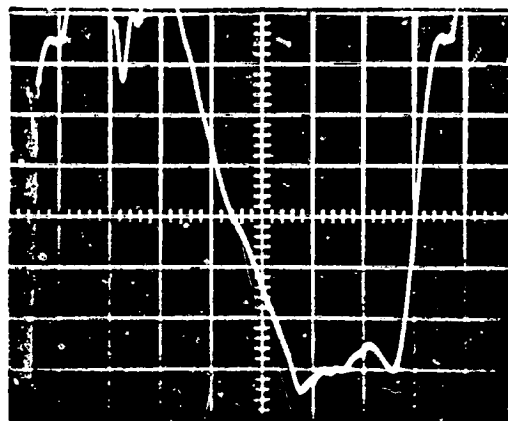
L/D = 1/2
TEST SPEED: 45,000 RPM
TEST LOAD: 6.54×10^4 N/m²
(9.5 PSI)

MINIMUM FILM
THICKNESS: $5.2 \mu\text{m}$
($205 \mu\text{IN.}$)
C: 0.0318 mm
(0.00125 IN.)

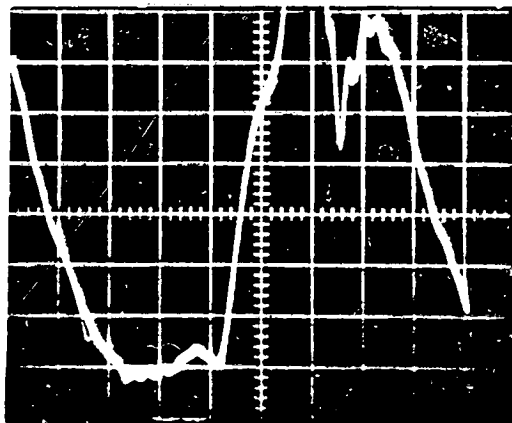
Fig. 11-13 Oscilloscope Traces Showing Effect of Bearing L/D Ratio on Film Thickness, Compliant Surface Bearing



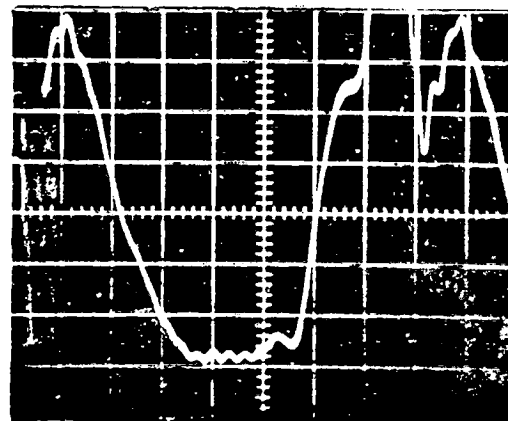
POSITION #1



POSITION #2



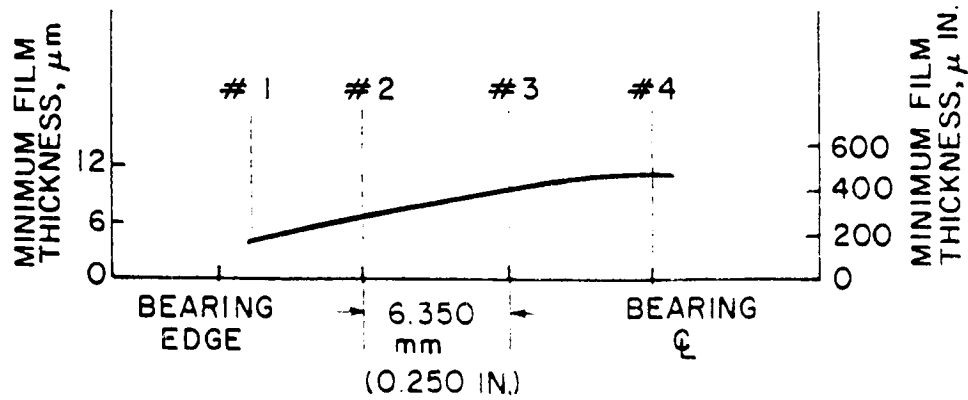
POSITION #3

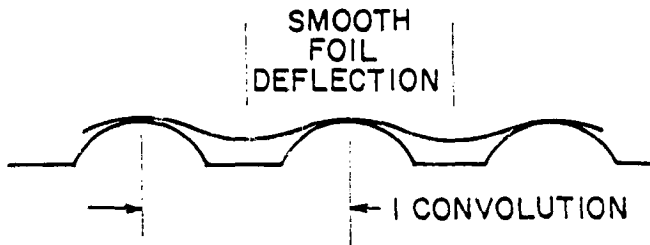


POSITION #4

L/D = 1
 TEST LOAD: $2.8 \times 10^4 \text{ N/m}^2$
 (4.1 PSI)

TEST SPEED: 30,000 RPM
 C: 0.0318 mm
 (0.00125 IN.)

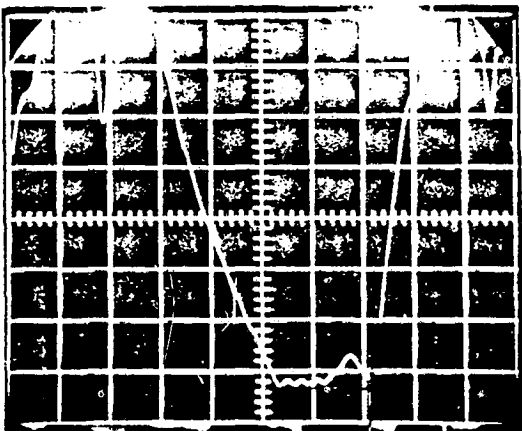




~27 CONVOLUTIONS/BEARING
1 CONVOLUTION = 13.3°

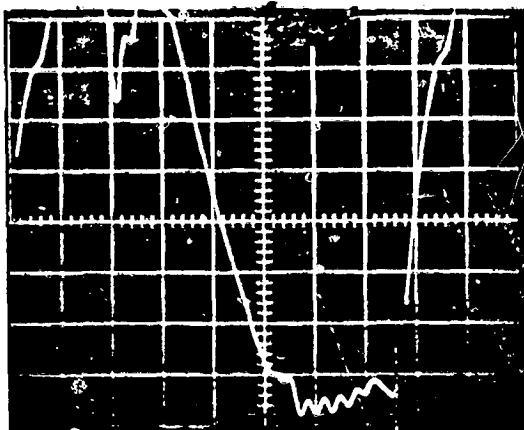
OSCILLOSCOPE TRACE
1 CYCLE = ~8 DIV.
1 DIV. = 45°

1 CONVOLUTION \approx .3 DIV.



L/D = 1
TEST SPEED: 30,000 RPM
TEST LOAD: $2.826 \times 10^4 \text{ N/m}^2$
(4.1 PSI)
C: 0.0318 mm
(0.00125 IN.)

MINIMAL SMOOTH FOIL
DEFLECTION UNDER LOAD

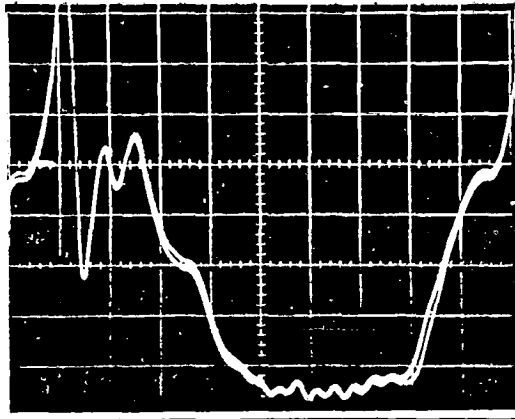


L/D = 1
TEST SPEED: 30,000 RPM
TEST LOAD: $1.11 \times 10^5 \text{ N/m}^2$
(16.1 PSI)
C: 0.0318 mm
(0.00125 IN.)

SMOOTH FOIL DEFLECTION
UNDER LOAD APPROXIMATELY
 $3.81 \mu\text{m}$ ($150 \mu\text{IN.}$) PEAK-TO-
PEAK

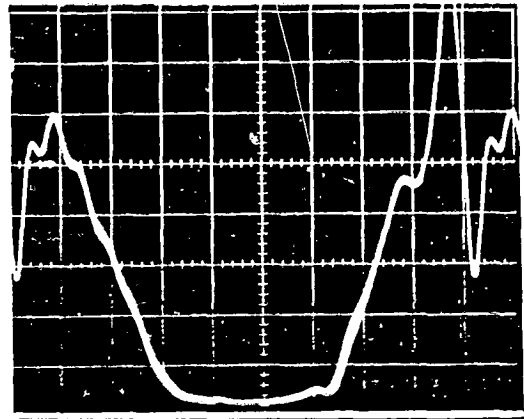
~ .3 DIV.

FIG. VII-15 Oscilloscope Traces Showing Effect of Load on Smooth Foil Deflection



A

INBOARD PROBE AT
BEARING CENTERLINE



B

OUTBOARD PROBE AT
6.35 mm (.25 INCH)
FROM BEARING EDGE

L/D = 1
 TEST SPEED: 30,000 RPM
 TEST LOAD: 9.24×10^4 N/m²
 (13.4 PSI)
 C: 0.057 mm
 (.00225 INCH)

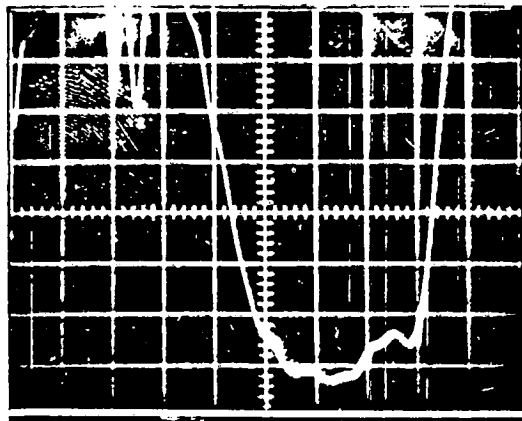
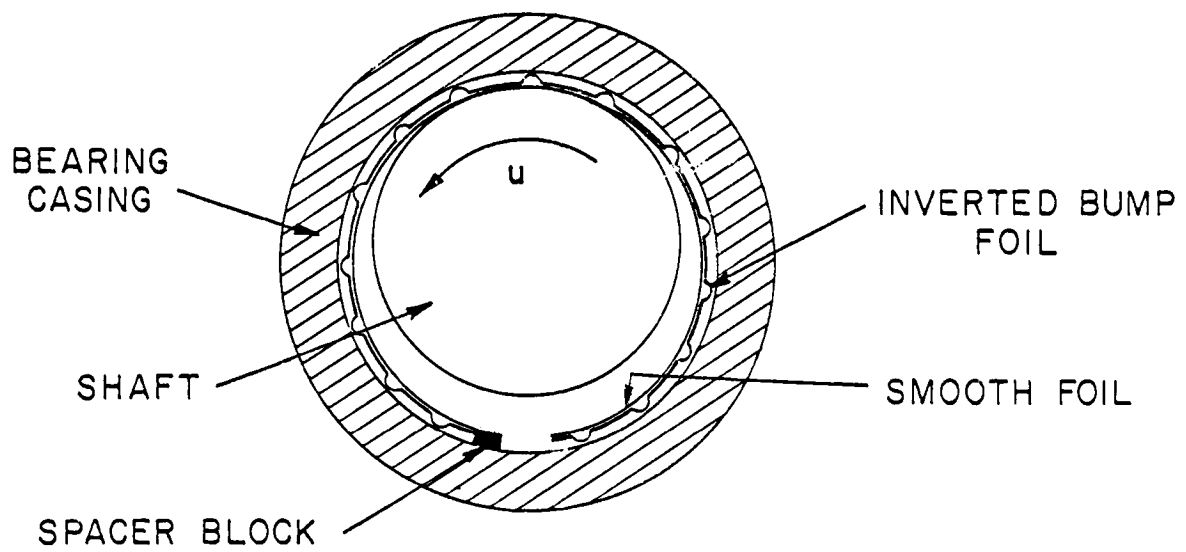
FIG. VII-1b Oscilloscope Traces Showing Effect of Axial Position on Smooth Foil Deflection

REPRODUCIBILITY OF THE
ORIGINAL PAGE IS GUARANTEED

band in the center of the bearing. The "dipping" of the smooth foil between the bumps was shown analytically in Reference [2] to be detrimental to bearing operation in that the more flexible the smooth foil, the smaller the predicted minimum film thickness. The axial grooves formed by the "dipping" can be seen to provide a source of escape for the air which would tend to diminish the buildup of hydrodynamic pressure. The film thickness profile traces reveal that the "dipping" is significantly more than anticipated in the design analysis and does affect the load capacity of the bearing.

The amount of smooth foil deflection can be controlled by varying bearing design parameters such as bump geometry or smooth foil thickness. Decreasing the bump pitch will reduce smooth foil deflection, however, the bearing stiffness and damping characteristics will also change. Increasing smooth foil thickness again will reduce "dipping", but will decrease bearing conformability and compliance.

The program schedule did not allow extensive testing to be conducted to experimentally determine the amount of increased load capacity that could be obtained by minimizing smooth foil deflection. One test was however conducted. A bearing was fabricated with the bump foil inverted as shown in Figure VII-17. This allowed the smooth foil to be supported over a 1.02 mm (0.040 inch) wide flat rather than at a line and effectively decreased the unsupported span of the smooth foil. During testing with the conventional Hydresil, the maximum steady state load capacity obtained at 45,000 rpm was $1.4 \times 10^5 \text{ N/m}^2$ (20.4 psi). Further attempts to increase the load resulted in a high speed rub. Utilizing the bearing with the inverted bump foil, a load of $1.65 \times 10^5 \text{ N/m}^2$ (24.0 psi) was obtained prior to a high speed rub occurring. Also shown in Figure VII-17 is a typical oscilloscope trace obtained during testing with the modified bearing. In the loaded region, the trace shows a minimal amount of smooth foil "dipping" and exhibits a different wave form than the conventional bearings. The wave form resembles the schematic shown below the oscilloscope trace. While inverting the bump foil did in this case increase the bearing load capacity, it may have other effects that might be detrimental to normal bearing operation. It did show however, that minimizing smooth foil dipping would increase bearing load capacity.



BUMP FOIL INVERTED
 L/D = 1
 TEST SPEED: 45,000 RPM
 TEST LOAD: 1.3×10^5 N/m²
 (18.9 PSI)

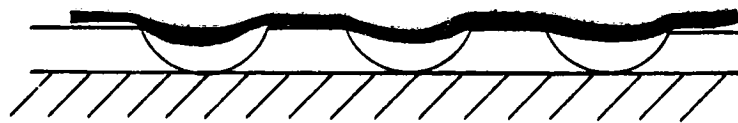


Fig. VII-17 Hydresil Bearing With Inverted Bump Foil

Changes in Film Thickness due to Test Parameters

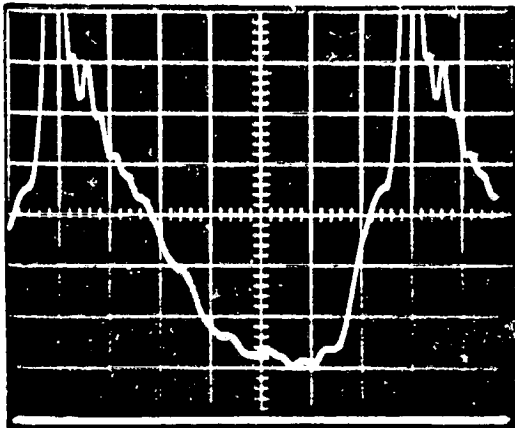
Test speed and load were varied in the program to determine the effects on minimum film thickness. During each test, the speed was maintained constant and the load increased in small increments. Figures VII-18 and VII-19 show the oscilloscope traces obtained at the same speed for three different load conditions for the $L/D = 1$ and $L/D = 1/2$ test bearings. Increased load decreased the film thickness in all cases.

One of the basic advantages of the compliant bearing is its ability to deflect under load and conform to the journal. This feature allows the load to be distributed over a relatively large area giving the compliant bearing greater load capacity than a rigid surface bearing. The oscilloscope traces shown in Figure VII-18 illustrate the load being distributed over a larger area with increased load. In Trace A the bearing is lightly loaded and the load support region, which coincides with the minimum film thickness, is approximately 25° (1 div = $\approx 50^\circ$) of the bearing. The bearing is heavily loaded in Trace C and the load support region has increased to approximately 85° of the bearing.

An expanded plot of a typical film thickness trace for the compliant surface bearing is shown in Figure VII-20. A comparison of Figure VII-20 with Figure VII-4, which is a similar plot for the rigid surface plain sleeve bearing, illustrates the vast difference in the load support region of the two bearings.

Figure VII-21 is a polar plot of the film thickness profile for the compliant test bearing. Indicated on the plot at Position ① is the start of the loose end of the smooth foil. At Position ② a "hump" appears. This "hump" is believed to be caused by the end of both the bump and smooth foils not being properly formed to the bearing diameter. Forming techniques now used produce a straight section at the end of the smooth foil which is believed to be the cause. Examination of bearings that have been tested, both in this program and others, show distinct polishing of the dry film in this area. The region of minimum film thickness which encompasses 80° of the bearing is shown at Position ③. The approximate location of the last support bump is indicated at Position

REPRODUCIBILITY OF THE
ORIGINAL PAGE IS POOR



A

L/D = 1

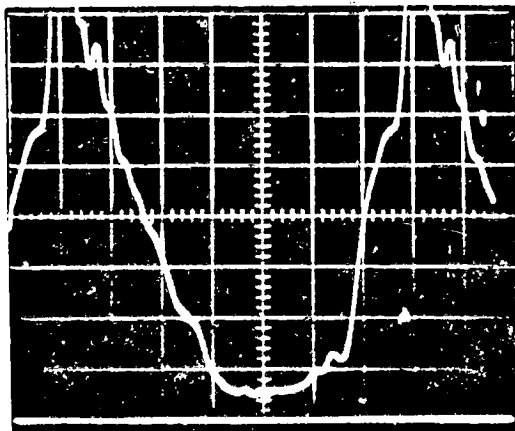
TEST SPEED: 30,000 RPM

TEST LOAD: $3.03 \times 10^3 \text{ N/m}^2$
(.44 PSI)

MINIMUM FILM

THICKNESS: $13.97 \mu\text{m}$
($550 \mu\text{IN.}$)

C: 0.0318 mm
(0.00125 IN.)



B

L/D = 1

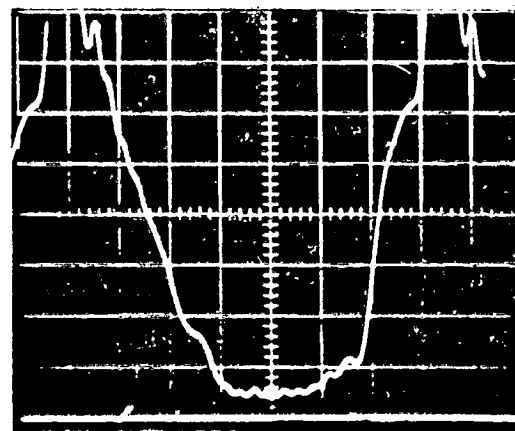
TEST SPEED: 30,000 RPM

TEST LOAD: $8.04 \times 10^4 \text{ N/m}^2$
(11.67 PSI)

MINIMUM FILM

THICKNESS: $6.35 \mu\text{m}$
($250 \mu\text{IN.}$)

C: 0.0318 mm
(0.00125 IN.)



C

L/D = 1

TEST SPEED: 30,000 RPM

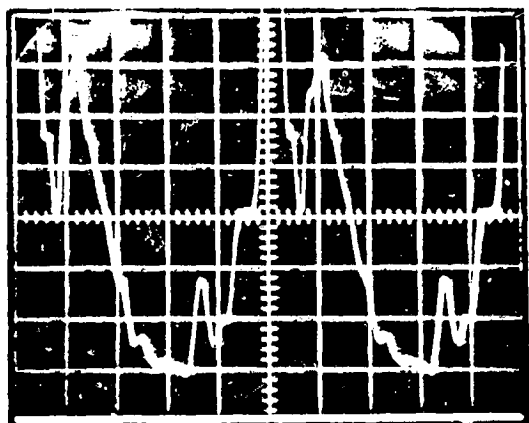
TEST LOAD: $9.86 \times 10^4 \text{ N/m}^2$
(14.3 PSI)

MINIMUM FILM

THICKNESS: $5.59 \mu\text{m}$
($220 \mu\text{IN.}$)

C: 0.0318 mm
(0.00125 IN.)

Fig. 11-10. Typical results of the film thickness measurement technique for a
lubricated journal bearing. The test conditions are: L/D = 1, 30,000 RPM, 0.0318 mm
C, and 0.44, 11.67, and 14.3 PSI test loads.

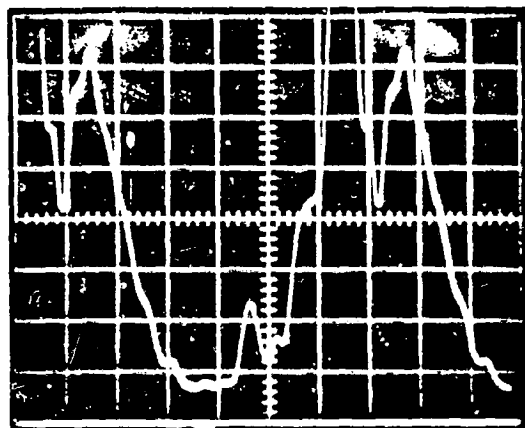


A

L/D = 1/2
 TEST SPEED: 45,000 RPM
 TEST LOAD: $6.13 \times 10^3 \text{ N/m}^2$
 (.89 PSI)

MINIMUM FILM
 THICKNESS: $10.67 \mu\text{m}$
 ($420 \mu\text{IN.}$)
 C: 0.0318 mm
 (.00125 IN.)

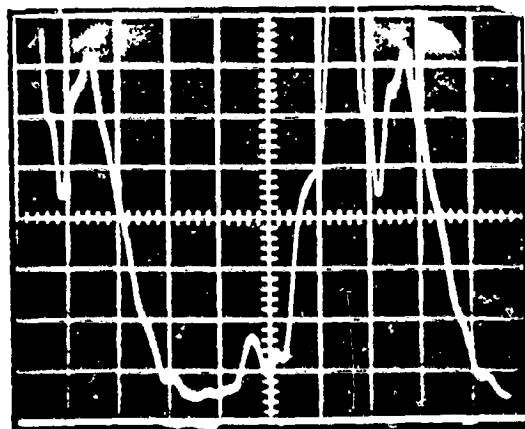
REPRODUCIBILITY OF THE
 ORIGINAL PAGE IS POOR



B

L/D = 1/2
 TEST SPEED: 45,000 RPM
 TEST LOAD: $3.83 \times 10^4 \text{ N/m}^2$
 (5.56 PSI)

MINIMUM FILM
 THICKNESS: $6.99 \mu\text{m}$
 ($275 \mu\text{IN.}$)
 C: 0.0318 mm
 (0.00125 IN.)



C

L/D = 1/2
 TEST SPEED: 45,000 RPM
 TEST LOAD: $8.85 \times 10^4 \text{ N/m}^2$
 (12.84 PSI)

MINIMUM FILM
 THICKNESS: $4.83 \mu\text{m}$
 ($190 \mu\text{IN.}$)
 C: 0.0318 mm
 (0.00125 INCH)

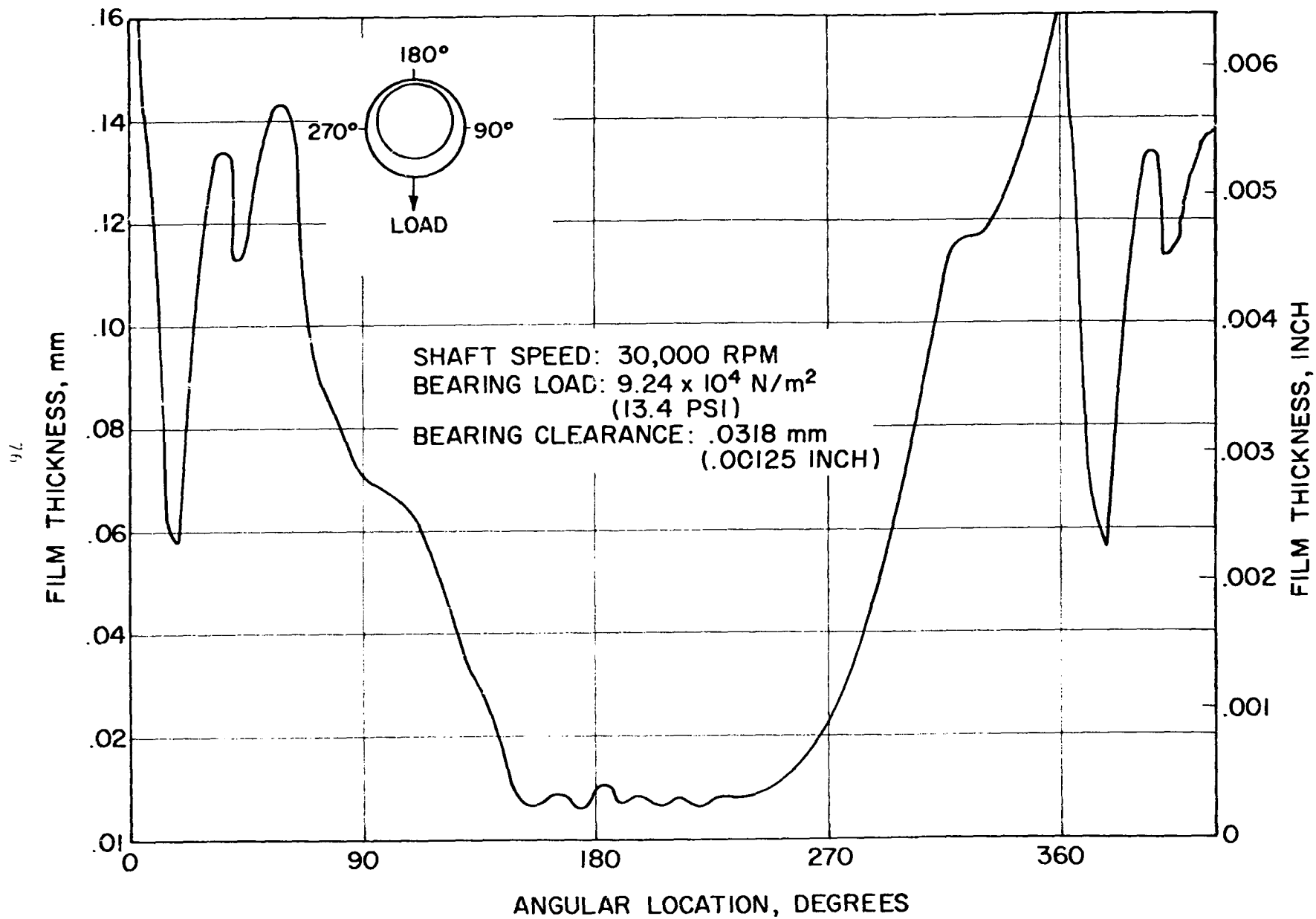


Fig. VII-20 Expanded Plot of Film Thickness Profile, Compliant Surface Bearing

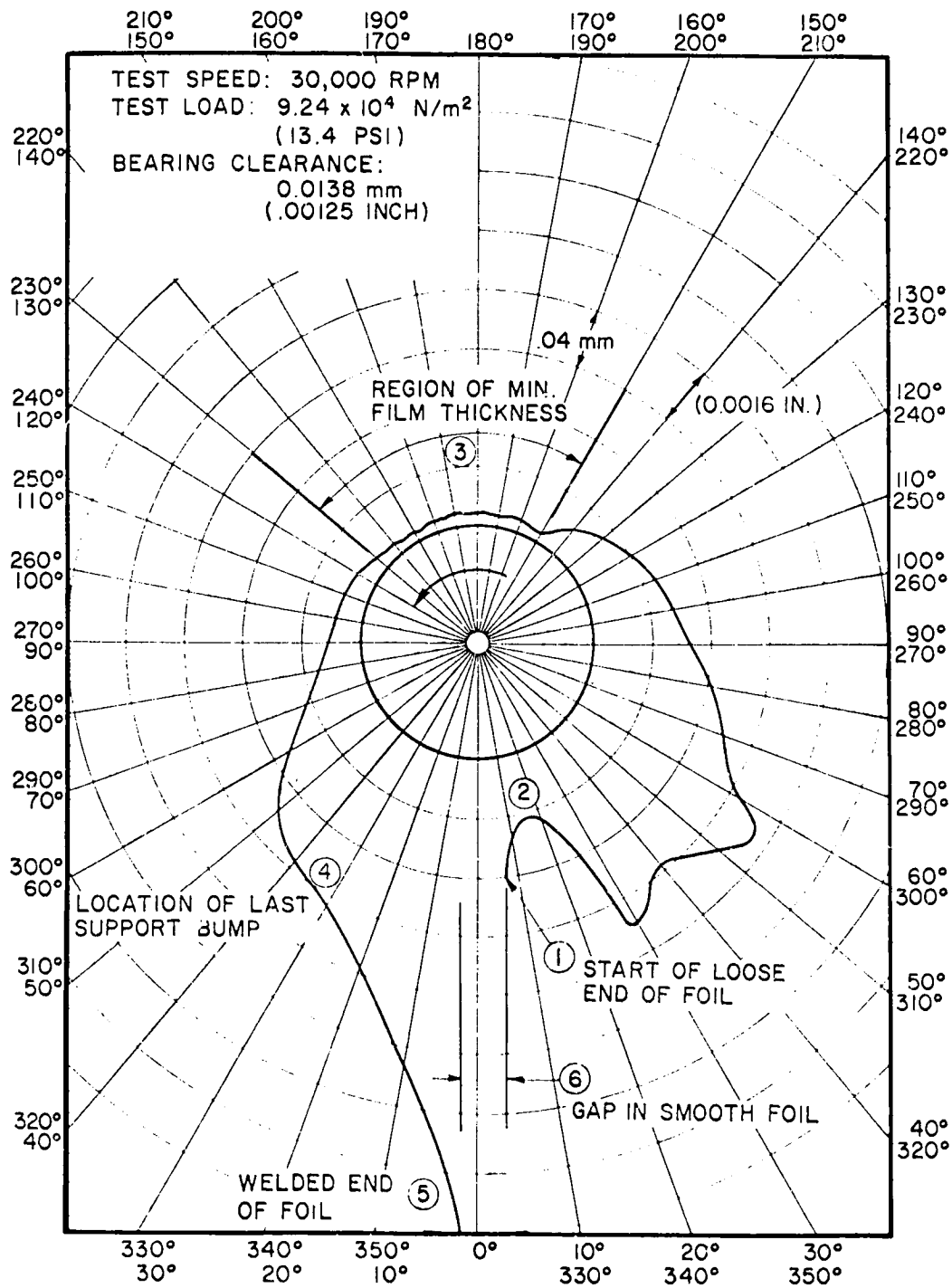


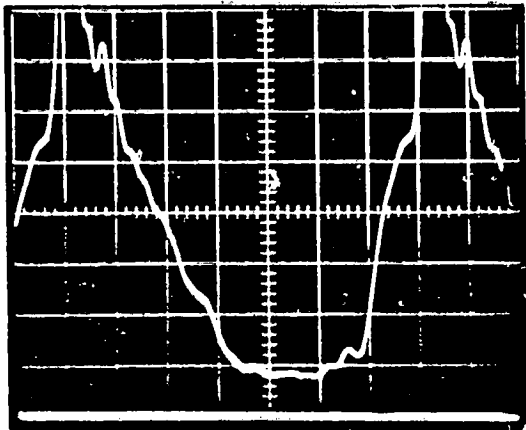
Fig. VII-21 Polar Plot of Film Thickness Profile, Compliant Surface Bearing

④. The smooth foil is welded to a spacer block which is 0.23 mm (.009 inch) smaller in height than the bump foil. The sharp change in the film profile between Positions ④ and ⑤ is due to the height difference between the bump foil and spacer block. The gap in the smooth foil which is equivalent to one bump pitch, 13° , is located at Position ⑥. Comparing Figure VII-21 with Figure VII-5 again illustrates the vast difference in film profiles of compliant and rigid surface bearings.

Bearing load capacity or minimum film thickness increases with increasing speed at a constant load. Figure VII-22 shows the oscilloscope traces for the film thickness profile obtained for three speeds at a constant load. At almost all test points, film thickness increased with increased speed. The test points obtained at high loads at 60,000 rpm with the $L/D = 1$, $C = 0.057$ mm (0.00225 inch) test bearing had approximately the same film thickness values as those obtained with the same bearing at the 45,000 rpm speed condition. This was believed to be caused by the increased shaft motion which occurred at 60,000 rpm. The increased shaft motion, which was discussed earlier in this section, was thought to be adding dynamic loads to the bearing. In the subsequent testing sequences, the maximum test speed was 55,000 rpm and, in all cases, the minimum film thickness value increased with increased speed. Increased rotor speed at constant load also varies the internal size of the bearing. Figure VII-23 is a polar plot showing the film thickness profile for the three speeds at a constant load. The plots indicate that as speed increases the internal bearing size increases.

Bearing attitude angle

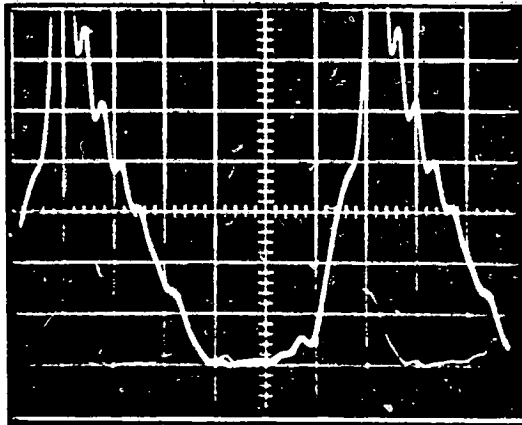
The test bearing attitude angle was obtained utilizing the oscilloscope trace of the film thickness profile. Angular orientation of the oscilloscope trace to the bearing was made by referencing the discontinuity in the trace to the gap in the smooth foil which was located 180° from the point where the load was being applied. The attitude angle is defined as the angle between the load line and the line between the bearing and journal centers. Using the oscilloscope traces the attitude angle was scaled as the angle between the load line and the midpoint of the region where the minimum film thickness occurs as shown in Figure VII-24. Table VII-8 is a summary of attitude angles obtained. These attitude angles are considerably less than in rigid surface bearings.



L/D = 1
 TEST SPEED: 30,000 RPM
 TEST LOAD: 4.34×10^4 N/m²
 (6.3 PSI)

MINIMUM FILM
 THICKNESS: 9.27 μ m
 (365 μ IN.)
 C: 0.0318 mm
 (0.00125 IN.)

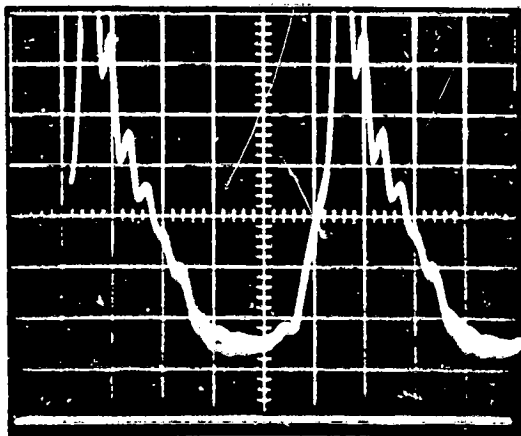
A



L/D = 1
 TEST SPEED: 45,000 RPM
 TEST LOAD: 4.34×10^4 N/m²
 (6.3 PSI)

MINIMUM FILM
 THICKNESS: 11.56 μ m
 (455 μ IN.)
 C: 0.0318 mm
 (0.00125 IN.)

B



L/D = 1
 TEST SPEED: 55,000 RPM
 TEST LOAD: 4.34×10^4 N/m²
 (6.3 PSI)

MINIMUM FILM
 THICKNESS: 16.38 μ m
 (645 μ IN.)
 C: 0.0318 mm
 (0.00125 IN.)

C

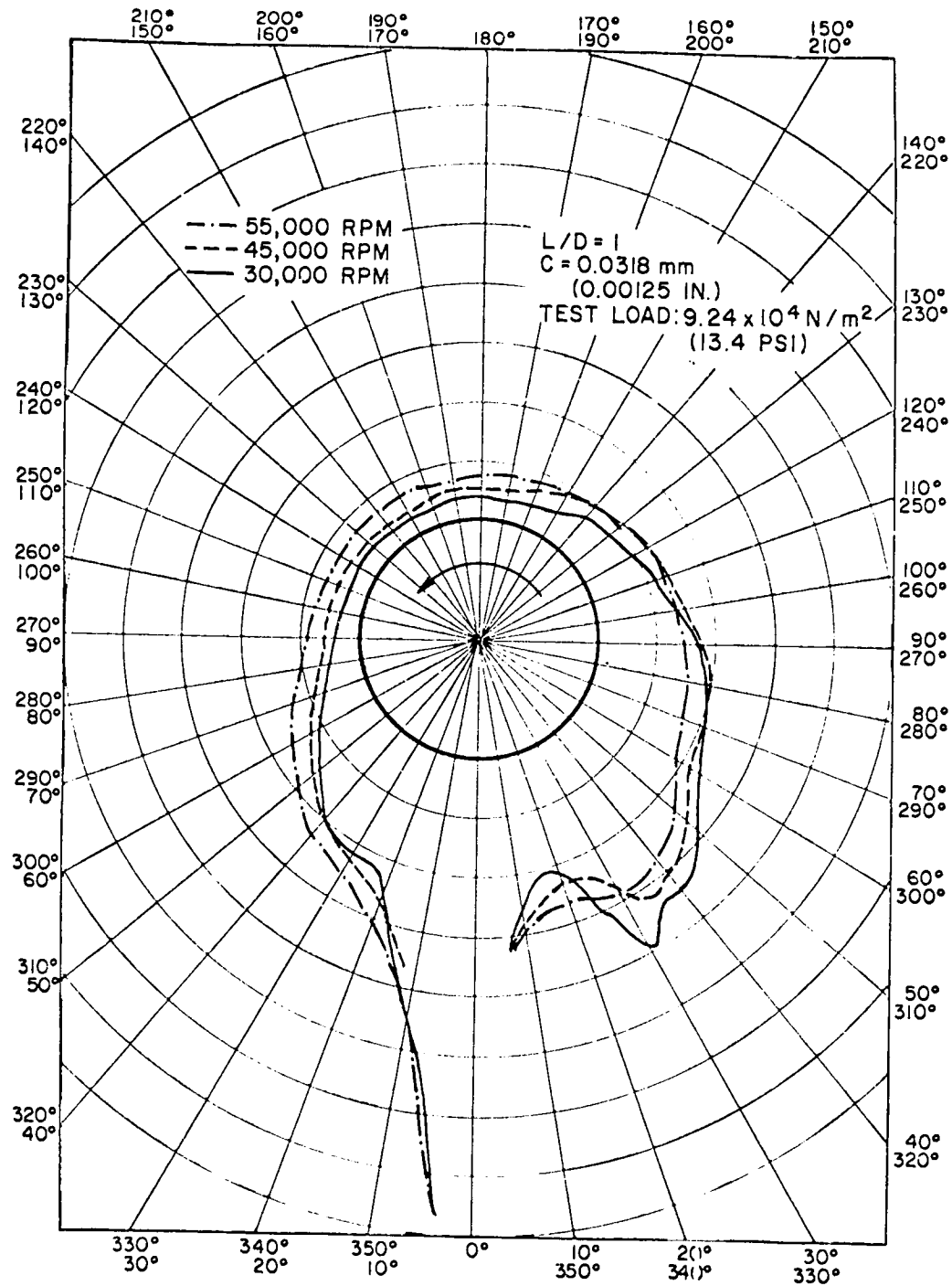


Fig. VII-23 Polar Plot Showing Effect of Speed on Internal Size of Compliant Surface Bearing

L/D = 1
 TEST SPEED: 30,000 RPM
 TEST LOAD: $3.03 \times 10^3 \text{ N/m}^2$
 (.44 PSI)

LOAD IS APPLIED AT 0°

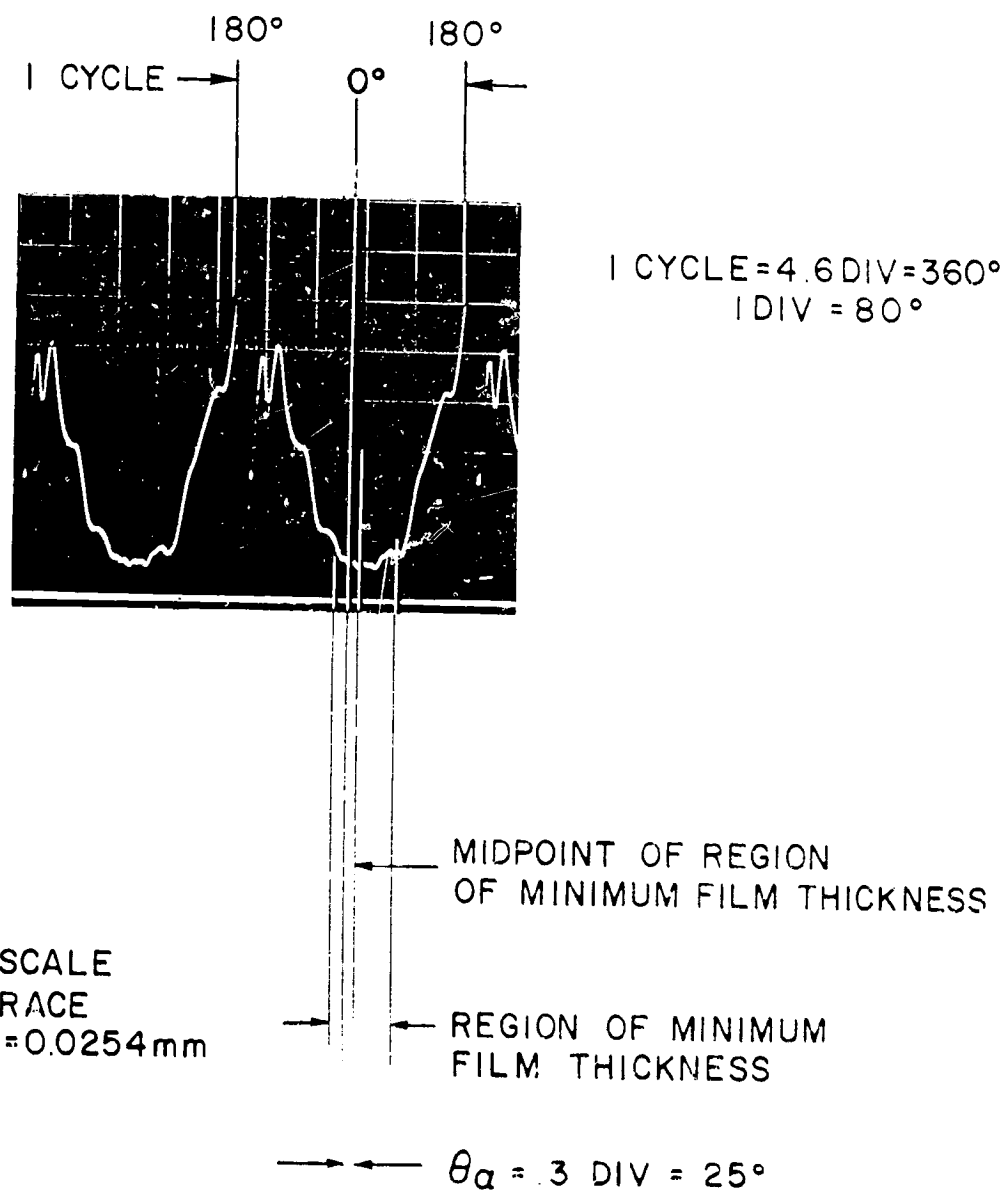


Fig. A11-24 Oscilloscope Film Thickness Trace Showing Method Used to Obtain At Grade Angle, Compliant Contact, etc.

TABLE VII - 8
TABULATED DATA FOR BEARING ATTITUDE ANGLE

L/D = 1; L x D = 14.6 cm² (2.25 in²) Test Speed: As Indicated
 Bearing Clearance: 0.0318 mm Test Temperature: Room Ambient
 (0.00125 inch)

N	Bearing Load	Speed	Attitude Angle
	pounds	rpm	degrees
4.4	1.0	30,000	25
41.1	9.25	30,000	20
63.4	14.25	30,000	18
90.1	20.25	30,000	15
116.8	26.25	30,000	13
142.3	32.0	30,000	12
18.9	4.25	45,000	25
63.4	14.25	45,000	22
98.3	22.1	45,000	18
135.4	30.45	45,000	15
163.0	36.65	45,000	14
18.9	4.25	55,000	28
63.4	14.25	55,000	25
107.0	24.05	55,000	22
142.3	32.05	55,000	17
169.0	38.0	55,000	15

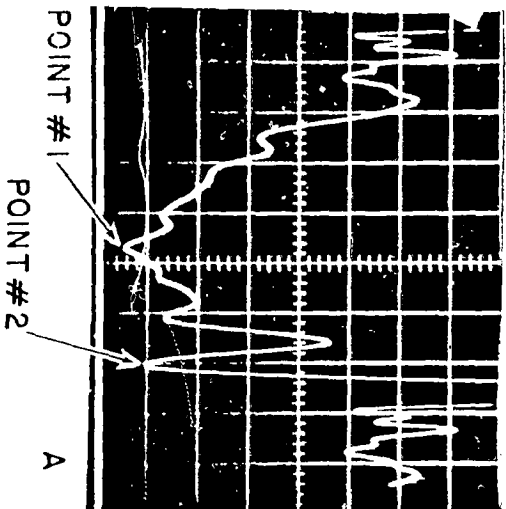
Influence of bearing accuracy on performance

The nature of the compliant surface bearing does not allow for an accurate dimensional inspection to be made after the bearing is fabricated. Components which make up the bearing such as bump and smooth foils and bearing cartridge are inspected prior to assembly, but a certain amount of art is still involved in the assembly procedure. Because of the small air film, minor discrepancies in the bearing can have a significant influence on performance. Normally, the discrepancies would not be noticed unless maximum bearing performance was sought. However, the rotating sensor system allowed bearing discrepancies to be readily noticed.

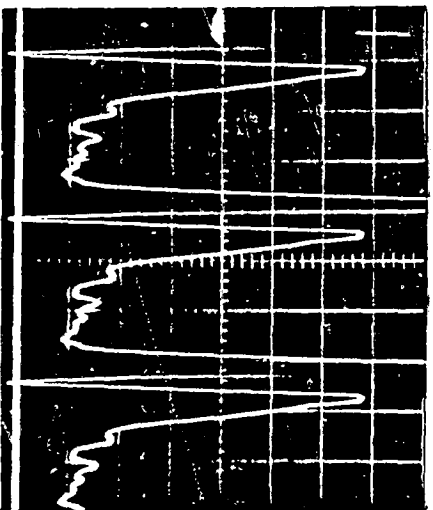
Trace A in Figure VII-25 shows the film thickness profile of a bearing which did not have a typical film thickness profile. The bearing operated normally under light loads and would have been considered a serviceable bearing had it not been for the film thickness trace. Close inspection of the bearing after running revealed that the bump foil had not properly conformed to the bearing cartridge creating a local high spot at Point #1 shown on the trace. The bearing also contained a clearance adjustment shim which was installed too close to the spacer block creating another irregularity in the bearing at Point #2. Trace B in Figure VII-25 shows the resulting film thickness profile when the loose end of the smooth foil is not properly formed. In this bearing, the loose end had a smaller radius than the bearing and air was drawn in under the smooth foil causing the very end of the smooth foil to contact the shaft. In another case, an irregular film profile was obtained which could not be completely explained as shown in Trace C of Figure VII-25.

The results of these tests indicate fabrication accuracy may be a potential problem with the compliant surface bearing for high performance applications such as the automotive gas turbine. Insights gained through this program, such as proper conformity of the smooth foil in the inlet region, have allowed advances to be made in eliminating this problem. It is also felt that with sufficient tooling, of the type that would be required for volume production, proper and consistent forming of the foils can be accomplished and accurate bearings can be fabricated.

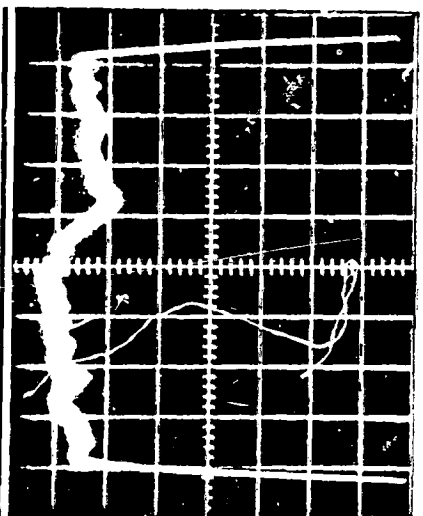
REPRODUCIBILITY OF THE
ORIGINAL PAGE IS POOR



L/D = 1
TEST SPEED: 30,000 RPM
TEST LOAD: 2.8×10^4 N/m²
(4.1 PSI)
C: 0.0318 mm
(0.00125 in)



L/D = 1
TEST SPEED: 30,000 RPM
TEST LOAD: 1.3×10^4 N/m²
(1.9 PSI)
C: 0.0318 mm
(0.00125 in)



L/D = 1
TEST SPEED: 30,000 RPM
TEST LOAD: 1.9×10^4 N/m²
(2.7 PSI)
C: 0.0318 mm
(0.00125 in)

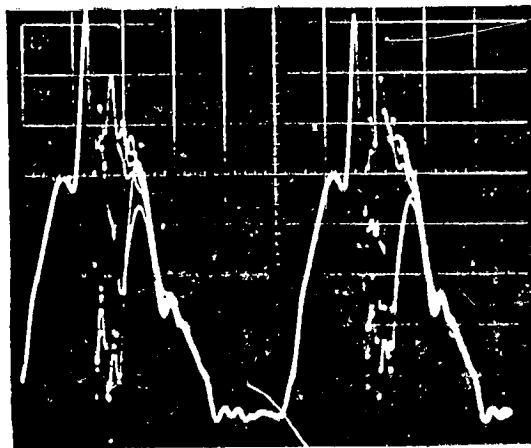
Foil excitation by cooling air

Shown in Figure VII-26 is an oscilloscope trace of the film thickness profile for a lightly loaded test bearing. In this test, a larger than normal flow of cooling air was introduced to the bearing. As the air entered the bearing, it excited the free end of the smooth foil causing it to vibrate and produce a audible high frequency pitch. Although there was no noticeable effect on bearing operation, if operation continued under these conditions, the smooth foil could have eventually failed under high cycle fatigue. The problem corrected itself when either the load was increased or the cooling air flow was reduced to the normal level.

This test illustrates the importance of properly designing the cooling air supply system. A discussion of various methods for supplying cooling air to the bearing is contained later in this section.

REPRODUCIBILITY OF THE
ORIGINAL PAGE IS POOR

REPRODUCIBILITY OF THE
ORIGINAL PAGE IS POOR



EXCITATION OF FREE END OF TOP FOIL
BY COOLING AIR SUPPLY

FIG. VII-25. (a) Free end of foil in air supply. (b) Smooth foil in air supply.

HIGH TEMPERATURE TESTS

The final series of tests were conducted at an ambient and bearing temperature of 315°C (600°F). These tests were conducted to measure the bearing cooling air flow requirements and to determine the effect of possible thermal distortion on bearing performance. For the tests, a solid non-instrumented test shaft with a plasma sprayed chrome carbide coating on the test journal surface was to be utilized. After initial testing, the chrome carbide was removed from the test journal for reasons discussed later in this section, and an uncoated wrought steel test journal was used.

The testing was conducted as follows: the test bearing housing temperature was maintained constant throughout the test at 315°C (600°F); the test bearing cooling air temperature was maintained constant at 205°C (400°F); and the test bearing temperature, which was measured on the back of the bump foil, was maintained constant at 315°C (600°F) by varying the quantity of cooling air supplied to the test bearing. While maintaining a constant test speed the bearing load was increased. Temperatures were allowed to stabilize, and adjustments were made to the cooling air flow to maintain the constant test bearing temperature. Testing was conducted at three (3) speeds: 30,000 rpm; 39,000 rpm; and 45,000 rpm.

Temperatures selected were chosen to be representative of temperatures anticipated in an automotive gas turbine engine.

RESULTS FOR ELEVATED TEMPERATURE TESTING

Test data for selected elevated temperature tests are shown in tabulated form in Tables VII-9 through VII-11. The complete bearing cooling air flow test data is presented in the graph of Figure VII-27. Figure VII-28 is a typical trace of the test bearing temperature, which shows it was maintained relatively constant throughout the testing. The test points noted correspond to the test conditions tabulated in Tables VII-10 and VII-11.

The final test conducted at the 315°C (600°F) temperature was for the

TABLE VII-9
COMPLIANT BEARING DATA FROM TEST #219

L/D = 1; LXD = 14.6 cm² (2.25 in.²)
 Bearing Clearance: 0.0318 mm
 (0.00125 in.)

Test Speed: 30,000 RPM
 Test Temperature: 315.6°C
 (600°F)

Bearing Load		Floating Housing Temp.		Test Bearing Temp.		Bearing Cooling Air Temp.		Cooling Air Flow	
N	lb	°C	°F	°C	°F	°C	°F	kg/min.	lb./min.
8.9	2	312.8	595	320.0	608	210.0	410	0.041	0.092
17.8	4	316.7	602	321.1	610	212.2	414	0.042	0.094
40.0	9	317.2	603	321.1	610	212.8	415	0.042	0.094
62.3	14	321.7	611	323.3	614	213.3	416	0.043	0.096
89.0	20	320.0	608	321.1	610	207.2	405	0.044	0.098
111.2	25	310.6	591	318.3	605	202.8	397	0.046	0.103

8 21472 UNGLAS

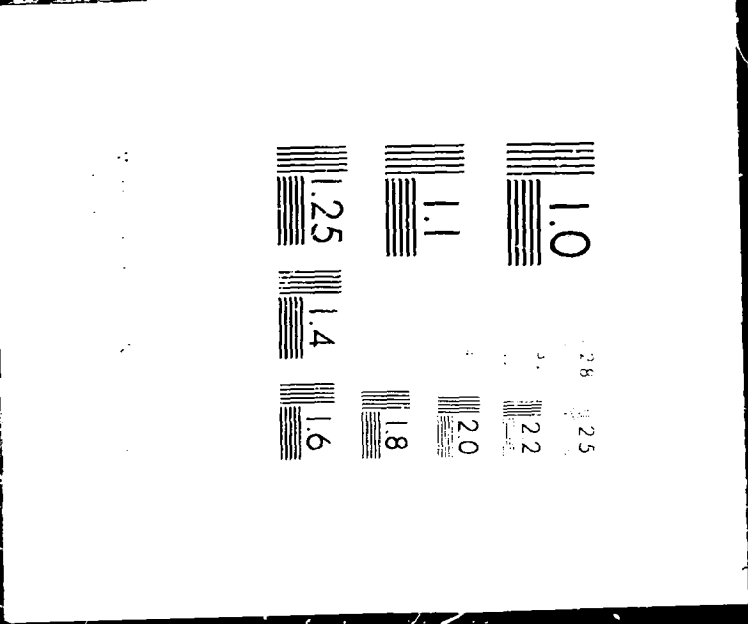


Table VII-10
COMPLIANT BLARING DATA FROM TEST # 220

L/D = 1; L x D = 14.6 cm² (2.25 in²)
 Bearing Clearance: 0.0318 mm
 (0.00125 in)

Test Speed: 39,000 RPM
 Test Temperature: 315.6 °C
 (600 °F)

Test Point Fig. VII-28	Bearing Load		Floating Housing Temp.		Test Bearing Temp.		Bearing Cooling Air Temp.		Cooling Air Flow	
	N	lb	°C	°F	°C	°F	°C	°F	kg/min	lb/min
①	8.9	2	315.0	599	321.1	610	204.4	400	0.043	0.096
②	31.1	7	315.0	599	319.4	607	205.6	402	0.044	0.098
③	53.4	12	320.6	609	321.1	610	206.7	404	0.046	0.103
④	75.6	17	318.3	605	319.4	607	203.3	398	0.048	0.105
⑤	97.9	22	316.7	602	319.4	607	203.9	399	0.049	0.107
⑥	120.1	27	317.8	604	319.4	607	206.7	404	0.051	0.113
⑦	142.3	32	321.1	610	323.3	614	207.2	405	0.053	0.117

Table VII-11
COMPLIANT BEARING DATA FROM TEST # 220

I/D = 1; L x D = 14.6 cm² (2.25 in²)
 Bearing Clearance: 0.0318 mm
 (0.00125 in)

Test Speed: 45,000 RPM
 Test Temperature: 315.6°C
 (600°F)

Test Point	Bearing Load		Floating Housing Temp.		Test Bearing Temp.		Bearing Cooling Air Temp.		Cooling Air Flow	
	N	lb	°C	°F	°C	°F	°C	°F	kg/min	lb/min
Fig. VII-28 ⑧	8.9	2	315.6	600	321.1	610	210.0	410	0.053	0.116
⑨	31.1	7	317.2	603	322.8	613	208.3	407	0.053	0.116
⑩	53.4	12	315.6	600	321.1	610	203.9	399	0.054	0.118
⑪	75.6	17	313.3	596	322.2	612	208.9	408	0.058	0.128
⑫	97.9	22	313.9	597	322.8	613	206.1	403	0.059	0.130
⑬	120.1	27	313.9	597	322.8	613	204.4	400	0.059	0.130
⑭	142.3	32	313.9	597	322.8	613	204.4	400	0.069	0.154
⑮	164.5	37	311.7	593	322.8	613	209.4	409	0.077	0.171

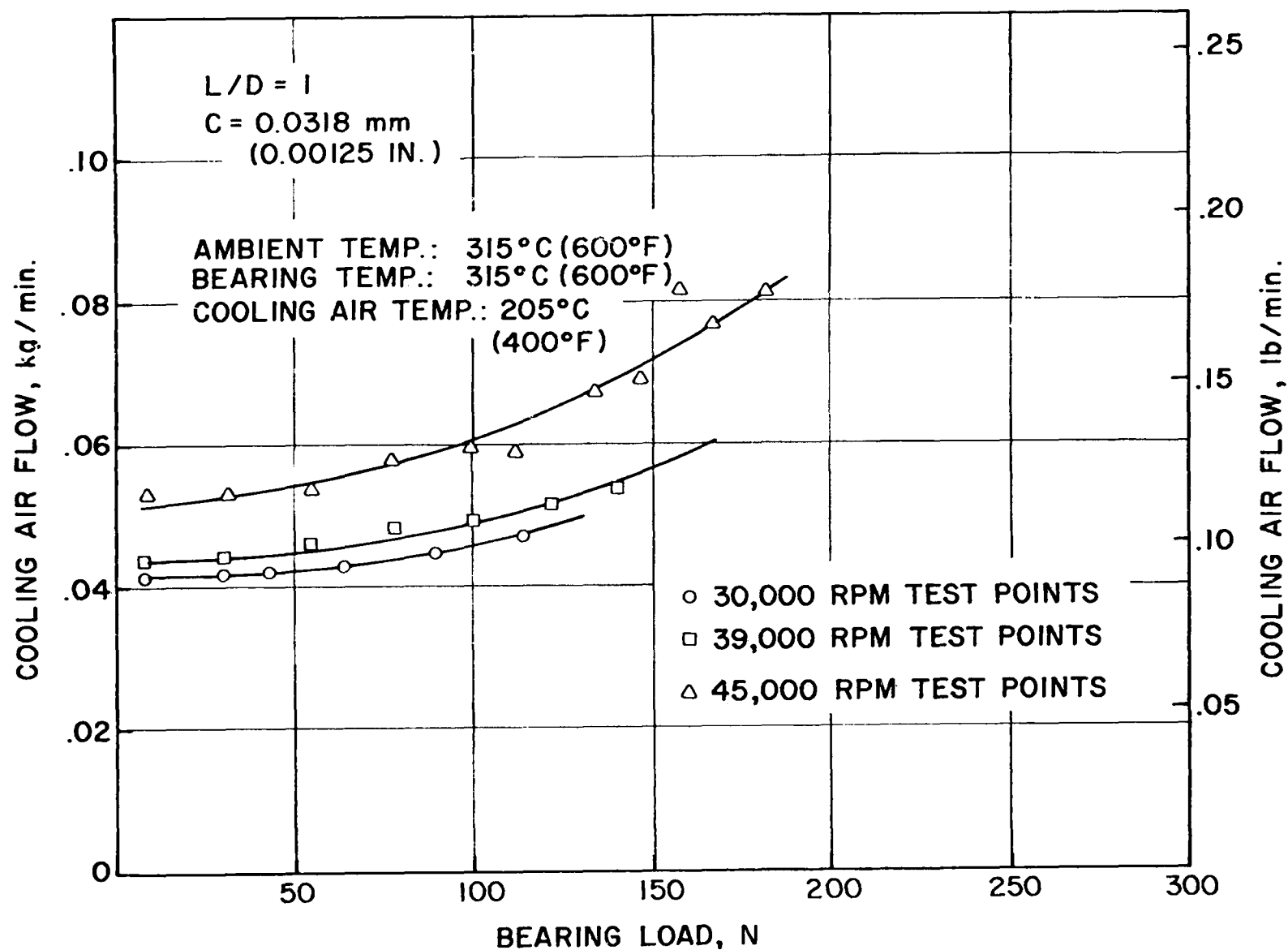
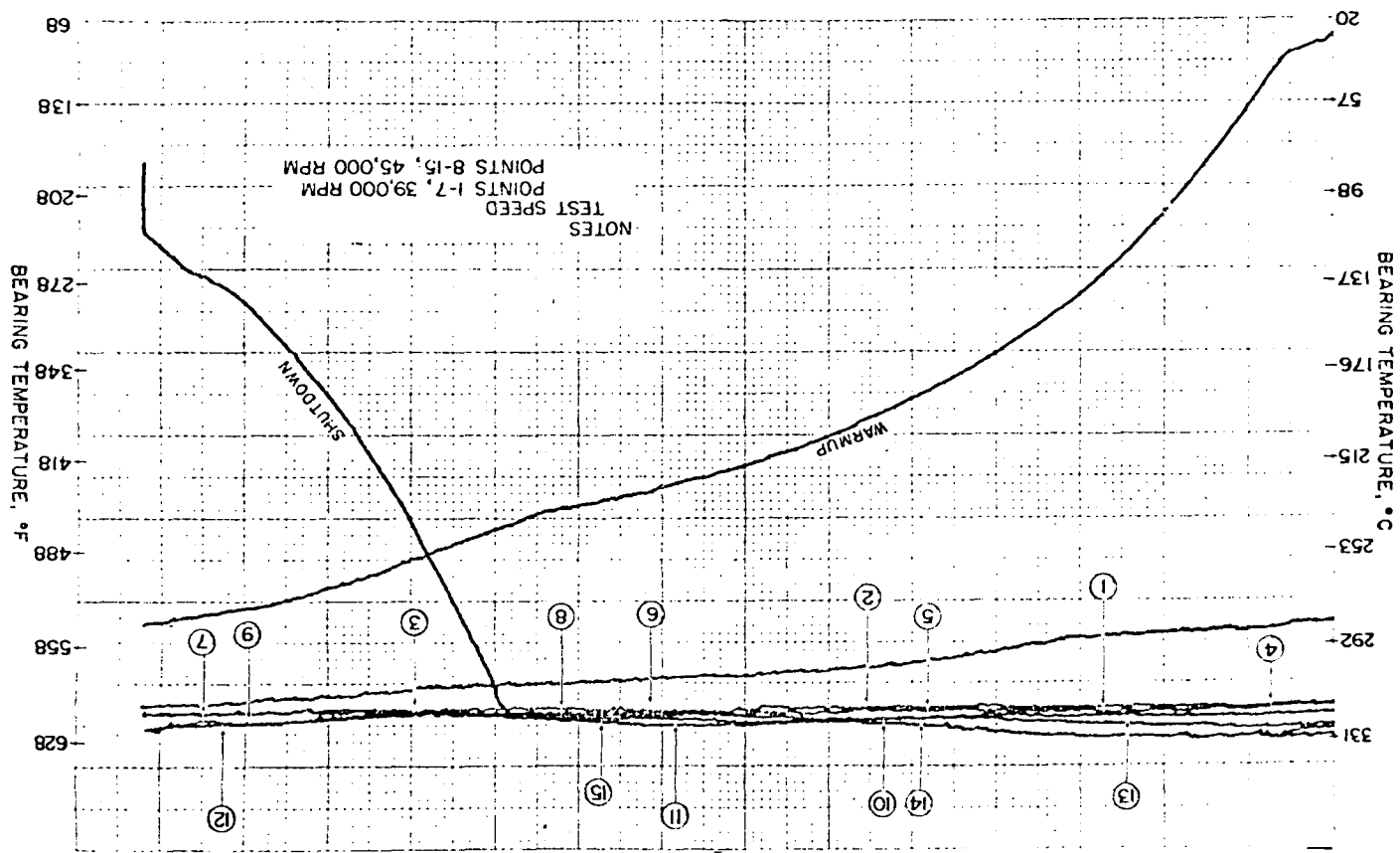


Fig. VII-27 Experimental Data for Bearing Cooling Air Requirements for Compliant Surface Bearing at 315°C

FIG. VII-28 Typical Trace of Test Bearing Temperature



purpose of obtaining the maximum bearing load performance capacity. A test speed of 45,000 rpm was selected, which corresponded with the test speed used when the maximum bearing load was obtained during testing at room temperature. The load was increased in 8.9 N (2 pound) increments, and the bearing temperature was allowed to stabilize. Figure VII-29 is the temperature trace for this test. The test points correspond to those tabulated in Table VII-12. A steady state load of $1.75 \times 10^5 \text{ N/m}^2$ (25.4 psi) was achieved with satisfactory bearing operation. An additional load of 8.9 N (2 pounds) was then added, for a total load of $1.80 \times 10^5 \text{ N/m}^2$ (26.1 psi). The bearing supported this load for approximately three (3) minutes before the air film broke down, causing a high speed rub. In Figure VII-29, test point (11) corresponds to the time the final 8.9 N (2 pound) load was added. The sharp vertical rise in the temperature at point (12) is caused by the bearing rub. The temperature trace shows that no significant rise in temperature occurred prior to the rub, and thus there was no indication of an impending breakdown in the air film.

DISCUSSION OF ELEVATED TEMPERATURE TEST RESULTS

Three (3) items of significant importance were determined from the elevated temperature testing:

- Influence of journal surface porosity on bearing load performance.
- Relatively low bearing cooling air requirements.
- No noticeable effects of elevated temperatures on bearing performance.

A detailed discussion of these items follows.

Effects of Bearing Journal Surface Porosity on Bearing Load Performance

During initial testing, both at room temperature and at elevated temperature, the load performance capability of the test bearing was significantly below the capacity achieved during the film thickness measurement tests. It was determined through further testing that the cause of the reduced bearing performance was the chrome carbide coating on the test journal surface. Plasma sprayed coatings, when finish ground, can result in a relatively porous surface when compared to a wrought ground steel surface. Utilizing a Taly Surf, it was found that a qualitative comparison could be made of journal surfaces. Figure VII-30 shows Taly Surf traces for the

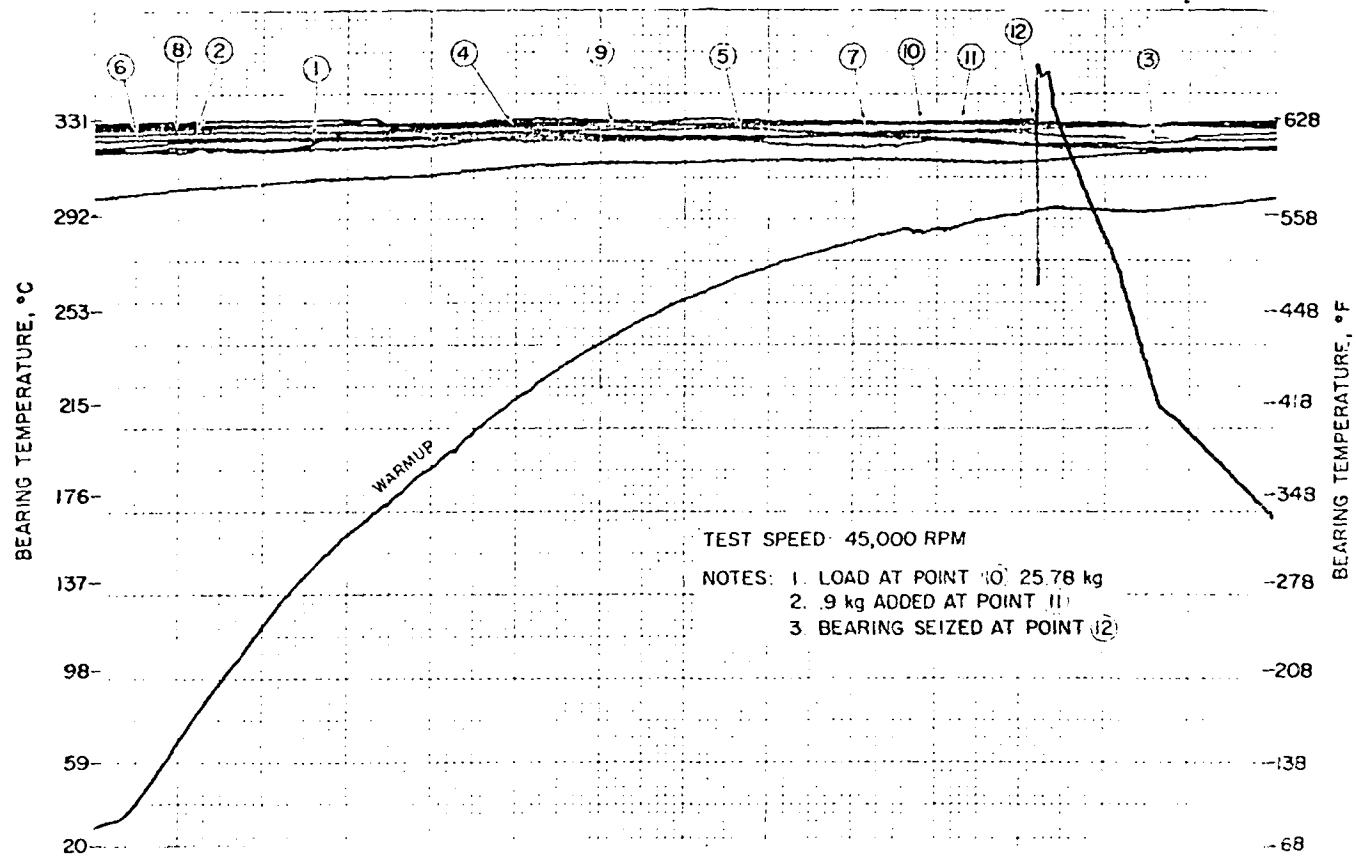


Fig. VII-29 Typical Trace of Test Bearing Temperature

Table VII-12
COMPLIANT BEARING DATA FROM TEST # 221*

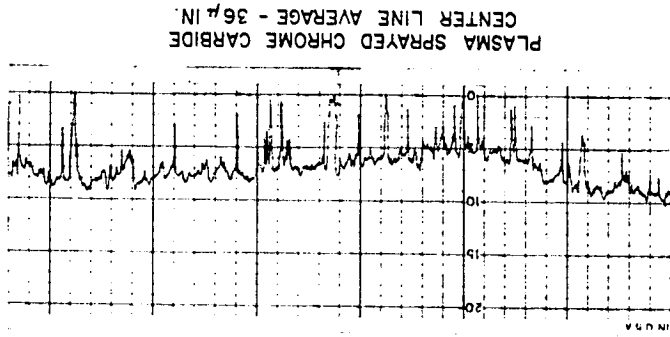
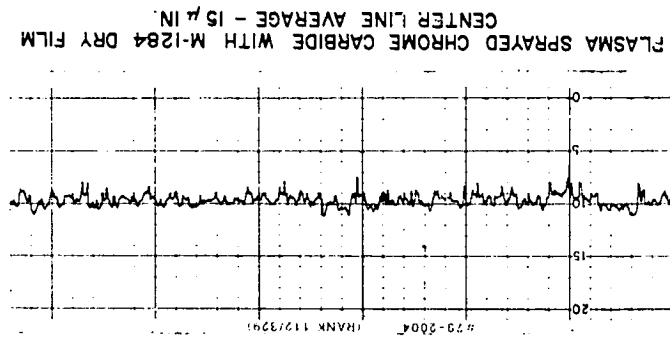
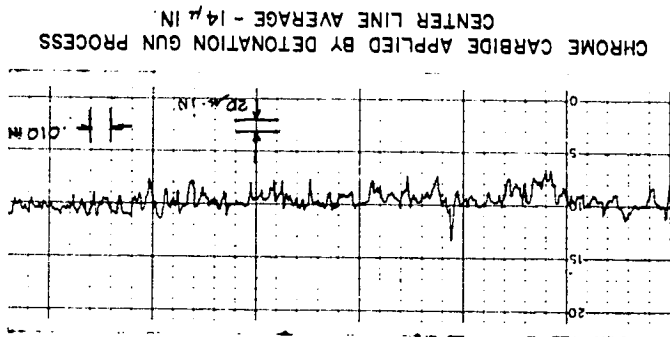
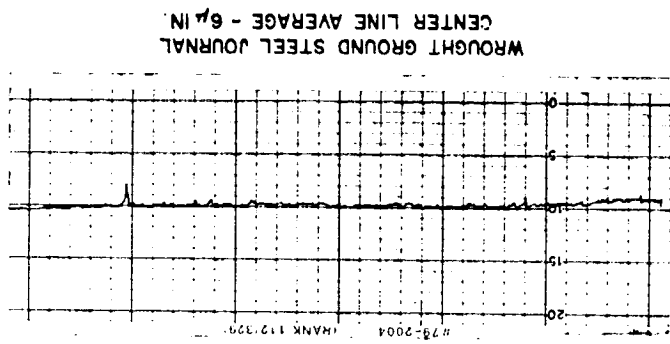
L/D = 1; L x D = 14.6 cm² (2.25 in²)
 Bearing Clearance = 0.0318 mm
 (0.00125 in)

Test Speed: 45,000 RPM
 Test Temperature: 315.6°C
 (600°F)

Test Point Fig. VII-29	Bearing Load		Floating Housing Temp.		Test Bearing Temp.		Bearing Cooling Air Temp.		Cooling Air Flow	
	N	lb	°C	°F	°C	°F	°C	°F	kg/min	lb/min
①	109.9	24.7	315.6	600	321.7	611	207.2	405	0.059	0.130
②	132.1	29.7	315.0	599	319.4	607	207.2	405	0.069	0.153
③	154.4	34.7	312.8	595	328.3	623	204.4	400	0.084	0.185
④	176.6	39.7	313.9	597	328.9	624	208.3	407	0.086	0.190
⑤	195.3	43.9	314.4	598	331.1	628	205.6	402	0.091	0.202
⑥	204.6	46.0	313.9	597	332.2	630	203.3	398	0.091	0.202
⑦	213.5	48.0	313.3	596	332.2	630	204.4	400	0.097	0.214
⑧	222.4	50.0	312.2	594	332.7	631	205.6	402	0.105	0.231
⑨	233.1	52.4	313.3	596	333.3	632	205.6	402	0.105	0.231
⑩	243.8	54.8	308.9	588	331.1	628	207.8	406	0.109	0.240
⑪	252.7	56.8	312.8	595	332.7	631	208.8	408	0.109	0.240
⑫	261.6	58.8	- Bearing siezed after 3 minutes at this load condition -							

* - The purpose of this test was to determine the maximum load capacity of the test bearing.

Fig. VII-30 Taly Surf Traces of Bearing Journal Surfaces



following journal surfaces:

- Chrome carbide coating applied by plasma spray process
- Same as above with dry film lubricant (Bohman M-1284) sprayed over the chrome carbide, then oven cured, and burnished smooth
- Chrome carbide coating applied by detonation gun process
- Wrought ground steel journal with no coating

The centerline average roughness reading is indicated on each trace and can also serve as another qualitative method for comparison of coating porosity, since roughness in the journal surface is predominately caused by depressions in the surface due to coating porosity.

The Taly Surf traces indicate that some voids in the coating surface are significantly large when compared to the minimum film thickness in the bearing. These large voids contribute in several ways to reducing bearing load performance. Basically they tend to create a dead air volume which will reduce the pressure generating capability of the bearing.

Tests to demonstrate the effect of journal surface porosity on load performance were conducted in the following manner: utilizing the same test bearing, two tests were conducted with all test conditions held constant; load was added to the test bearing in small increments until the bearing capacity was reached. The bearing capacity was defined to be the load after which any further increase in load would result in a sharp increase in test bearing temperature and/or a sharp decrease in rotational speed. During the first test, the test journal surface was plasma sprayed chrome carbide and the bearing load capacity was $5.51 \times 10^4 \text{ N/m}^2$ (8 psi) at 33,000 rpm. The test journal surface was then coated with dry film, oven cured, and burnished smooth. This procedure partially filled in the voids in the chrome carbide coating, creating a denser test journal surface. The test was repeated and the bearing load capacity was determined to be $7.58 \times 10^4 \text{ N/m}^2$ (11 psi). Based on this test, the test shaft for the high temperature testing was ground undersize to remove the chrome carbide and the bearing diameter adjusted to maintain the bearing clearance. Testing at elevated temperature was

therefore conducted on an uncoated wrought steel journal. During initial testing of the uncoated test journal at room temperature, a load of $8.62 \times 10^4 \text{ N/m}^2$ (12.5 psi) was supported at 30,000 rpm. The maximum load capacity was not determined at this time to avoid the risk of a high speed rub and damage to the soft journal surface.

Bearing Cooling Air Requirements

The experimental values obtained for the cooling air flow, shown in Figure VII-27, are considered to be very conservative requirements for typical compliant journal bearing applications for the following two reasons:

- The method of supplying the cooling air to the test bearing
- The requirement to maintain the ~~bearing temperature~~ the same as the ambient temperature.

Method of supplying cooling air

Test bearing cooling air for the high temperature testing was supplied through a flexible hose connected to the floating bearing housing at the top. The hose was suspended by springs, as shown in Figure VII-31, to eliminate the influence of the hose on test bearing alignment. The cooling air was manifolded to three (3) circumferential grooves in the floating housing which fed three (3) 2.3 mm (0.090 inch) diameter holes in the test bearing cartridge. The cooling air entered the test bearing at the gap in the smooth foil, between the welded and loose end, 180° from the load region.

This method of supplying cooling air to a journal bearing is, in most cases, not the most efficient manner. In many applications, the cooling air is best utilized in an arrangement which allows the cooling air to pass axially through the bearing. A typical cooling air configuration is shown in Figure VII-32. In this arrangement, the cooling air is introduced at one end of the bearing into a cavity, and forced to flow axially through the bump foil and air film to remove the heat generated by the bearing. In the method used for the test program, which is used in applications that do not incorporate seals, when the cooling air enters at the gap in the smooth foil a significant portion travels

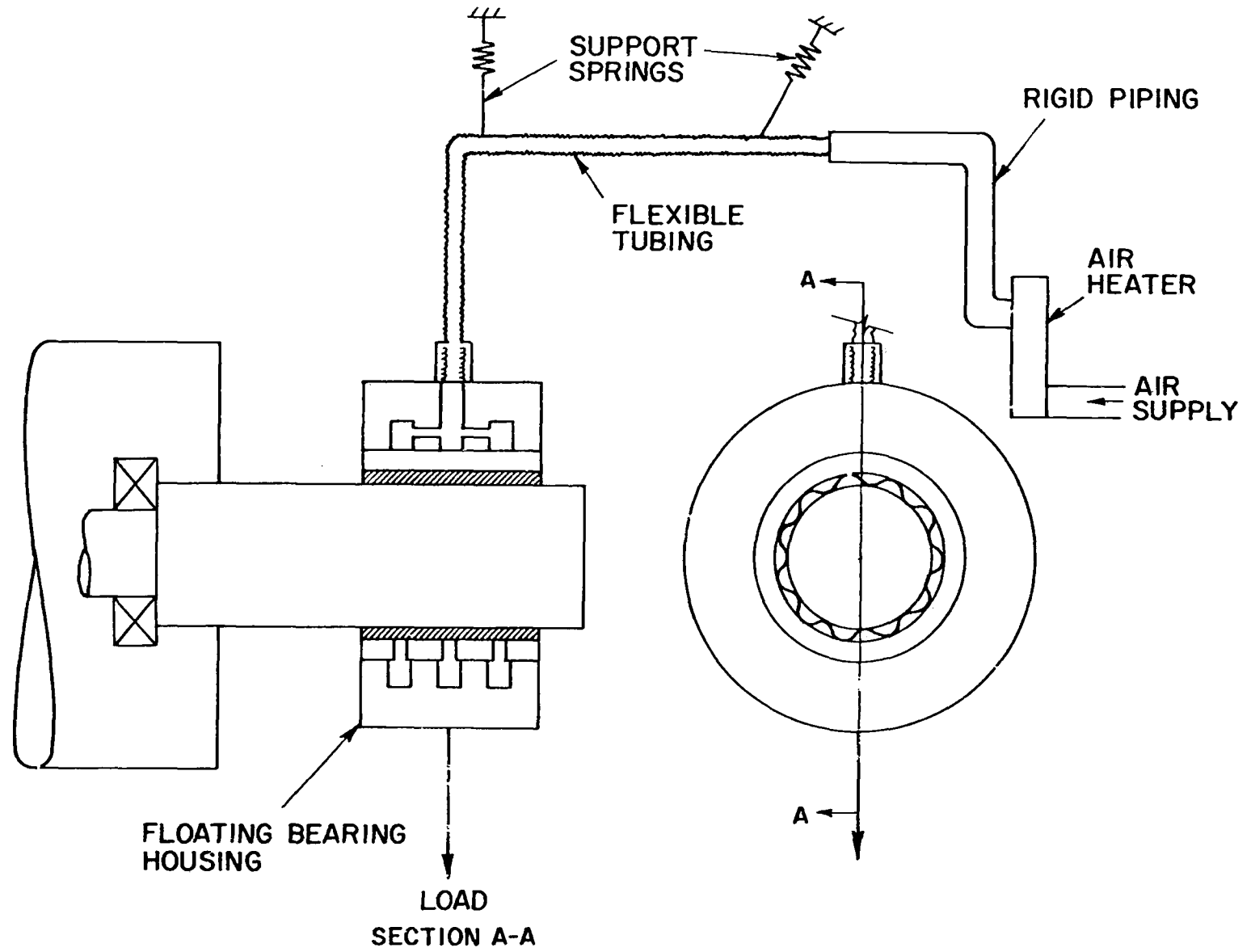


Fig. VII-31 Schematic Showing Method of Supplying Cooling Air to Test Bearing

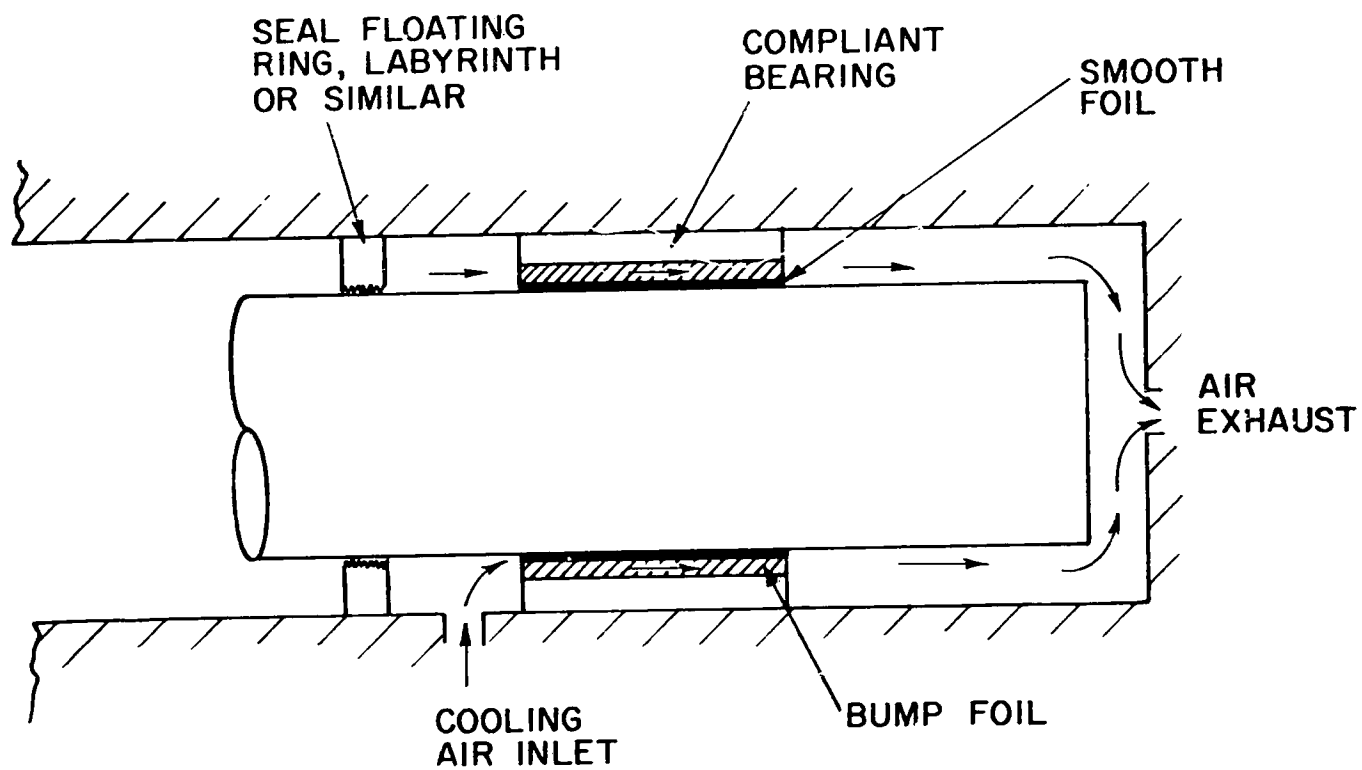


Fig. VII-32 Schematic Showing Alternate Method of Supplying Cooling Air to Bearing

axially in the gap out each end of the bearing. The cooling effect of the air was gained by the rotating shaft drawing the cooling air radially around the bearing through the air film. The cooling effect increased with increasing speed. In addition, in extreme temperature applications when the cooling air enters the bearing at one radial location, the possibility exists for local thermal distortion of the bearing to occur due to temperature gradients caused by the cooling air.

In the test rig, the shaft position is fixed, and the bearing is free to float, which is opposite to most applications of the compliant bearing, where the bearing is fixed and the shaft is free to float. Because of the test requirement that the bearing must be free to float, the cooling air configuration, which forces the air to pass axially through the bump foil and air film, could not be used without a complicated system of a cavity with seals being incorporated on the floating bearing housing.

Maintaining bearing temperature constant with ambient temperature

The second reason for considering the measured air flows conservative is the requirement that the bearing temperature be held constant and at the same temperature being maintained on the bearing housing. This requirement was self-imposed and selected for the purpose of maintaining as many test conditions as possible constant throughout the entire test sequence. At a set of constant test conditions, the bearing temperature will increase as the cooling air flow is reduced. Although specific tests in this area were not conducted during this program, it is known that the bearing temperature will stabilize at a higher temperature with a reduced cooling air flow. The lower the flow, the higher the temperature. Some point will be reached, however, where more internal heat is being generated by the bearing than can be removed by the cooling air and the bearing temperature will not stabilize. When these conditions occur, local thermal distortions will start to occur in the loaded area, potentially rupturing the air film and causing the bearing to seize.

It is believed that lower cooling air flows may have been achieved during these tests if the bearing temperature were allowed to stabilize at a temperature higher than the ambient temperature.

Comparison of Cooling Flows with Typical Gas Turbine Engine Flows

The bearing cooling air flows measured, conservative as they are, still represent insignificant flows when compared to typical total gas turbine engine flows. The design flow for the Chrysler/ERDA Upgraded Automotive Gas Turbine is approximately 22.4 kg/min (50 lbm/min) at 45,000 rpm. The maximum steady state foil bearing load anticipated for this condition is 111.2 N (25 pounds). Using the curve of Figure VII -27, the cooling air flow required based on the experimental test data, would be approximately 0.06 kg/min (0.13 lbm/min) or 0.26 percent of the total engine flow.

Effects of High Temperature on Load Performance

Throughout the elevated temperature testing there were no indications that, if thermal distortions were occurring, they were affecting bearing performance. The maximum steady-state load capacity obtained during these tests was $1.75 \times 10^5 \text{ N/m}^2$ (25.4 psi), which was approximately $1.38 \times 10^4 \text{ N/m}^2$ (2 psi) more than obtained during testing at room temperature. Some of the additional capacity obtained may be attributed to the increase in air viscosity at the higher temperature, but is more likely caused by a combination of small differences between the two tests, i.e., variations in the two test bearings and journals, dynamic shaft motion, and test conditions.

The testing was positive in showing, however, that the bearing performance was not degraded by possible thermal distortions occurring at the elevated temperatures. Although test journal temperatures were not measured, an axial thermal gradient along the journal existed due to the extensive oil and water cooling of the test end support ball bearing. Thermal distortion of the bump foil, smooth foil, and/or bearing housing was also considered a possible factor in limiting the bearing performance at elevated temperatures. No measurements could be obtained to determine the extent of distortion, however; again the effect on performance was insignificant due to the combination of bearing compliance and bearing cooling air limiting the distortion.

BEARING LIFT OFF SPEED

The lift off speed of a self-acting bearing is the speed required to generate a hydrodynamic air film capable of supporting the dead weight load on the bearing. The lift off speed was obtained by displaying on a high speed chart recorder, the conditioned signal from one capacitance probe used in the friction torque system and the conditioned signal from the speed sensor. During the start cycle, prior to the lift off speed being reached, the frictional drag of the bearing is significantly higher than the frictional torque after lift off occurs. The lift off speed is defined as the speed at which the frictional torque decreased sharply. Figure VII-33 shows a typical trace with the method for obtaining lift off speed illustrated. Table VII-12 lists lift off speeds obtained with the various dead weight loads on the bearing.

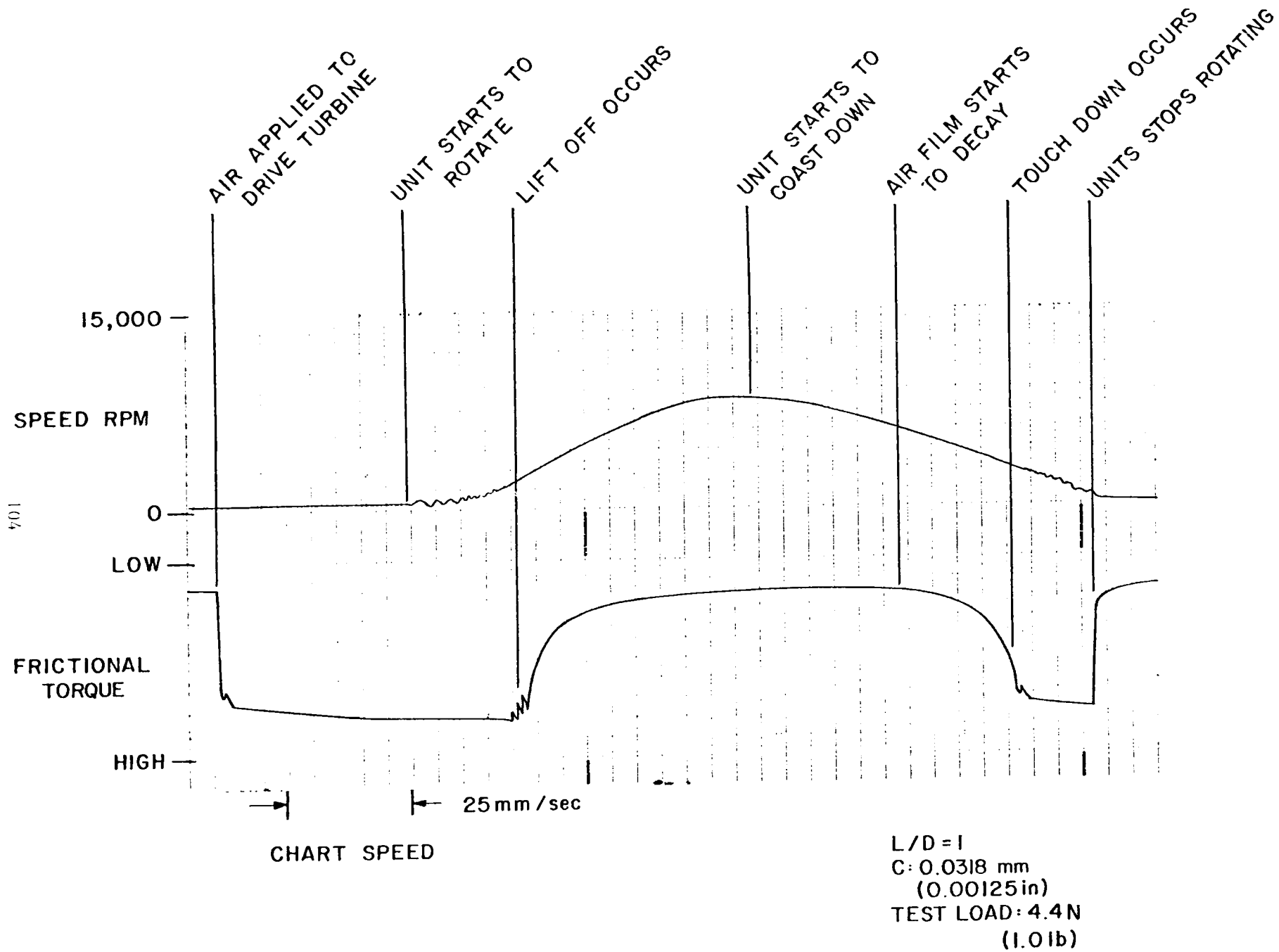


Fig. VII-33 Typical Trace for Obtaining Lift Off Speed, Compliant Surface Bearing

TABLE VII - 13
TABULATED DATA FROM LIFT OFF SPEED TEST

L/D = 1; L x D = 14.6 cm² (2.25 in²)
Bearing Clearance: C as indicated

Test Speed: As indicated
Test Temperature: Room Ambient

Bearing Load		Lift Off Speed, RPM	
		C = 0.057mm (0.00225 in)	C = 0.0318 mm (0.00125 in)
N	pounds		
4.4	1	2400	2100
18.9	4.25	3600	2400
27.8	6.25	3900	2600
36.7	8.25	4200	3000
45.6	10.25	4600	3300

BEARING FRICTIONAL POWER LOSS

Frictional power loss measurements were to be obtained utilizing two restraining flexures and the loading parallelogram as shown in Figure IV-1. The principle consideration in designing the torque measurement system was to have a system in which the dead weight load would always pass through the bearing centerline. If this was achieved, no error moment would be introduced into the system and the measurements would be accurate. The loading parallelogram was designed to ensure no error moment would be introduced; however, when testing was initiated it was apparent that the system was producing an error moment of significant value when compared to the very low bearing frictional torque losses.

An alternate and preferred method considered for applying the dead weight load was to utilize a hydrostatic gas bearing. Although it was felt that this method would produce accurate bearing frictional power loss data, it was not feasible to incorporate a hydrostatic gas bearing into the test rig design without a very complicated design for the brush and slip ring assembly. In addition, this system would have had its own inherent problems when operated at the elevated test temperatures.

The existing computer program predicts the bearing frictional power loss based on the film thickness calculated at a finite number of points around the bearing. Calculated frictional power loss for the test bearing at 60,000 rpm and $1.53 \times 10^5 \text{ N/m}^2$ (22.2 psi) bearing load is 70 watts (0.094 hp), which is less than 0.1 percent of the horsepower rating of the Chrysler/ERDA Upgraded Automotive Gas Turbine Engine.

VIII. ANALYSIS OF FILM THICKNESS TEST DATA

An objective of the test program was to obtain experimental data that could be used to correct the film thickness values obtained from the one-dimensional (infinitely-long) compliant foil bearing theory discussed in Section II of this report. An end leakage correction factor was sought which would give good agreement between the analytical bearing performance (infinitely long solution corrected for finiteness) and the experimentally obtained bearing performance. The solution of the one-dimensional foil bearing expression was modified to include the effects of finiteness assuming a solution of the form:

$$\bar{\Psi}(\theta', \eta) = \bar{\Psi}_\infty(\theta') + M(\theta') N(\eta) \quad (1)$$

- where:
- $\bar{\Psi}$ - PH, corrected dimensionless pressure solution
 - P - $\frac{p}{p_a}$, dimensionless pressure solution
 - H - $\frac{h}{C}$, dimensionless film thickness
 - p - Actual gas film pressure, atmosphere (psia)
 - p_a - Ambient pressure, atmosphere (psia)
 - θ' - Angular displacement measured from line of centers in direction of journal rotation, radians
 - η - $\frac{z}{L}$, coordinate along bearing axis, dimensionless
 - z - Actual distance along bearing axis, mm (inch)
 - L - Length of bearing, mm (inch)
 - M - is a function of θ' only
 - N - is a function of η only

The functions M and N are sought which degrade the pressure distribution to obtain an approximate finite bearing solution. These functions were not obtained due to the high non-linearities introduced into Reynolds Equation by the compliant effects of the smooth and bump foils.

A second attempt to derive an end leakage correction factor was made using the experimental data. A functional relationship was sought of the form:

$$K' = f(\bar{\omega}, \Lambda, \beta, \gamma) \quad (2)$$

Where $\tilde{\omega}$ = load capacity $\frac{\omega}{P_a L D}$ dim.

Λ = compressibility number $\frac{6\mu U_o R}{C^2 P_a}$ dim.

β = ratio $\frac{\alpha_B}{\Lambda}$ dim.

α_B = bump compliance $\frac{6\mu U_o R S}{K_B C^3}$ dim.

S = bump pitch

K_B = unit bump stiffness

γ = aspect ratio (L/D) dim.

then $K' = e^{a_0 \tilde{\omega}^{a_1} \Lambda^{a_2} \beta^{a_3} \gamma^{a_4}}$ (3)

where $K' = \left(\frac{h \text{ min actual}}{h \text{ min theoretical}} \right)$

and $h \text{ min}_A = CK' \left(\frac{h \text{ min}}{C} \right) T$ (4)

The exponents in equation 3 were determined by curve fitting the ratio of the experimentally obtained to the theoretical film thickness using a least squares algorithm and then taking the log on both sides of the equation to linearize it. A Gauss elimination routine was then employed to solve for the exponents in the relationship. The expression was used to correlate all the data.

The expression obtained could reproduce some experimental minimum film thickness values from the computer predicted values with reasonable accuracy for the exact test bearing configuration. However, when slight changes were made to any of the bearing parameters, such as L/D ratio, bump compliance, diameter, or clearance, the corrected minimum film thickness values obtained from the computer predicted values using the derived expression were not reasonable. It should be noted that the one-dimensional compliant foil bearing theory used in the computer program contains assumptions that have not yet been shown

experimentally to be correct. As was discussed previously in Section VI, if a bearing with an L/D ratio of 2 or 3 could be tested in the proper speed and load range, some of the assumptions in the theory could be changed to better approximate the actual behavior of the bearing.

Figures VIII-1 through VIII-6 show in dimensionless form at a specific speed and bearing clearance the minimum film thickness values at various loads for bearings with an $L/D = \infty$, $L/D=1$, and $L/D = 1/2$. The curve for the $L/D = \infty$ bearing is obtained from the computer program using the existing foil bearing theory. The curves for the $L/D = 1$ and $L/D = 1/2$ bearings are drawn from the test data obtained in this program.

It is recognized that these curves were generated from data obtained from a single bearing design with relatively limited testing at specific speeds and loads, and thus should be used only as guides in designing bearings with design parameters different from the tested bearing. However, it should also be recognized that these curves are unique and were generated utilizing a direct measurement of the film thickness value and profile. It is also re-emphasized at this point that the experimental film thickness values used to plot the curves contained in this report are film thickness values obtained at the bearing centerline. As discussed earlier in Section VII, the centerline film thickness value was used based on the major load support capability being contained in the center region of the bearing. Smaller film thickness values were measured near the bearing edge. The computer program predicts a constant film thickness value axially across the bearing.

In each figure the two curves representing the experimental data for the $L/D = 1$ and $L/D = 1/2$ test bearings are very similar in shape and trends. Since all bearing and test parameters, except the L/D ratio, were held constant for the two test bearings, the difference in film thickness values at a constant unit load is due only to end-leakage effects which are significantly greater for the shorter bearing. An approximate value for use in degrading the minimum film thickness value of an $L/D = 1/2$ bearing in the size and configuration of the program test bearing is 50 percent of the film thickness value of an $L/D = 1$ bearing. Again it should be recognized that this degradation factor is based on the limited testing performed in this program.

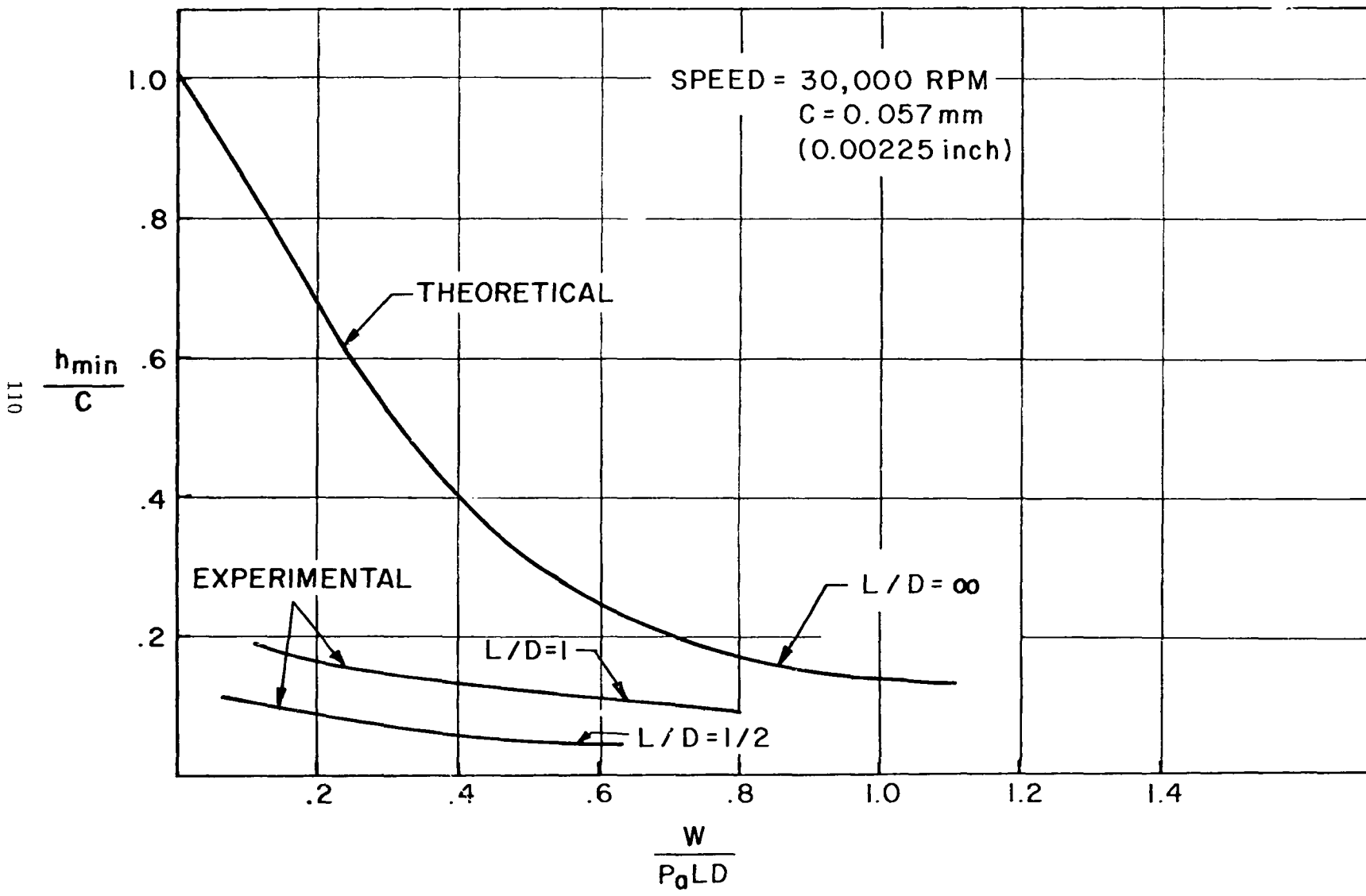


Fig. VIII-1 C=0.057 mm; 30,000 rpm: Dimensionless Minimum Film Thickness Values for 3 L/D Ratios, Compliant Surface Bearing

111

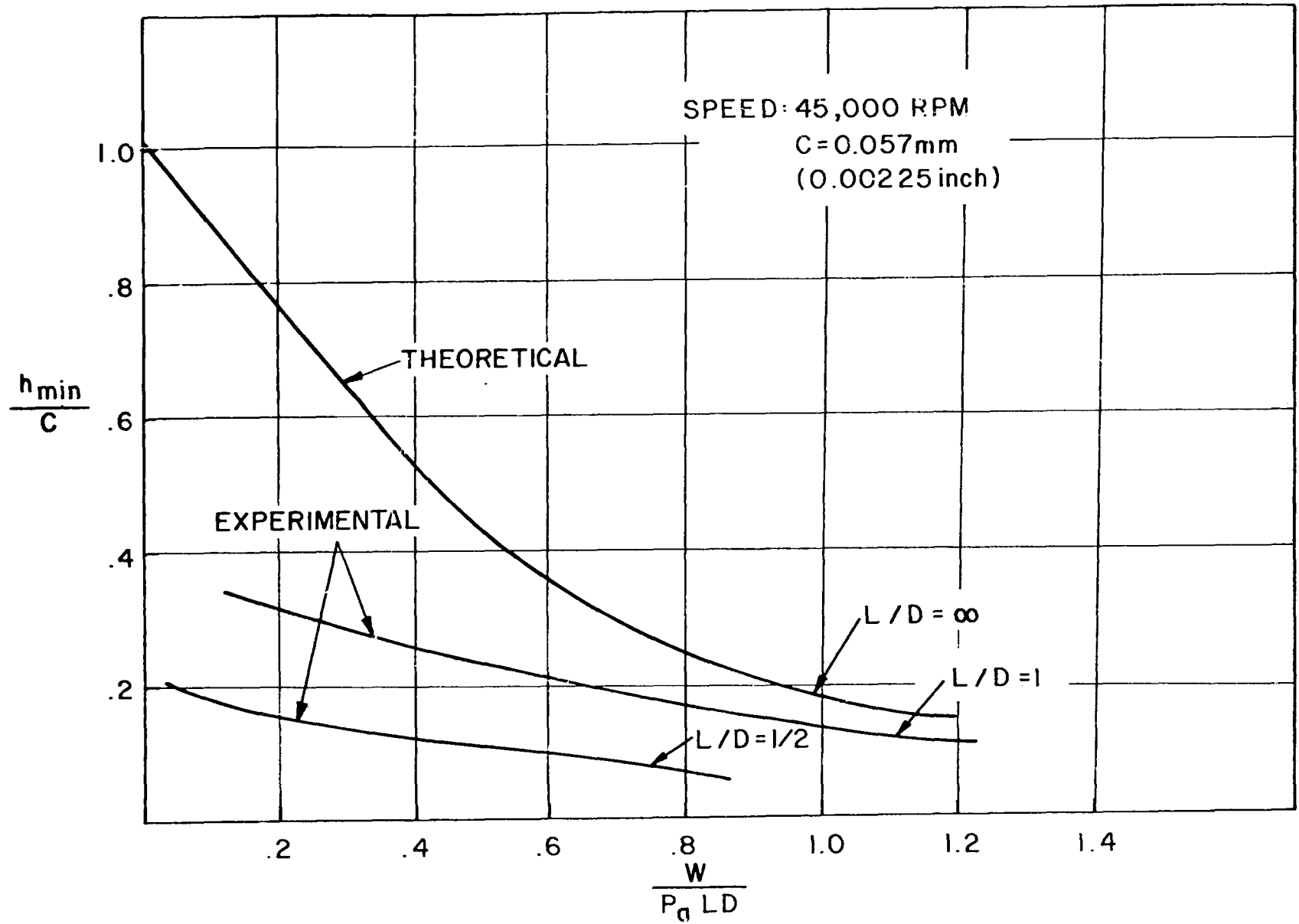


Fig. VIII-2 C=0.057 mm; 45,000 rpm: Dimensionless Minimum Film Thickness Values for 3 L/D Ratios, Compliant Surface Bearing

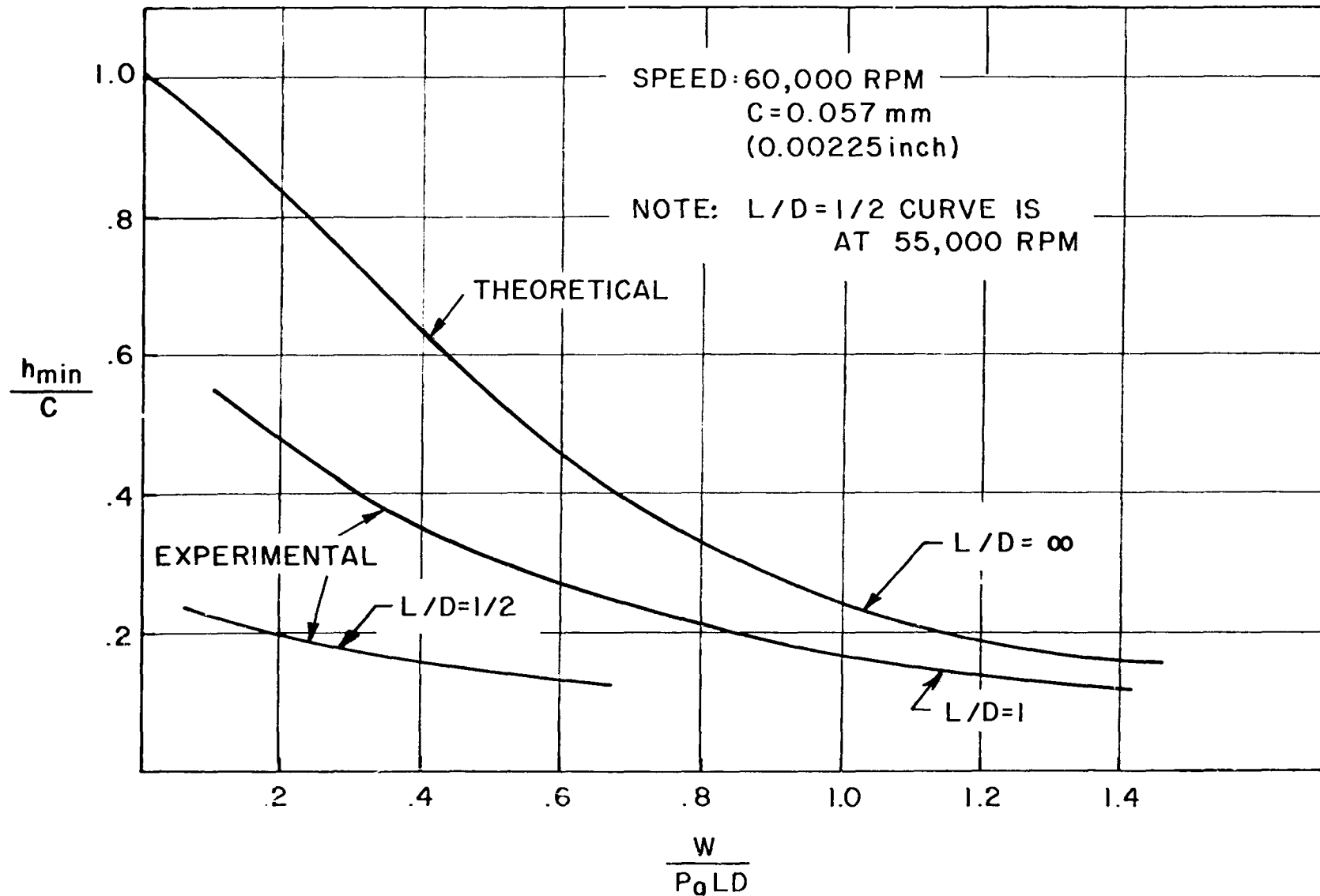


Fig. VIII-3 C=0.057 mm; 60,000 rpm: Dimensionless Minimum Film Thickness Values for 3 L/D Ratios, Compliant Surface Bearing

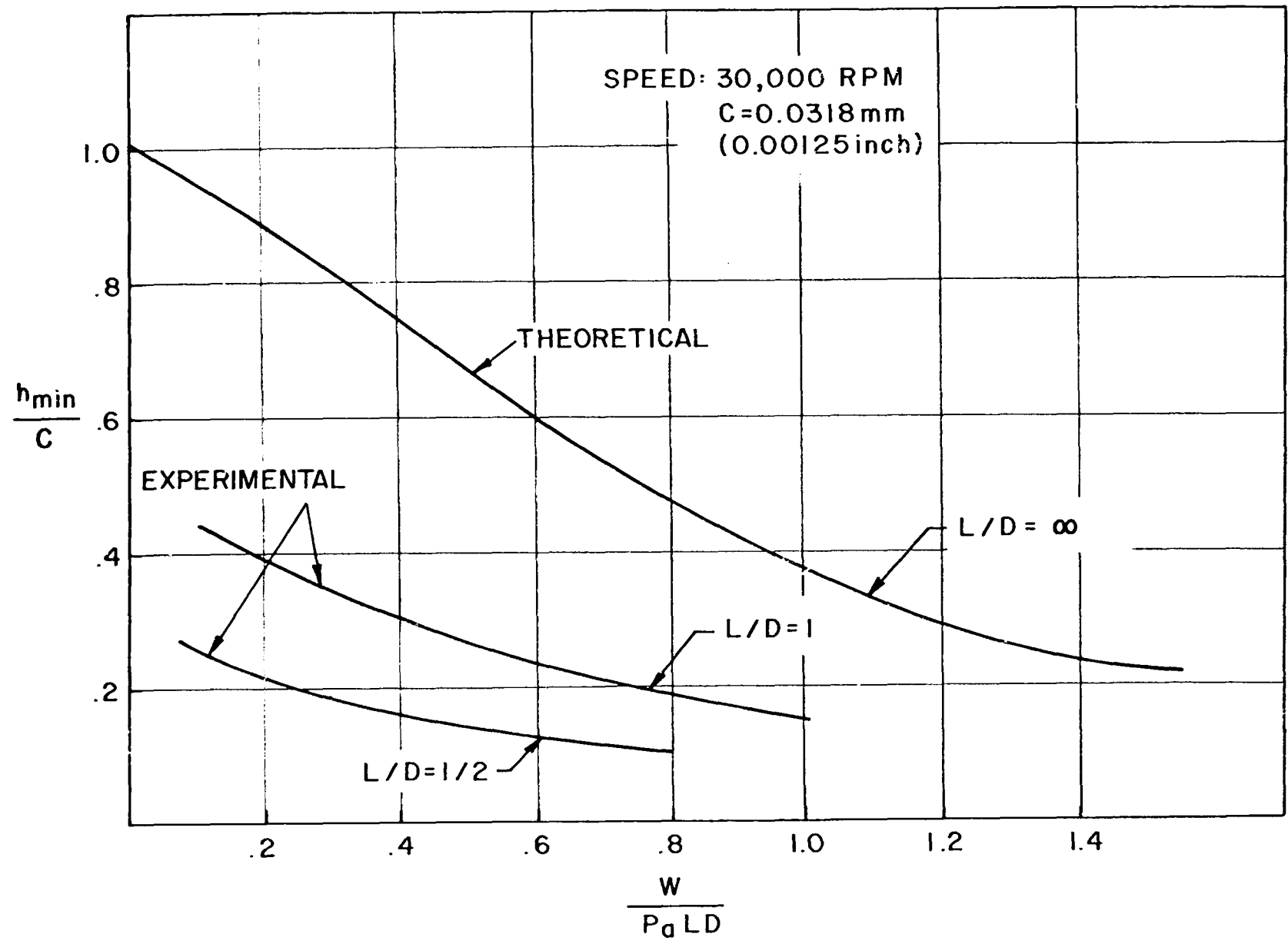


Fig. VIII-4 C=0.0318 mm; 30,000 rpm: Dimensionless Minimum Film Thickness Values for 3 L/D Ratios, Compliant Surface Bearing

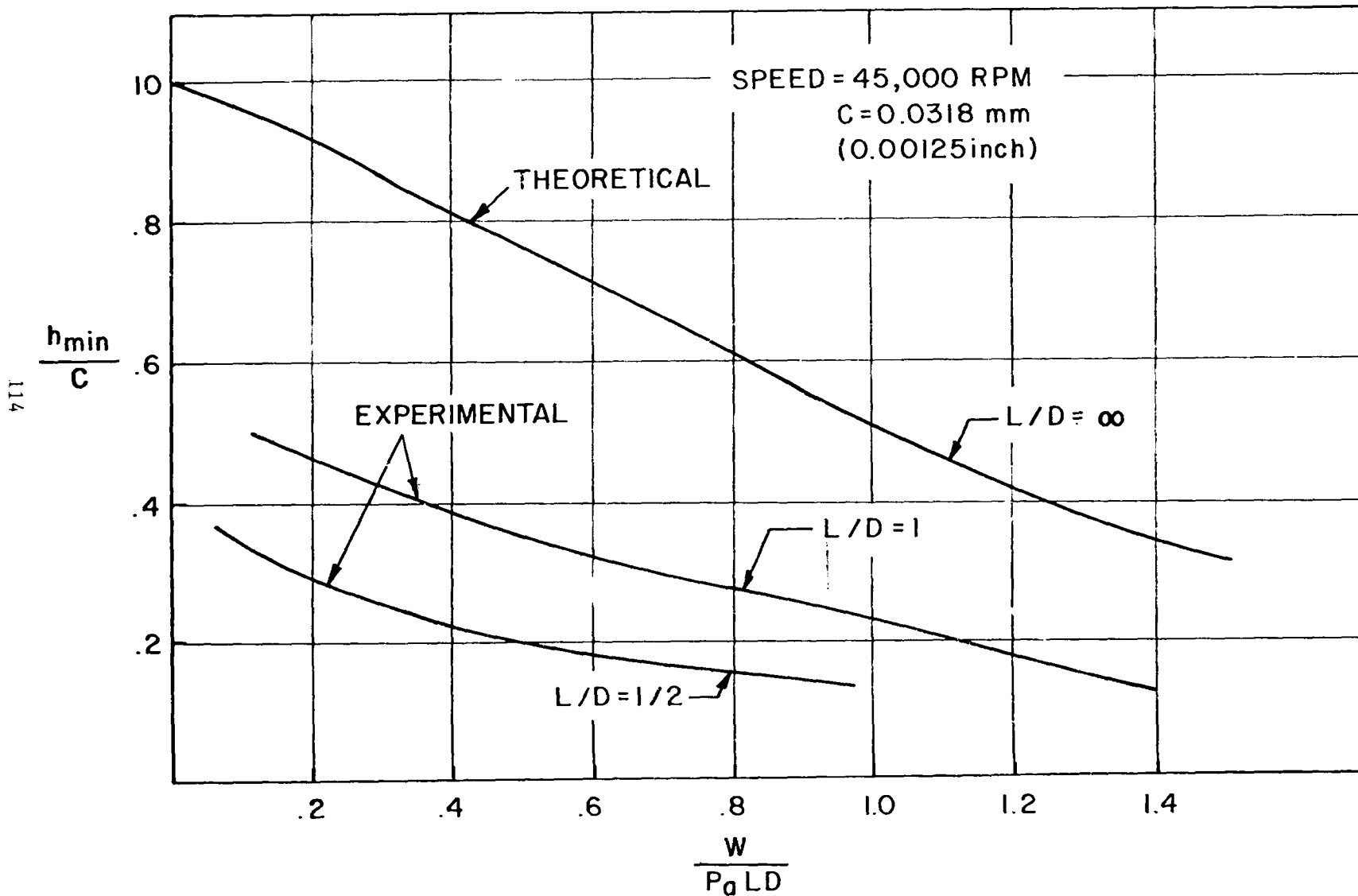


Fig. VIII-5 C=0.0318 mm; 45,000 rpm: Dimensionless Minimum Film Thickness Values for 3 L/D Ratios, Compliant Surface Bearing

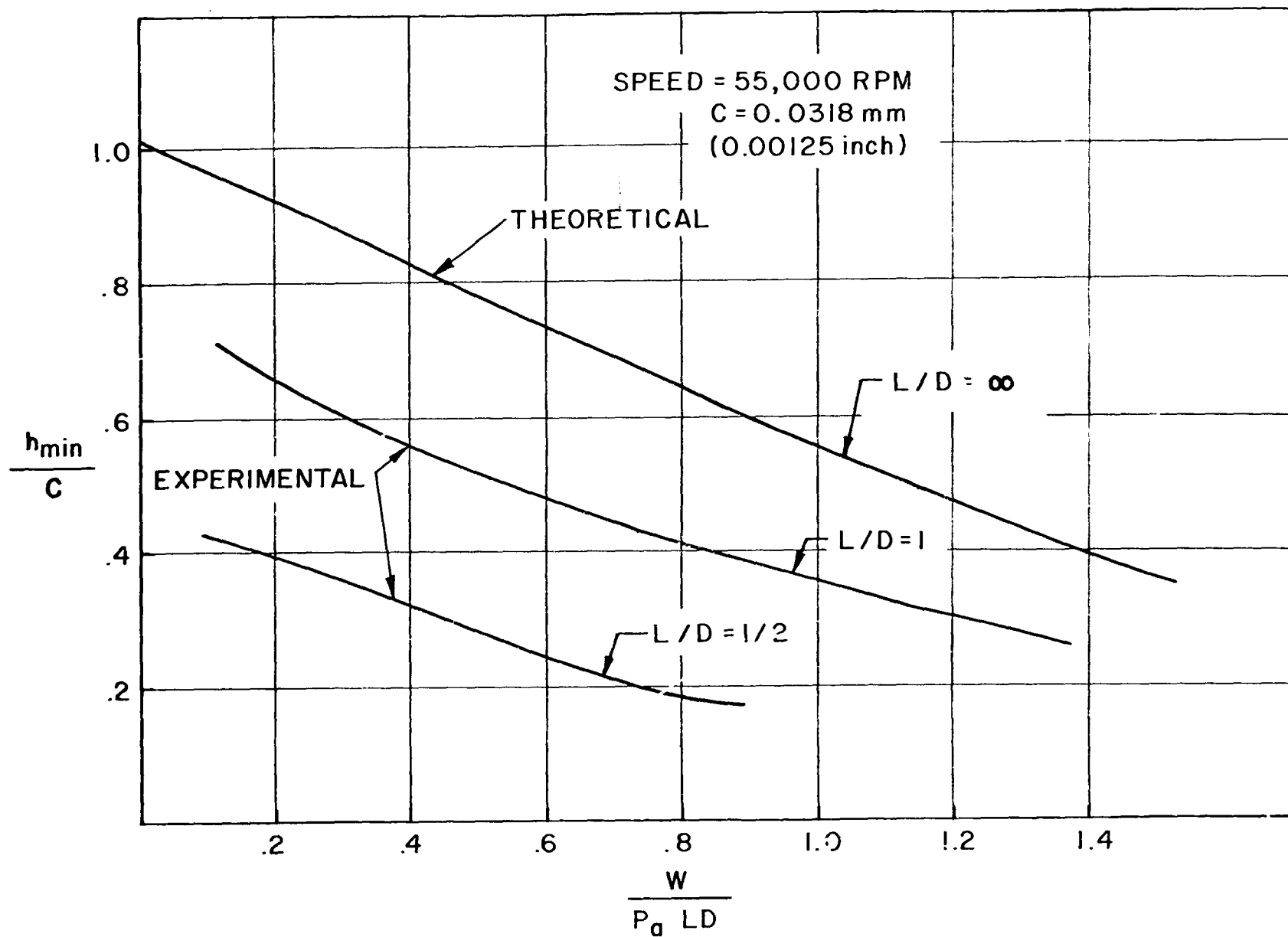


Fig. VIII-6 C=0.0318 mm; 55,000 rpm: Dimensionless Minimum Film Thickness Values for 3 L/D Ratios, Compliant Surface Bearing

Figure VIII-7 is a plot similar to those being discussed for a rigid surface plain sleeve bearing. The curves were generated solely from Raimondi's analytical results presented in Reference [3]. In the very limited band of unit loading between 0.1 and 0.3, a rough approximate degradation of the $L/D = 1/2$ film thickness value to the $L/D = 1$ value is 50 percent. This comparison is not intended to correlate foil bearing test data with rigid bearing analytical data, but rather is presented only to show that the experimentally derived degradation factor has a reasonable value.

Examining the plots for the compliant surface bearing reveals significant differences in the shape of the curves for the two L/D bearings tested and the $L/D = \infty$ bearing, especially at the lightly loaded conditions. The primary difference is that the experimental curves do not originate at $\frac{h_{min}}{C} = 1$ at zero unit loading.

The predicted $L/D = \infty$ curve in each of the six plots exhibits the same shape and trend as similar plots for any rigid hydrodynamic bearing. This can be readily observed by comparing the curves of Figure VIII-7 with the $L/D = \infty$ curves in Figures VIII-1 through VIII-6.

Although no test data was obtained at zero load, which would require an upward load to eliminate the weight of the floating housing, it can be stated with certainty that at zero load, $\frac{h_{min}}{C} = 1$ would NOT have occurred. This condition can only occur in a compliant bearing if both the bump foil and smooth foil are formed exactly to the proper diameters and are firmly seated against the bearing housing and each other. In addition, the bearing clearance must be known to the same accuracy as the film thickness values. In an actual bearing neither of the two conditions can be satisfied. The present analysis assumes these two conditions exist; hence, this is one reason for the significant difference at light loads between predicted and experimental film thickness values. The shape of the predicted and experimental curves tend to become more similar as bearing load increases.

The expanded plot of both the predicted and experimental film thickness profile around the bearing, shown in Figure VIII-8, offers another possible explanation

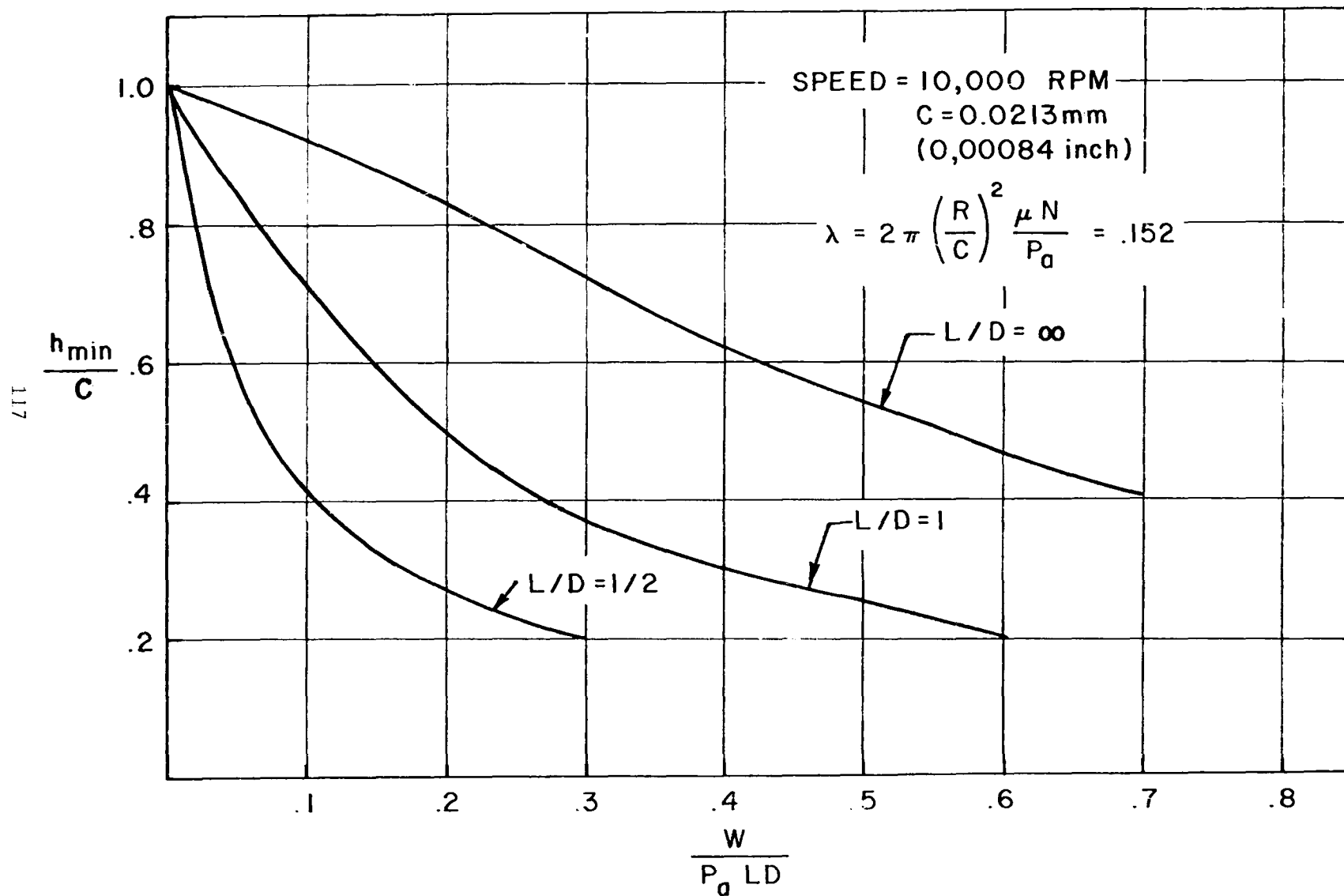


Fig. VIII-7 C=0.0213mm; 10,000 rpm: Dimensionless Minimum Film Thickness Values for 3 L/D Ratios, Rigid Surface Plain Sleeve Bearing

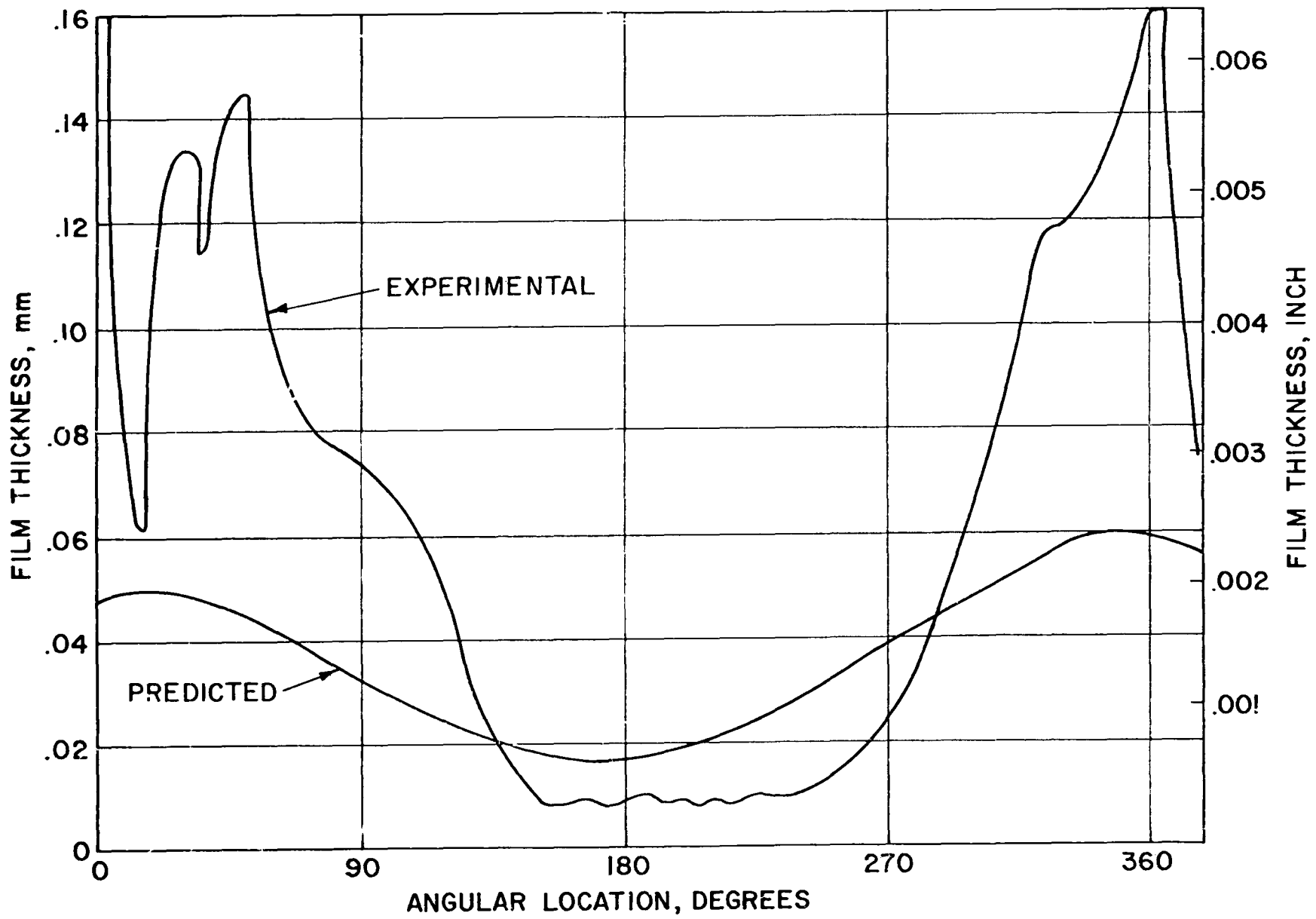


Fig. VIII-8 Expanded Plot of Predicted and Experimental Film Thickness Profile

as to why the experimental curves differ from the predicted curves. The film profile predicted is a symmetrical curve where the region of minimum film thickness is finite. The region of minimum film thickness which accounts for the majority of load support does not increase substantially with increasing load over the load range examined, therefore causing rapid changes in the minimum film thickness value with increased load. The experimentally obtained profile, however, contains a region of minimum film thickness over a substantial portion of the bearing. As load is increased, the minimum film thickness region, or main load support region, increases because of the bearing's compliance and conformity resulting in less of a change in minimum film thickness value for each change in load.

It was not the intent of this program to correct the existing one-dimensional analysis and computer program based on test data, but rather to establish guides for correcting minimum film thickness values obtained from the present computer program for an $L/D = \infty$ bearing for end leakage effects. Since the $L/D = \infty$ curve is significantly different compared to the $L/D = 1$ and $L/D = 1/2$ curves, it is hard to establish a general degradation factor for the complete load range. At a unit loading of 0.8, which represents approximately one-half the load capacity of the $L/D = 1$ test bearing, the minimum film thickness value of an $L/D = 1$ bearing is approximately 50 percent of the computer predicted minimum film thickness value for an $L/D = \infty$ bearing. A degradation factor based on a specific speed and clearance for a bearing similar to the program test bearing can be obtained by using the graphs of Figures VIII-1 through VIII-6. Again, it is recognized that these graphs are based on limited test data for a specific bearing design, but it does offer an approximate correction for side leakage effects in the compliant bearing.

LX. CONCLUSIONS AND RECOMMENDATIONS

A 38.1 mm (1.50 inch) diameter Hydresil compliant surface journal bearing was designed using an existing computer program and the bearing performance characteristics calculated. The bearing was then extensively tested at speeds up to 60,000 rpm and loads up to 1.75×10^5 N/m² (25.4 psi) to determine experimentally the bearing's performance characteristics both at room temperature and 315°C (600°F). A measurement system for obtaining direct film thickness measurements which utilized a modified capacitance proximity probe system mounted in a high speed journal was designed and fabricated for the test program. Accurate film thickness profiles and minimum values were obtained at room temperature for L/D=1 and L/D=1/2 test bearings at two clearances each for various speeds and loads. Testing was conducted at 315°C (600°F) on the L/D=1 test bearing, and bearing cooling air requirements and load performance capacity were determined.

The Hydresil Compliant Surface Air Lubricated Journal Bearing successfully demonstrated performance characteristics that can fulfill the requirements of present and proposed automotive gas turbine engines. The load performance demonstrated at both room temperature and 315°C (600°F) ambient and bearing temperature represents a significant advancement for compliant surface bearings.

SPECIFIC CONCLUSIONS

Following is a list of specific conclusions relating to the compliant surface journal bearing. These conclusions are substantiated by the test results documented in Section VII.

Journal Bearing Load Capacity Performance

A maximum steady state load of 1.75×10^5 N/m² (25.4 psi) was successfully supported at 45,000 RPM at a bearing temperature of 315°C (600°F). This capacity is considered sufficient for use in present and proposed automotive gas turbine engines.

Influence of L/D Ratio on Minimum Film Thickness

The minimum film thickness value was found to significantly decrease at constant speed and load conditions as the L/D ratio decreased. The computer predicted minimum film thickness value for an L/D=∞ bearing was found to decrease by 50 percent for an L/D=1 bearing and 75 percent for an L/D=1/2 bearing in a typical load range for the test bearing due to the end leakage effects occurring in a bearing of finite length. These degradation factors are of the same order as values for rigid surface bearings.

Influence of Bearing Fabrication Accuracy on Load Performance

The assembled compliant surface bearing when built on a small volume basis without production type tooling presents a quality control problem when maximum bearing performance is sought. Close visual inspection of the completed bearing provides the best check on the bearing as the flexible foils do not allow precise measurement checks to be made. Improper bearing conformity was shown to influence the film thickness profile and reduce bearing performance. Proper tooling and large volume manufacturing techniques should eliminate this problem.

Bearing Journal Surface Porosity

The effect of bearing journal surface porosity was determined experimentally to be a significant factor on bearing load performance. The maximum bearing capacity was obtained using a wrought ground steel journal which had essentially no porosity. The porosity of plasma sprayed chrome carbide coatings, which are currently being used on journal surfaces to obtain good wear properties at high temperatures, were found to degrade the hydrodynamic pressure field. Denser coatings which can be obtained by applying the chrome carbide by methods other than plasma spray offer a compromise solution.

Bearing Cooling Air Requirements

The cooling air required by the compliant surface bearing to remove the self-generated heat was shown to be a very small portion of the total air flow of typical turbomachinery utilizing the bearing. Cooling air requirements per bearing of as low as approximately 0.25 percent of total engine flow can be expected.

Effects of Thermal Distortion on Bearing Performance

While no attempts were made to deliberately introduce thermal distortions into the tests, the load performance capacity of the test bearing was experimentally shown not to have been reduced by operating at a temperature of 315°C (600°F) where thermal distortions might be anticipated. A combination of the bearings compliant characteristics and the cooling air supplied to the bearing allowed the bearing to successfully operate at the elevated temperatures.

RECOMMENDATIONS

The following recommendations are made based on the results of the work performed in this program.

Continued Technology Advancement

Further testing should be conducted on a journal bearing of L/D of 2 or 3 using the film thickness measurement techniques developed in this program. Use of the longer bearing will more closely approximate the model of the current one-dimensional analysis and allow the assumptions now in the analysis to be verified and corrected if required. These assumptions include among others the influence of foil seating and the use of a meaningful bearing clearance. After the infinite length bearing is correctly modeled, the analysis can be extended possibly by finite element bearing analysis to accurately represent a bearing of finite length for use in correctly predicting the finite length bearing performance characteristics. The test measurement techniques developed should be utilized for investigation of the influence of foil bearing design parameters in order to optimize bearing design.

Additional Journal Bearing Tests

Additional testing of compliant surface journal bearings should be conducted for use in verifying a complete set of design charts. Various design characteristics and higher test speeds should be evaluated based on anticipated requirements for the advanced automotive gas turbine engine. Testing compliant surface bearings of other designs, such as the tension foil and cantilevered beam, should also be conducted in the same test equipment to obtain data which is directly comparable.

Thrust Bearing Tests

A program similar to the one reported here is recommended for compliant surfaces thrust bearings.

REFERENCES

1. Gray, S., Sparks, N., McCormick, J., "The Application of Gas and Oil Lubricated Foil Bearings for the ERDA/Chrysler Automotive Gas Turbine Engine," ASME Paper No. 76-GT-115, March, 1976.
2. Walowit, J., Murray, S. F., McCabe, J., Arwas, E. B., and Moyer, T., "Gas Lubricated Foil Bearing Technology Development for Propulsion and Power Systems," AFAPL-TR-73-92, December 1973, Contract NAS3-9433.
3. Raimond, A. A., "A Numerical Solution for the Gas Lubricated Full Journal Bearing of Finite Length," ASLE Paper 60LC-14.

APPENDIX A

FABRICATION OF THE FILM THICKNESS SENSOR

All components for the rotating sensors and slip ring assemblies, with the exception of the commercially purchased metal fiber brushes, were designed, fabricated and assembled by the Instruments Group at MFI. Two test shafts were instrumented; one for film thickness measurements and one for film pressure measurements. Two similar probes were installed in each journal surface 90° out of phase with a slip ring assembly at each end of the shaft allowing for simultaneous reading of both probes. Figure V-1 shows the actual probe and Figure V-2 shows the installation. A detailed cross-section of the film thickness sensor is shown in Figure A-1.

A major consideration in the design of the sensors was to minimize the effect of speed on the mechanical shifting (zero shift) of the sensor in the shaft. To achieve this, the capacitance probes were constructed to provide high axial stiffness and stability under varying radial loads. At 60,000 RPM the radial load on the center electrode was calculated to be 22.7 kilograms (50 pounds). An experiment conducted on a completed probe using a special fixture showed that the center electrode would displace approximately 2.79×10^{-4} mm/kg (5×10^{-6} in/lb) of load. Under full speed loading, the center electrode will displace 6.35×10^{-3} mm (2.5×10^{-4} inch). This displacement is due to compression of two separate .1 mm (.004 inch) thick layers of mineral filled epoxy resin.

To reduce the effect of speed on zero shift, and to obtain a positive electrical connection, jacks were used to preload the probe assembly. The center of gravity of the jack was located below the journal axial centerline (with respect to the probe) which tended to reduce the preload at high speeds resulting in a fairly constant pressure on the probe support face over the speed range. A special #6-40 screw in the jack was used to apply 59 kgm (130 pounds) of preload to the probe. The jack screw connector contacted the shaft bore through a steel ball.

Figure A-2 shows the complete installation consisting of (left-to-right):

- End shield with slip ring; connection from a large to a miniature coaxial cable; connector to probe.

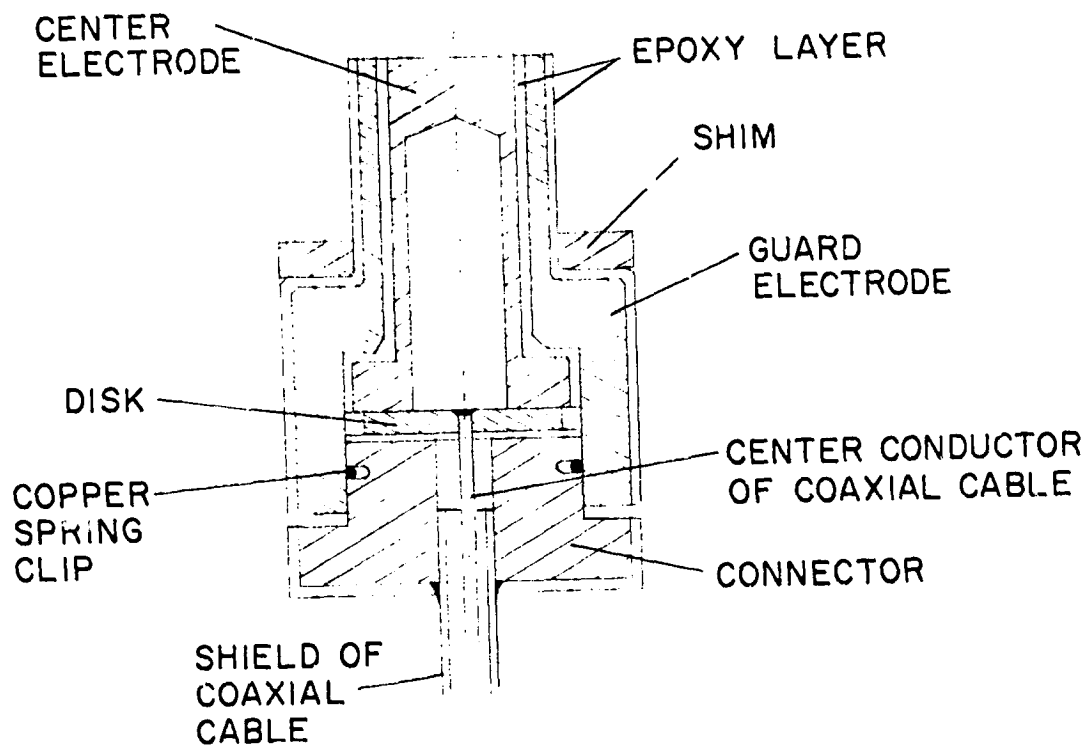
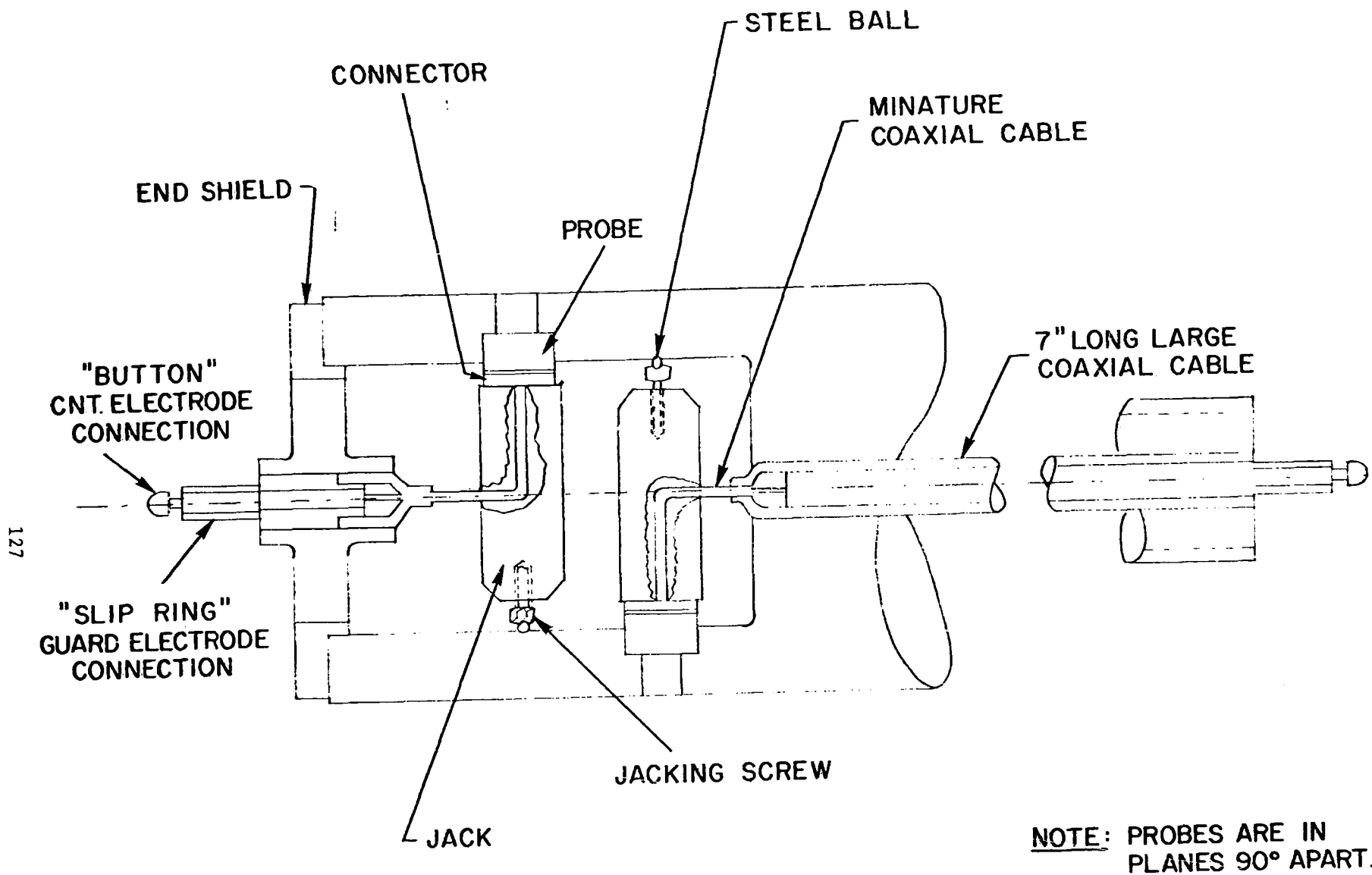


Fig. A-1 Detail Cross Section of Film Thickness Probe



NOTE: PROBES ARE IN PLANES 90° APART.

Fig. A-2 Detail Cross Section of Film Thickness Sensor System Installed in Test Shaft

127

- Probes (2)
- Jacks (2)
- Connector to probe; miniature coaxial cable; connection to large coaxial cable; slip ring.

Both channels of instrumentation were identical in their layout and dimensions, except for the length of the large coaxial cable. Figures A-3 and A-4 show the actual hardware.

The film thickness sensor was a 3.25 mm (.128 inch) diameter capacitance probe with a maximum range of .127 mm (.005 inch). Figure A-1 shows a detailed cross section of the sensor. The center electrode and guard electrode were made of 400 series stainless steel. The outside of the center electrode was coated with Ecobond 104 Epoxy containing an aluminum oxide filler. The epoxy coating was machined to give a light interference fit with the inside of the guard electrode. The final thickness of the epoxy layer was approximately .1 mm (.004 inch). The outside of the guard electrode received a similar treatment. The fit of the assembled probe into the shaft was line on line to slightly loose.

The sensors were initially installed in the shaft with the probe tip above the journal surface. The journal surface was masked and the probe tip lapped to conform to the shaft radius. The sensors were then removed, and the shim between the guard electrode and shaft increased in thickness so that when the sensors were reinstalled in the shaft the probe tip was approximately .038 mm (.0015 inch) below the journal surface. The probe tips were recessed to protect the tip surface during starts and stops and in the event of a high speed rub.

The connector was fabricated from the same stainless steel material as the probe assembly. The center conductor of the miniature coaxial cable was brazed to a disk that made the connection to the center electrode. The disk was insulated from the rest of the connector by a layer of epoxy. The shield of the coaxial cable was brazed to the connector which fitted inside the guard electrode. A spring clip made of copper insured a good electrical connection between the connector and the guard electrode.

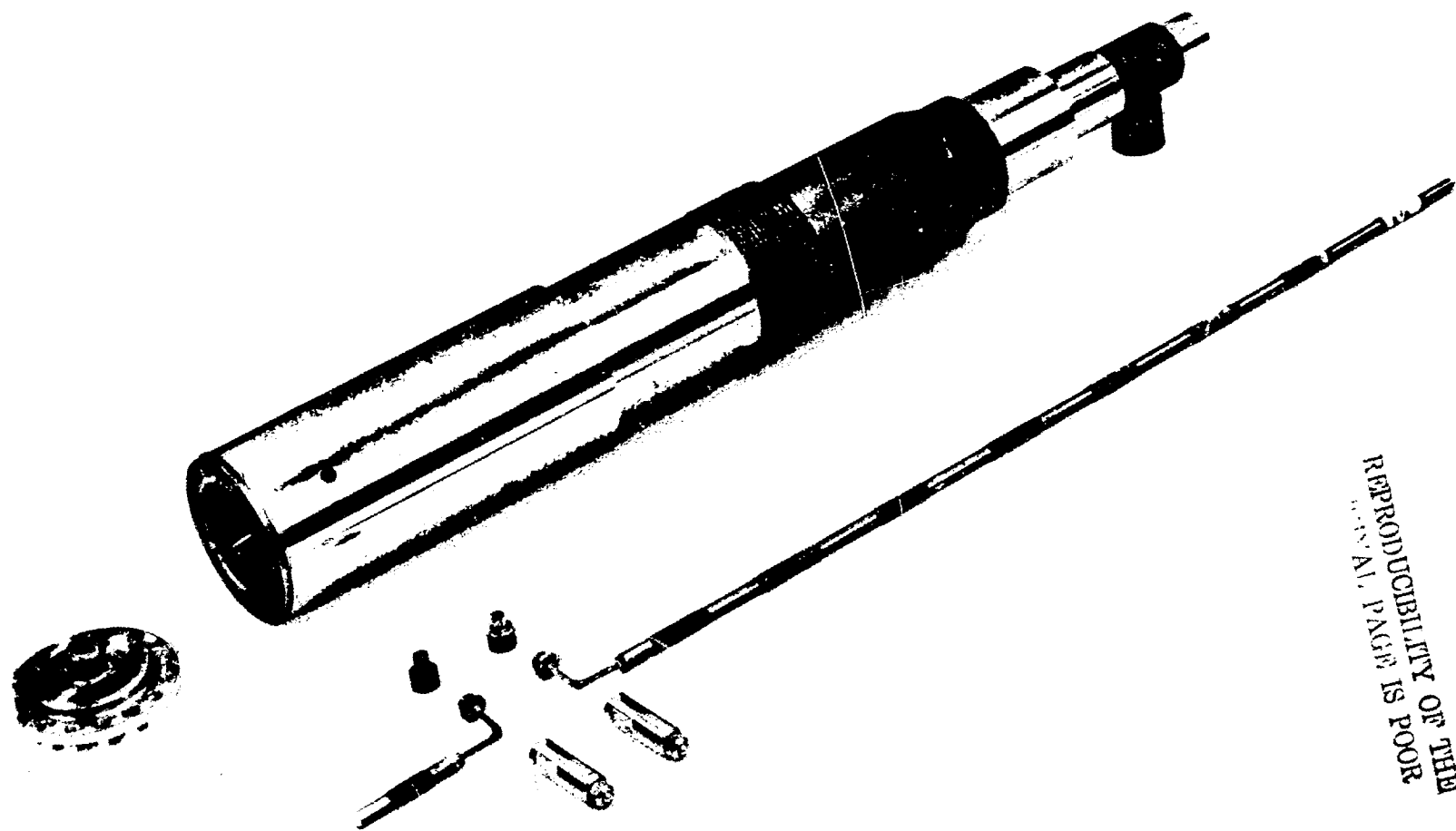


Fig. A-3 Rotating Film Measurement Sensors and Test Shaft

REPRODUCIBILITY OF THIS
ORIGINAL PAGE IS POOR

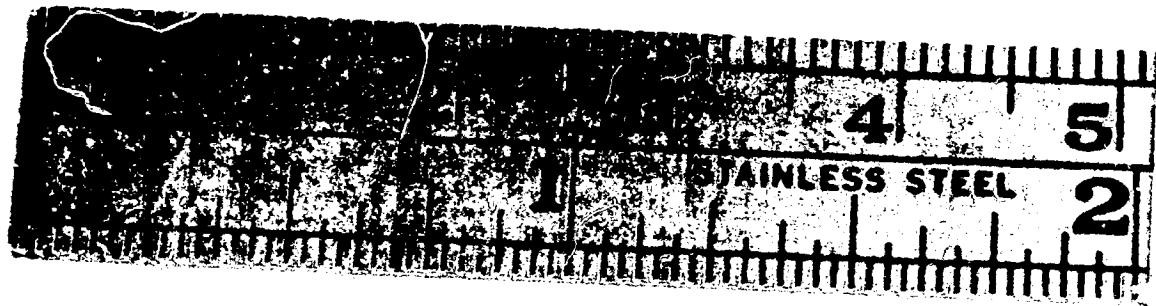
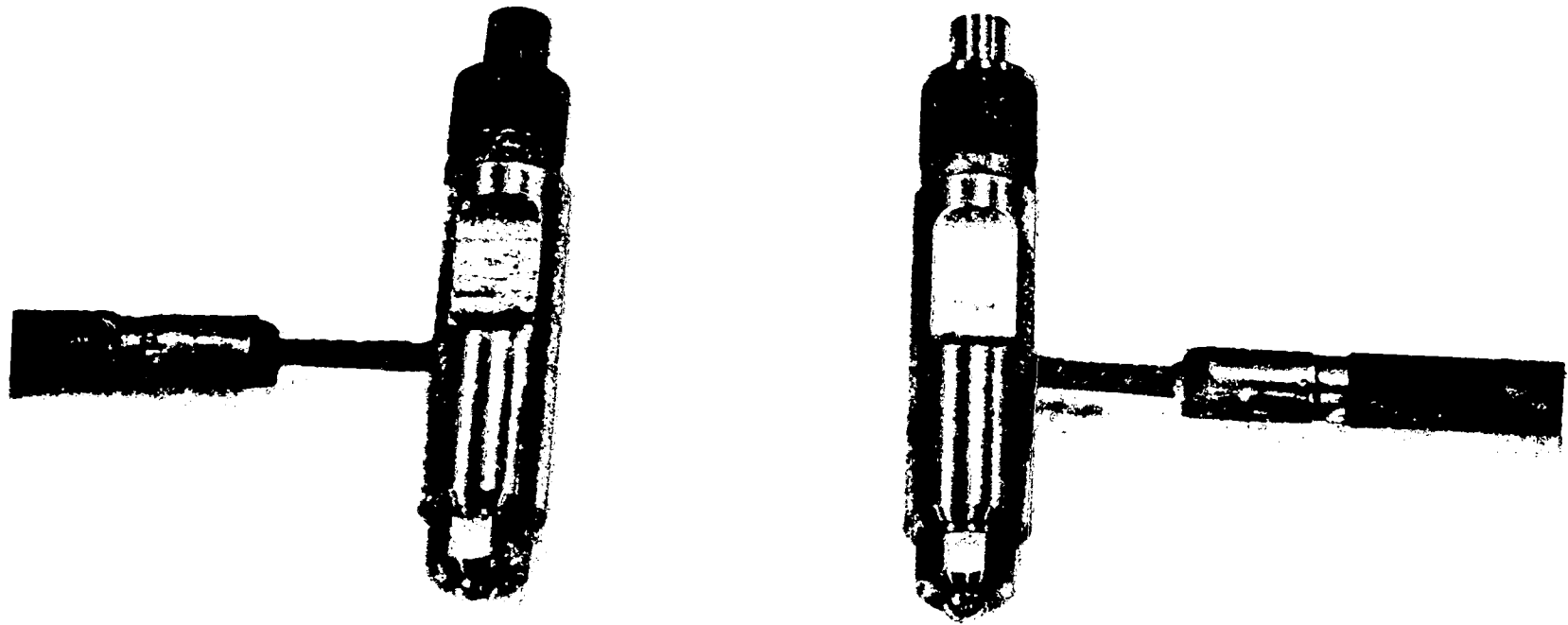


Fig. A-4 Film Measurement Sensors

The miniature coaxial cable was connected to the large coaxial cable utilizing a special adapter. The center conductors were spot welded and the shields brazed as shown in Figure A-5. The long coaxial cable received bands of epoxy approximately 12.7 mm (.5 inch) wide spaced 19mm (.75 inch). These epoxy bands were then machined to obtain a line fit with the bore in which the cable was to be installed. After both large coaxial cables were installed in the shaft and connected they were potted in place with epoxy. The coaxial cable at each end was then machined to receive the gold plated brass slip ring which made the guard electrode connection, and the "button" tip which made the center electrode connection. Also shown in Figure A-5.

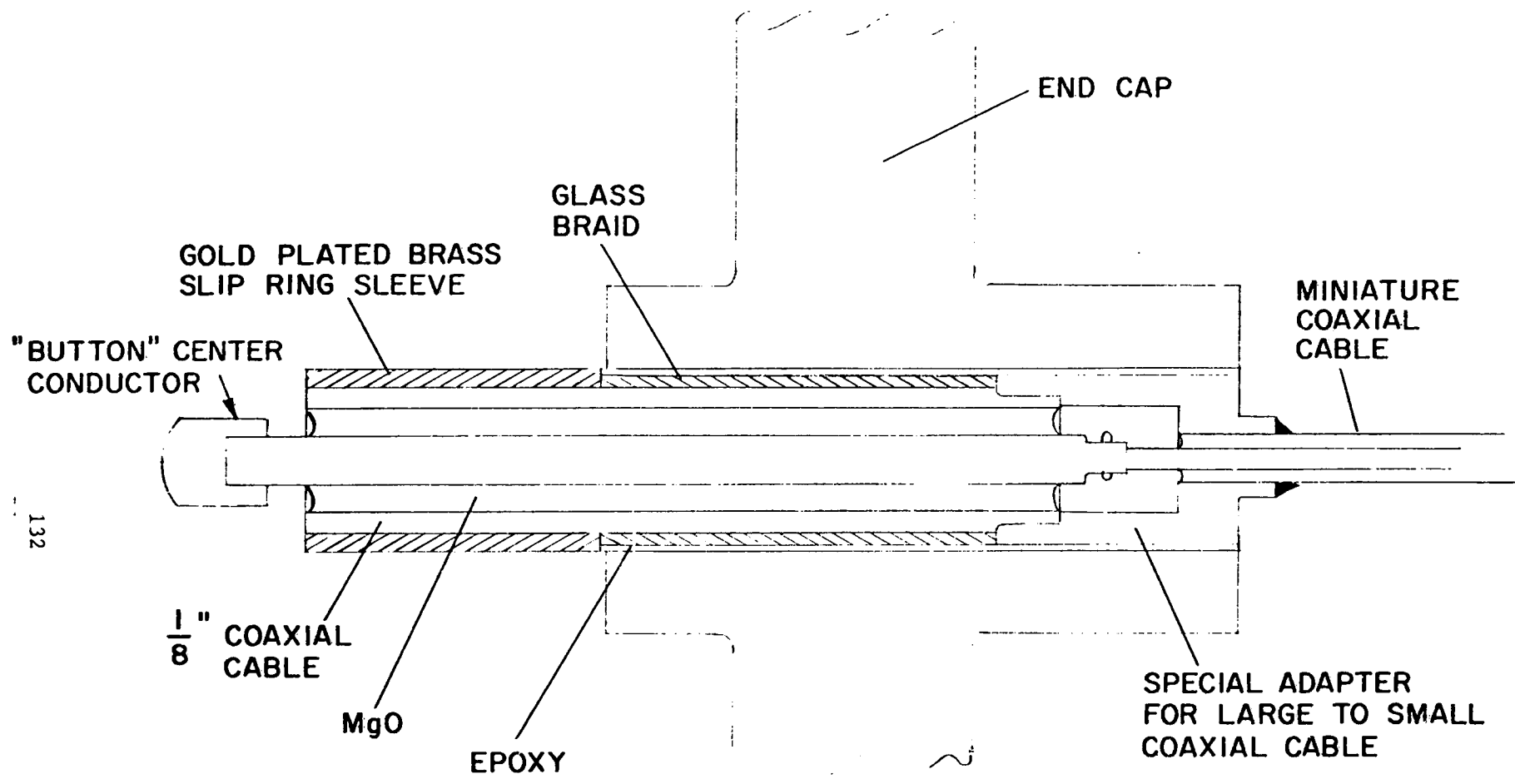


Fig. A-5 Detail Cross Section of Slip Ring

APPENDIX B

FABRICATION OF BRUSH AND SLIP RING ASSEMBLY

A detailed cross section of the brush and slip ring assembly is shown in Figure V-2. The use of a capacitance system required a completely shielded slip ring assembly which was designed and fabricated at MTI for this program. The high shaft speed required the slip ring size to be as small as practical in order that the surface velocity be kept at a reasonable level. At the 60,000 RPM speed condition the surface velocity of the slip ring was 9.96 m/sec (32.7 ft/sec). A hard gold wire brush running on a hard gold plated brass slip ring provided the circuit for the guard electrode. A silver graphite brush against a silver alloy "button" completed the center electrode circuit. Both circuits terminated in a regular coaxial cable micro-dot connector.

The coaxial cable which protruded from each end of the test shaft was prepared to accept the slip ring and "button" by machining the outer shield and inner conductor concentric with the support ball bearing surfaces. The brass slip ring sleeve, which was plated with a .025 mm (.001 inch) thick coating of a hard gold alloy, was a light press fit onto the outer diameter of the shield of the coaxial cable. The silver button was a light press fit onto the center conductor. When the shaft was assembled and rotated on its support ball bearings the total indicated runout at the slip ring surface was less than .005 mm (.0002 inch).

The brush housings were doweled to the test rig after the instrumented shaft was installed to ensure the housings were centered around the slip rings. Two metal-fiber brushes supplied by the Wendon Company were used in each brush housing. The brushes were threaded into a pivot arrangement which enabled the brushes to be rotated in and out of contact with the slip rings and also allowed for the adjustment of brush pressure. The entire brush housing was at the guard electrode potential which required the housing to be electrically insulated from ground.

The silver graphite brush was spring loaded against the "button" on the center conductor. A special connector was used to make the connection to the center terminal of the micro-dot connector. The brush, spring and connector

were electrically insulated from the rest of the brush housing.

Figure B-1 shows the brush housing and internal components.

During initial tests, the slip rings and metal fiber brushes were exhibiting excessive wear. To reduce the wear rate a system of lever arms with magnetic stops was devised to allow the brushes to be conveniently lifted from the slip rings while the shaft was running but when no test data was being obtained. A counter weight at one end of the lever arm held the brushes off the slip rings. A magnet at the opposite end of the lever arm would hold the brushes in a preset position on the slip ring to allow test data to be obtained. This system greatly reduced the wear rate of the brushes and slip rings.

Figure B-2 shows the brush housing installed at the test end.

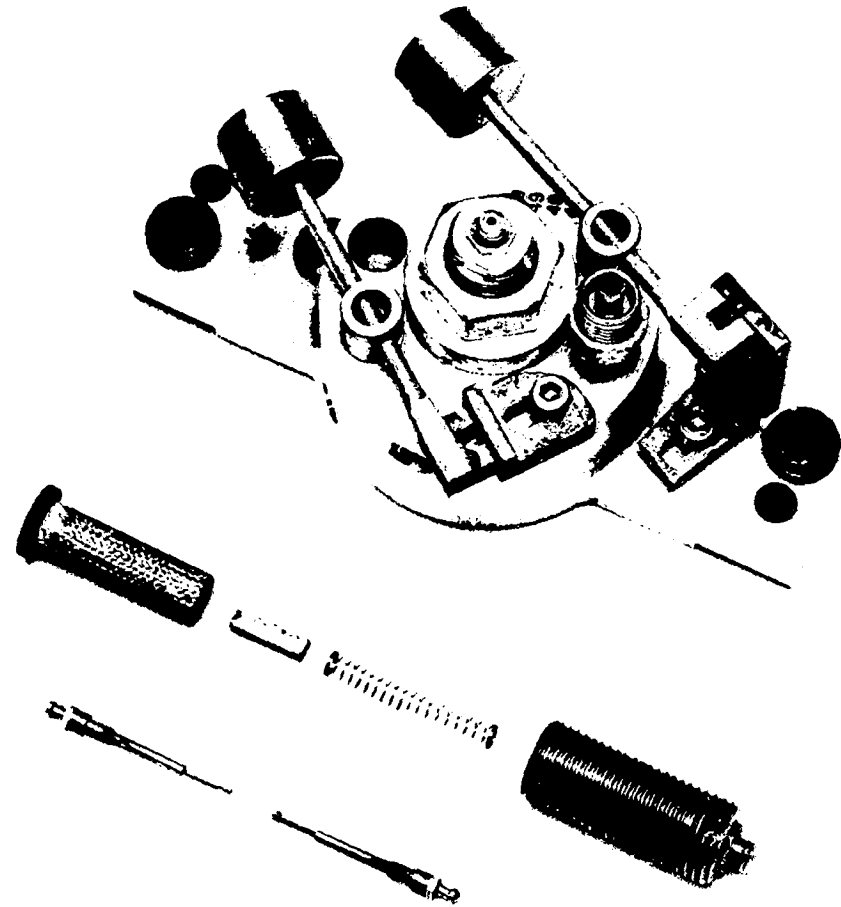


Fig. B-1 Brush Housing and Brushes

REPRODUCIBILITY OF THE
ORIGINAL PAGE IS
NOT GUARANTEED

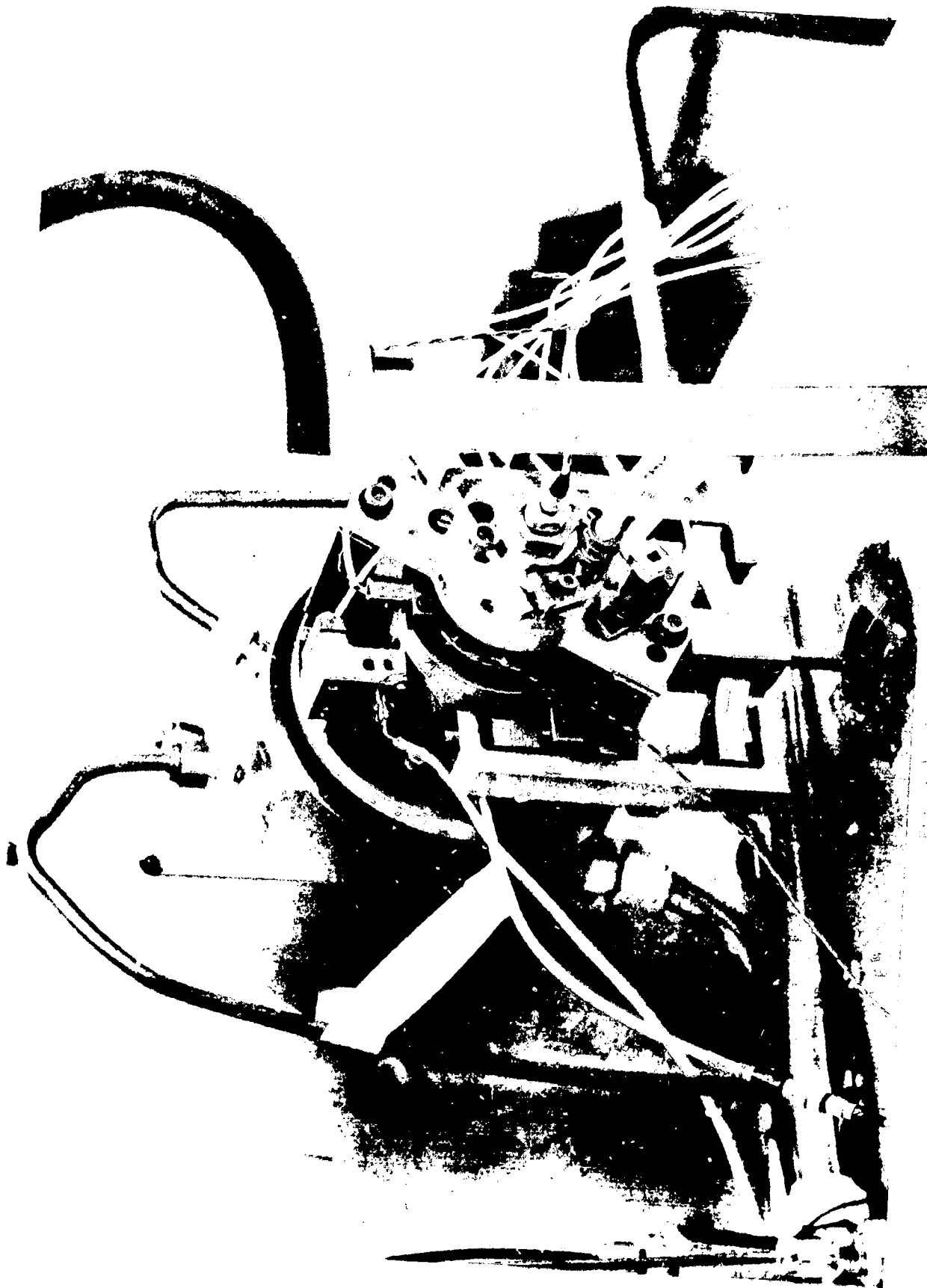


Figure 1. Turbine Engine Installed on Test Rig